CHARACTERIZATION OF THE HOST TISSUE RESPONSE INDUCED BY A BIOSYNTHETIC MATERIAL COMPOSED OF POLY (4-HYDROXYBUTYRATE)

by

Catalina Pineda Molina

Biomedical Engineer, Antioquia's School of Engineering with CES University, 2007

Master in Biotechnology, National University of Colombia, 2013

Submitted to the Graduate Faculty of

Swanson School of Engineering in partial fulfillment

of the requirements for the degree of

Doctor of Philosophy

University of Pittsburgh

2018

UNIVERSITY OF PITTSBURGH

SWANSON SCHOOL OF ENGINEERING

This dissertation was presented

by

Catalina Pineda Molina

It was defended on

June 28, 2018

and approved by

Bryan M. Brown, PhD, Assistant Professor, Department of Bioengineering and Obstetrics, Gynecology, and Reproductive Sciences

Janet S. Lee, MD, Professor, Department of Medicine

Kacey Marra, PhD, Associate Professor, Department of Plastic Surgery and Bioengineering

Jon D. Piganelli, Associate Professor, Department of Surgery, Immunology and Pathology

Dissertation Director: Stephen F. Badylak, DVM, PhD, MD, Professor, Departments of Surgery and Bioengineering

CHARACTERIZATION OF THE HOST TISSUE RESPONSE INDUCED BY A BIOSYNTHETIC MATERIAL COMPOSED OF POLY (4-HYDROXYBUTYRATE)

Catalina Pineda Molina, PhD

University of Pittsburgh, 2018

Biomaterial-associated infections and bacterial resistance to antibiotics represent two of the major causes of implant failure. Pre-clinical and clinical studies have associated the use of biosynthetic surgical mesh materials composed of poly (4-hydroxybutyrate) (P4HB) with decreased surgical site infection (SSI) and an improved long-term remodeling response. The mechanisms driving these beneficial effects of P4HB remain unknown. 4-hydroxybutyrate (4HB), the main degradation product of P4HB, is an endogenous short chain fatty acid (SCFA) that has been exhaustively studied for its role as a modulator of the neurotransmitter γ-aminobutyric acid (GABA) in the central nervous system (CNS) and as a modulator of reactive oxygen species (ROS) in endothelium. Other functions of 4HB within non-CNS tissues have been less studied; however, this SCFA is a hydroxylated form of butyrate, a known histone deacetylase (HDAC) inhibitor, which is secreted by commensal bacteria within the gastrointestinal tract. Butyrate exerts its immunomodulatory functions by suppressing pro-inflammatory macrophage activation and promoting antimicrobial peptide (AMP) secretion. However, the immunomodulatory effects of 4HB upon cells of the immune system and the ability of 4HB to induce the expression of AMP have not been studied.

The present dissertation evaluates the 4HB-mediated effects upon macrophage expression. The molecular mechanisms by which a specific AMP, cathelicidin LL-37, is expressed are described. A rat model of a partial thickness abdominal wall defect and a rat model of deliberate contamination in a subcutaneous tissue pocket are used to evaluate the host macrophage response and the expression of cathelicidin LL-37 in the presence of P4HB surgical mesh.

4HB promotes a pro-remodeling, regulatory phenotype and increases expression of AMP in subjected macrophages. The associated molecular mechanism involves transcriptional activation of cathelicidin LL-37 through MAP-kinase and NF-κB pathways. *In vivo*, P4HB mitigates the acute, pro-inflammatory host response and provides an increased resistance to bacterial contamination. The results of this work expand the understanding of the biologic activity of 4HB in cells of the immune system and show its potential to promote a constructive tissue remodeling effect for regenerative medicine applications.

TABLE OF CONTENTS

LIST OF TABLES

LIST OF FIGURES

PREFACE

This journey and this work would have not been possible without the contribution of many people that have influenced my academic and personal development.

I want to express my most sincere gratitude to my advisor and mentor, Dr. Stephen Badylak. Thank you for accepting me in your lab; thank you for your patience and your constant guidance during this time. I will forever value the unique opportunity you gave me.

I want to acknowledge the valuable ideas and constructive feedback I received from my advisory committee. Thank you, Dr. Kacey Marra, Dr. Janet Lee, Dr. Bryan Brown, and Dr. Jon Piganelli for your critical insights.

I want to thank former and current Badylak lab members for their support in my academic process. The Badylak lab has been a place not only for the construction of a collaborative environment, but also for the generation of a long-lasting friendship. Special thanks to Dr. George Hussey, Dr. Brian Sicari, Dr. Jenna Dziki, Dr. Jonas Eriksson, Dr. Neill Turner, Dr. Li Zhang, Dr. Lina Quijano, Dr. Xue Li, Scott Johnson, Janet Reing, Maddie Cramer, Lindsey Saldin, Mark Murdock, Jordan Chang, Joe Bartolacci, Yoojin Lee, Lori Walton, Dr. Ricardo Londono, Dr. Crisanto Torres, Dr. Alessandra Costa, Dr. Nazia Mehrban, Dr. Luai Huleihel, Dr. Lisa White, Dr. Juan Diego Naranjo, Dr. Denver Faulk, Dr. Tim Keane, and Dr. Michelle Scarritt for your helpful discussions and assistance.

I want to express my gratitude to former and current administrative members of the Badylak lab for keeping us organized. Thank you, Rachel Thomas, Emily Henderson, Hadley

Pratt, Jocelyn Runyon, Emily Stayshich, Eve Simpson, and Allyson Lacovey for assisting me since the day I contacted Dr. Badylak for my application.

I want to thank the undergrad and rotational students that facilitated the development of this work. Thank you, Ross Giglio, Derek Wang, Francesca Torri, Riddhi Gandhi, Angela Ramirez, Laura L. Cárdenas B., Michael Shulock, Neil Khurana, Salma Elmossier, for your exceptional work and your valuable ideas.

I want to acknowledge the McGowan Institute for Regenerative Medicine, the Bioengineering Program, and the Center for Latin American Studies (CLAS) at the University of Pittsburgh, as well as their faculty and administrative members for their valuable assistance. The University of Pittsburgh, through these institutions, received me with open hands and allowing my academic growth during the past few years.

I am also grateful with COLCIENCIAS – Fulbright Colombia and the Tuition Remission Fellowship from CLAS, programs that sponsored my academic activity. I would also like to thank additional support given by Dr. Badylak and the McGowan Institute for Regenerative Medicine to participate in academic diffusion strategies, such as conferences, symposiums, and technical meetings. And I would like to thank the industrial partnership between the McGowan Institute for Regenerative Medicine at the University of Pittsburgh and Becton, Dickinson and Company, that supported the development of this work.

I am forever grateful to my parents, Luz Elena and José Uriel, who are the best examples of dedication, discipline, and hard work. Thank you for teaching me that there are no limits to pursue my dreams. Your encouragement to work for what I want and your endless love have been my day-to-day motivation.

I want to express my deepest gratitude to Yesid, the best big brother someone can ask. Thank you for your life-long mentorship, for being an inspiration, for teaching me to be independent, and for introducing the biomedical engineering field into my life.

I also want to thank my sisters in law Carolina, Ángela, and Sara, my parents in law Mérida y Ramiro, and my extended family for their support and motivation.

Finally, I want to express my gratitude to my beloved husband, Juan Fernando. Thank you for your patience and understanding. Your love and support have been essential throughout this journey.

This thesis is dedicated to my little angel, Andrés Felipe. You came to this world to teach me how to value every single step in life, no matter how small it was.

1.0 INTRODUCTION

The use of biosynthetic materials composed of poly 4-hydroxybutyrate (P4HB) in medical devices has increased significantly over the past decade [1]. The rationale behind the use of P4HB-based materials as a surgical mesh for ventral hernia repair applications includes its beneficial mechanical properties and its ability to degrade *in vivo*, among others[2]. Pre-clinical [3, 4] and clinical studies [5-7] have shown that implanted surgical meshes composed of P4HB prevent a long-term adverse host response and are associated with both a decreased hernia recurrence rate and a lower incidence of surgical site infection (SSI) when compared with other surgical meshes. The mechanisms by which P4HB mesh promotes these beneficial clinical outcomes are unknown; however, it is hypothesized that the early host macrophage response to P4HB plays a significant role in determining the long-term outcomes.

The present dissertation evaluates the host macrophage response to P4HB and compares it with the host response to other non-degradable and degradable synthetic and biologic surgical meshes. The immunomodulatory activity of P4HB and its ability to promote endogenous antimicrobial peptide expression in macrophages are investigated. The cellular and molecular mechanisms by which 4-hydroxybutyrate, the degradation product of P4HB, drives these modulatory effects are also investigated. Finally, the role of macrophages in promoting a particular long-term outcome [foreign body response (FBR) vs. constructive tissue remodeling] and their

contribution to resistance to bacterial contamination when interacting with a subset of non-degradable or degradable synthetic, biosynthetic, and biologic surgical meshes are evaluated.

The present chapter provides a general background on the host response to implanted biomaterials, and more specifically the role of macrophages as critical modulators of this response. A second aspect of the host response, the endogenous secretion of antimicrobial peptides (AMP), is discussed and presented in the context of implanted biomaterials. The general characteristics of polymers and monomers of 4-hydroxybutyrate are described. Finally, the significance of the present work is explained.

1.1 THE HOST RESPONSE TO IMPLANTED BIOMATERIALS

1.1.1 The wound healing process

Disruption of the normal structure of tissues, produced either by surgical or traumatic injuries, prompt a wound healing process leading towards the recovery of tissue homeostasis. The wound healing involves a series of strictly coordinated molecular and cellular events and is classically divided into three, overlapping phases: 1) inflammation, 2) proliferation, and 3) tissue repair (Figure 1A) [8]. Immediately after injury, aggregation of platelets produced by the rupture of vessels results in an activation of the coagulation cascade and the release of chemotactic signals to induce cell migration. Cells of the innate immune system (i.e., neutrophils and macrophages) are the predominant cell types present during the inflammation phase. Neutrophils migrate within the first 48 hours, followed by macrophage infiltration. Macrophages activate along a broad

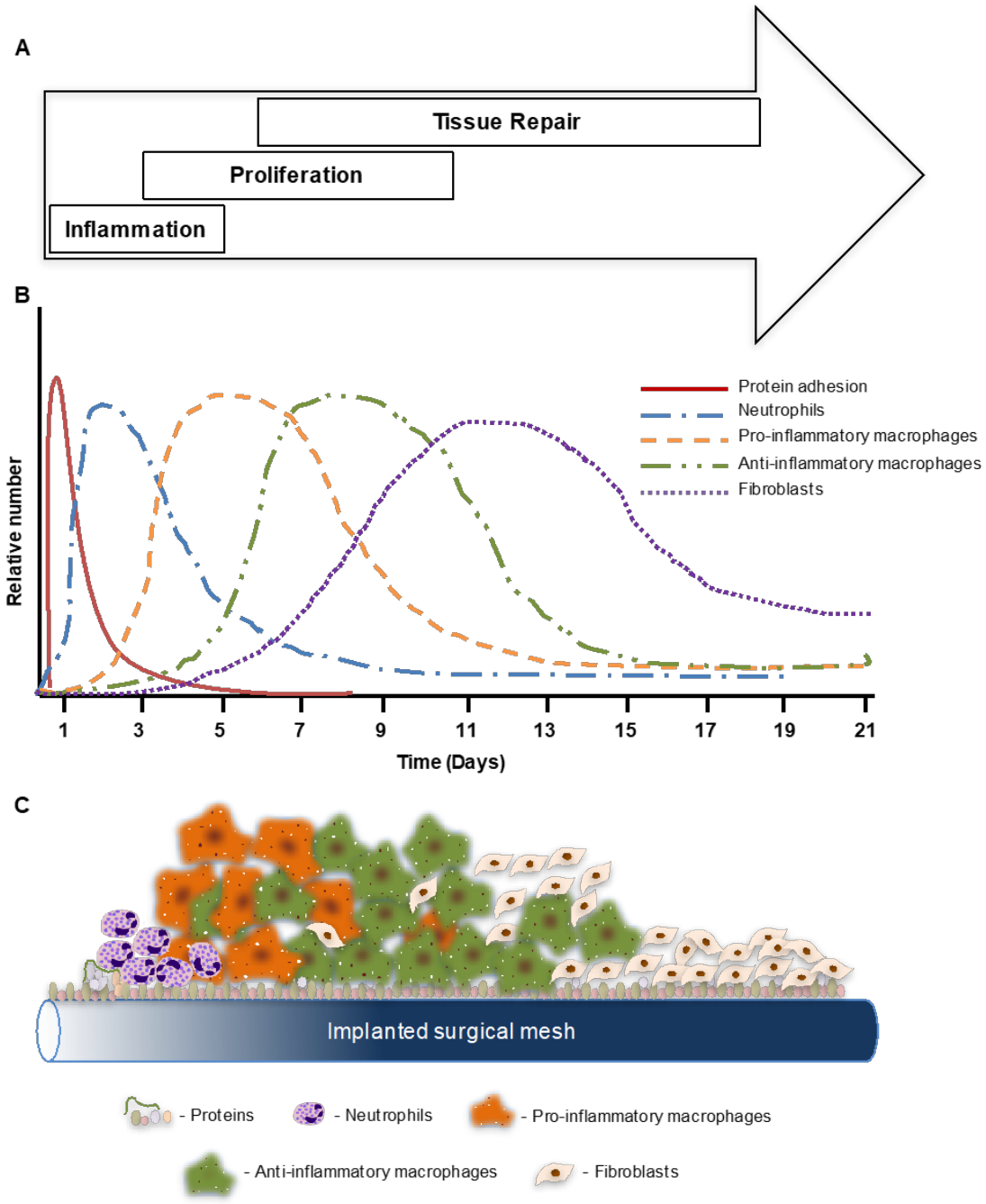

Figure 1. Host response to wound healing and to implanted biomaterials.

A. Phases of healing process following an implantation of a surgical mesh material. B. Timeline of molecular and cellular events at the mesh-tissue interface. C. Schematic view of protein adhesion (Vroman effect), and cellular interactions with an implanted surgical mesh. (A & B, adapted from [8, 9]).

spectrum of phenotypes, orchestrating the pro-inflammatory response to injury at early time points, but also regulating the tissue repair process and recovery of tissue homeostasis during the proliferative and maturation phases (Figure 1B) [10]. An appropriate transition from a pro-inflammatory state to an alternative, regulatory phenotype of macrophages is critical for a successful wound healing process. For instance, a perpetuated inflammatory response, promoted by the maintenance of a pro-inflammatory macrophage phenotype at the injured site is one of the hallmarks of chronic wounds, commonly associated with poor healing outcomes [11].

1.1.2 The host response to biomaterials

The present dissertation considers implanted biomaterials in the form of surgical mesh materials and both terms will be used interchangeably. All implanted materials elicit a host immune response, which is the ultimate determinant of their downstream success or failure within the body [12, 13]. After biomaterial implantation, an early transition from pro- to anti- inflammatory macrophages, particularly in response to implanted, extracellular matrix (ECM) bioscaffolds, is a predictor and determinant of long term site-appropriate tissue repair, a process known as "constructive remodeling" [14-16]. Conversely, non-degradable and slowly degradable polymeric scaffolds typically prompt a chronic inflammatory host response, promoted by the perpetuation of a pro-inflammatory macrophage phenotype at the material-tissue interface, resulting in a FBR [15, 17, 18]. As a response to frustrated phagocytosis, macrophages fuse together to form multinucleate foreign body giant cells characterized by chronic active inflammation, seroma formation, fibrotic scar tissue, and increased risk of infection [15, 19, 20]; all of which may be associated with tissue contraction and pain, among other complications [21, 22].

Different strategies have been used to mitigate the effects of an adverse host immune response to implanted materials. Such strategies include functional coating with biologic molecules such as cytokines or extracellular matrix components that modulate the phenotypic transition of macrophages at the host-material interface and prevent the development of FBR [15, 16, 23]. Other strategies include the development of absorbable polymers with tunable mechanical properties and controlled degradation times [24], promoting only a temporary substrate and therefore, a temporary host response. These materials include polymers and copolymers of poly-glycolide (PGA), poly-lactide (PLA), poly-hydroxyalcanoates (PHA), poly-4-hydroxybutyrate (P4HB), and poly-trimethylene carbonate (TMC), among others [3, 25, 26]. Additionally, other physical and chemical characteristics of absorbable materials also influence the final outcome of the implanted material. For example, the micro- and macro-structure of polymers affect molecular and cellular interactions. Patterns of polymer degradation, such as rate and release of acid monomers into the microenvironment, which in turn decrease the local pH, promote a prolonged pro-inflammatory stage, affecting the functionality of the repaired tissue (i.e., fibrotic or site-appropriate tissues). The chemical composition of polymeric scaffolds can facilitate or inhibit bacterial adherence.

1.1.3 Wound healing and bacterial infection

Bacterial infiltration is facilitated by the disruption of tissues during the injury or by their adhesion at the surface of implanted biomaterials. Perpetuation of bacterial colonies within biofilms increases the levels of bacterial proteases and pro-inflammatory cytokines, orchestrated by a prolonged presence of polymorphonuclear cells and pro-inflammatory macrophages, impairing effective wound healing [27, 28].

1.2 BACTERIAL-BIOMATERIAL INTERACTIONS

Interactions of bacteria with adherent proteins at the surface of implanted materials allows for their attachment and subsequent secretion of a biofilm. Bacterial biofilms are an organized hydrated matrix of extracellular polymeric substances (EPS) [29, 30] that provides protection from host defense mechanisms and allows bacterial survival within the tissue [31, 32]. Bacterial biofilms are less susceptible to antimicrobial agents. Mechanisms which account for this increased resistance include: 1) EPS-mediated formation of a thick structure that isolates bacteria and inhibits the entrance of immune cells or diffusion of antimicrobial agents and 2) slow growth rate of bacteria within the EPS thus rendering antimicrobial agents ineffective [30, 32].

Bacterial concentrations greater than $1*10^5$ colony forming units (CFU) per gram of wound tissue can lead to the development of infections [33]. It is estimated that more than 70% of bacterial infections, which include those associated with soft tissues and implanted biomaterials, are involved in the formation of biofilms [30, 34]. Given the intrinsic resistance of biofilms to current antimicrobial therapies, there is an imminent need of new approaches that effectively decrease/impede bacterial interactions and thus biofilm formation.

1.3 ENDOGENOUS ANTIMICROBIAL PEPTIDES

Antimicrobial peptides (AMP) have long been recognized as part of the innate immune system defense against pathogens. AMP can be effective even when bacteria are in a quiescent stage within a biofilm, providing an advantage over most current antibiotic agents [30], and can prevent bacterial-associated biofilm formation [32] and persistent infection [35, 36].

The major groups of AMP in mammals are defensins, cathelicidins, and histatins [37]. The mechanisms of action of AMP include their ability to interact with negatively charged bacterial membranes because of their cationic polarity, and promote disruption and permeabilization of the bacterial membrane. AMP can also target and block specific molecules of bacterial metabolic pathways [32]. Various AMP have been shown to downregulate the gene expression of molecules required for bacterial motility and matrix synthesis through inhibition of transcriptional activators of the quorum-sensing (QS) systems and the intracellular stringent response signal (p)ppGpp, affecting bacterial communication within the biofilm [30]. The functions of AMP extend beyond antimicrobial activity. For example, defensins and cathelicidins are chemoattractants for immune cells to enhance the host response to bacterial contamination or infection [38, 39]. The role of cathelicidin LL-37, the only human cathelicidin, in wound healing processes [40-42] and angiogenesis [43] has also been recognized. Cathelicidin LL-37 is also implicated in a seemingly paradoxical response, since it promotes the expression of anti-inflammatory cytokines in already activated pro-inflammatory immune cells, acting as modulator of the immune response and promoting local tissue homeostasis [39].

The functions of AMP at the material-tissue interface importantly prevent bacterial-associated biofilm formation [32] and therefore, persistent infections [35, 36]. Small fragments of AMP have been synthetically produced to functionalize biomaterials. For instance, the small peptide sequence (LLKKK18), derived from cathelicidin LL-37, conjugated to dextrin and indirectly linked to Carbopol® hydrogels (based on acrylic acid polymers), is being investigated for skin burn treatments [40]. Strategies intended to enhance the natural production of AMP using biologically-derived biomaterials, however, have not yet been explored. The use of implanted

biomaterials able to trigger the immune system to produce AMP could provide a sustained and more potent response compared with the extrinsic addition of these peptides within the biomaterial.

1.4 BIOSYNTHETIC POLYMERS COMPOSED OF P4HB

Medical devices composed of P4HB have been gaining attention within the biomaterials field. P4HB-based materials are FDA approved and indicated for a variety of soft tissue repair procedures in plastic and reconstructive surgeries (i.e., sutures, meshes for hernia and tendon repair, etc.) [1]. P4HB is a polyester that belongs to the group of polyhydroxyalcanoates (PHA), which are polymers naturally assembled by microorganisms and further processed (e.g., molded, extruded, knitted, woven, etc.) to produce a highly reproducible material with mechanical properties comparable to synthetic polyesters. Pre-clinical and clinical evidence indicate the ability of P4HB to promote tissue integration [3, 5], vascularization [3], and functional tissue reconstruction [44], prevent long-term adverse response [3, 7, 45], and resist bacterial contamination [4]. The mechanisms associated with the advantageous responses of implanted P4HB still need to be further studied.

The main forms of degradation of P4HB are surface erosion and enzymatic degradation, releasing monomers of 4HB. Moreover, it has been shown that unlike PGA or poly-ε-caprolactone (PCL), *in vivo* degradation of P4HB does not decrease the local pH, reducing the risks of inflammation and bacterial infection at the host-material interface [3]. Following hydrolysis of P4HB, monomers of 4HB are quickly degraded through the Krebs cycle, finally being eliminated from the body through CO_2 and H_2O, without harmful accumulation of secondary metabolites [46].

1.4.1 4-Hydroxybutyrate

4HB is an endogenous bioactive molecule commonly found in mammalian tissues [47-49], it belongs to the group of short chain fatty acids (SCFA), and it is actively studied for its role as metabolite of the neurotransmitter γ-aminobutyric acid (GABA). In the central nervous system (CNS), this molecule modulates the extracellular concentrations of GABA, dopamine, and glutamate to regulate neural responses [50]. Endogenous 4HB has been identified in peripheral organs (i.e., hearth, kidney, liver, lungs, muscle, and brown fat) at concentrations that exceed the normal values in brain [51]. Although the functions of 4HB within these tissues remain mostly unclear, a protective effect of 4HB has been identified. In particular, 4HB has been shown to mitigate cellular responses to stress and ischemia by decreasing the production of reactive oxygen species (ROS) and shifting metabolism towards the production of NADPH [52]. Exogenous administration of 4HB is currently approved by the FDA for the treatment of narcolepsy and is being evaluated for the control of fibromyalgia in a phase 3 clinical trial [53, 54].

Other functions of 4HB within the tissues have been less studied. This SCFA is a hydroxylated form of butyrate, a known histone deacetylase (HDAC) inhibitor secreted by commensal bacteria within the gastrointestinal tract. Butyrate exerts its immunomodulatory functions as a suppressor of pro-inflammatory macrophages to prevent the development of chronic inflammation, and promotor of AMP secretion to prevent bacterial infection [55-57]. A group of SCFA, which include butyrate, valeric acid, propionate, and a series of butyrate derivatives such as sodium-4-phenylbutyrate, have been shown to modulate favorable responses and induce the gene expression of AMP in a variety of cells of the immune system (i.e., epithelial cells, neutrophils, macrophages) [58-60]. It is plausible, therefore, that similar responses will be elicited

by 4HB. The immunomodulatory influence of 4HB upon cells of the immune system and its ability to induce the expression of AMP have not yet been explored.

1.5 SIGNIFICANCE

Biomaterial-associated infections and the emergence of antibiotic resistant bacteria represent significant challenges for surgeons and the field of biomaterials in general. Surgical site infections (SSI) are considered the main cause of implant failure [61], with an incidence as high as 33% [62]. The primary source of variability are factors associated with the type of application (i.e., contact lens, meshes for hernia repair, catheters, etc.) and the intrinsic properties of the implanted biomaterial (i.e., biologic vs. synthetic, microstructure, degradability, etc.) [62]. The incidence of infection increases when non-degradable synthetic mesh materials such as polypropylene, poly(tetrafluorethylene) (ePTFE) or multifilament polyester are employed [63]. New approaches in manufacturing of synthetic materials are focused on functionalization and coating with antimicrobial agents [64, 65]. Such strategies, however, provide only short-duration protection for the time that the active component is released and involve a high risk of developing bacterial resistance [66]. Additionally, it has been shown that sub-optimal concentrations of antibiotics (which could be induced by slow, long-term release) promote an increased release of extracellular DNA (eDNA) into the bacterial biofilms and therefore, increased resistance to the antibiotic [30]. The recognition that AMP kill bacteria through mechanisms that do not depend on the metabolic activity of the pathogens, provides an effective mode of protection against them without the risk of developing resistance. The exogenous administration of AMP is being explored [40], however, this mode of use raises questions regarding the stability of the peptides and the methods for

delivery, and provides only temporary protection. The present study investigated an alternative approach that enhances endogenous antimicrobial activity of the immune system via increased production of AMP by host cells, thus generating a stronger and more prolonged response.

Biosynthetic materials composed of P4HB have been shown to facilitate site appropriate tissue remodeling and resist persistent bacterial contamination [4]. The mechanism(s) by which these materials, which do not contain bona fide AMP, can promote a favorable wound healing and resist bacterial contamination remain unknown. The activity of 4HB, the main degradation product of P4HB, as an endogenous metabolite within the CNS has been recognized. The use of 4HB as an endogenous inductor of AMP represents an attractive alternative to prevent biofilm-associated infections and potentially contribute to improved tissue repair outcomes due to their associated secondary functions in the wound healing process. Identification of the mechanisms mediating the effects induced by 4HB will prompt the development of newly derived composites able to promote functional tissue reconstruction in challenging, contaminated clinical environments. The present work provides significance within a basic science understanding via opportunities for clinical translation.

1.6 CENTRAL HYPOTHESIS

The present study hypothesizes that the biosynthetic surgical mesh material composed of P4HB promotes a predominantly constructive, anti-inflammatory macrophage phenotype, increased antimicrobial activity through expression of AMP, and a favorable tissue remodeling outcome when compared to synthetic counterparts.

1.7 SPECIFIC AIMS

1.7.1 Specific aim 1

Determine the phenotypic response of macrophages following exposure to degradation byproducts of P4HB.

Sub Aim 1.1: Compare the phenotypic response of macrophages exposed to degradation byproducts of a subset of biosynthetic, synthetic, and biologic surgical mesh materials.

Hypothesis 1: Degradation byproducts of P4HB promote a predominant constructive anti-inflammatory macrophage phenotype compared to other synthetic mesh materials. Degradation byproducts of P4HB suppress the pro-inflammatory macrophage phenotype.

Rationale: Macrophage activation within a diverse phenotypic spectrum plays an important role in the host response to biomaterials [67]. The anti-inflammatory effect of butyrate in IFN-γ-stimulated macrophages [57], and its facilitating role in the activation of anti-inflammatory (M2-like) macrophages [68] have already been demonstrated. The ability of 4HB, the main degradation product of P4HB, to modulate the macrophage response remain unknown. The present study uses use immunolabeling and gene expression to examine the phenotype of murine bone marrow-derived macrophages induced by P4HB vs. synthetic and biologic mesh materials *in vitro*.

1.7.2 Specific aim 2

Identify the mechanisms responsible for the antimicrobial activity associated with the biosynthetic material composed of P4HB.

Sub Aim 2.1: Determine the direct and indirect (macrophage-mediated) antimicrobial effect of degradation byproducts of P4HB.

Sub Aim 2.2: Compare the expression of AMP of macrophages exposed to degradation byproducts of a subset of biosynthetic, synthetic, and biologic surgical mesh materials.

Hypothesis 2: The antimicrobial activity of P4HB is mediated by an indirect effect involving the transcriptional activation of AMP in macrophages exposed to degradation byproducts of the biosynthetic material.

Rationale: Activated macrophages express AMP [69] with bactericidal and chemoattractant functions within the wound healing process [39, 41, 70-72]. The role of AMPs within the host response to implanted surgical biomaterials, however, has not been previously evaluated. Further derivatives of butyrate (i.e., sodium-4-phenylbutyrate) have been shown to share butyrate's activity [59, 60] either acting as HDAC inhibitors or as signaling molecules activating the mitogen-activated protein (MAP)-kinase pathway and therefore, inducing the expression of AMP. Whether 4HB is capable of inducing transcriptional activation of AMP is unknown. The proposed study evaluates antimicrobial activity, gene expression, and inhibition immunoassays to target intermediate proteins involved in the expression of AMP in macrophages exposed to byproducts of P4HB.

1.7.3 Specific aim 3

Evaluate the host tissue response to biosynthetic materials composed of P4HB *in vivo*.

Sub-Aim 3.1: Evaluate the spatiotemporal pattern of host tissue response to biosynthetic materials composed of P4HB implanted in a rat partial thickness abdominal wall defect model.

Sub-Aim 3.2: Compare the resistance to deliberate bacterial contamination of biosynthetic, synthetic, and biologic surgical mesh materials implanted in a rat subcutaneous model.

Hypothesis 3: Biosynthetic material composed of P4HB promotes increased antimicrobial activity through AMP expression, and a constructive macrophage phenotype when compared to other mesh devices.

Rationale: The early spatiotemporal phenotype of macrophages as part of the host immune response to implanted biomaterials is a determinant and predictor of long term outcomes (i.e., pro-remodeling or chronic inflammation) [14]. The host immune response to implanted P4HB and the expression of AMP have not been evaluated in the pre-clinical setting. The mechanisms behind the resistance of P4HB to persistent bacterial contamination remain unknown. The cell types involved and their association with secretion of AMP need to be further evaluated. The proposed study examines the *in vivo* macrophage phenotype and AMP expression following P4HB mesh implantation in a rat partial thickness abdominal wall defect model.

2.0 COMPARATIVE PHENOTYPIC RESPONSE OF MACROPHAGES EXPOSED TO DEGRADATION BYPRODUCTS OF BIOSYNTHETIC, SYNTHETIC, AND BIOLOGIC SURGICAL MESH MATERIALS[1]

2.1 INTRODUCTION

The use of biomaterials from synthetic, biosynthetic, and biologic sources has become commonplace for the repair of damaged tissues for different clinical applications. The clinical outcome, however, ranges from successful tissue repair to implant failure. The early macrophage response to implanted biomaterials, specifically their phenotypic profile, is predictive and determinant of such disparate downstream outcomes [14]. An earlier transition of pro-inflammatory (M1-like) macrophages to pro-remodeling (M2-like) macrophages has been associated with a successful tissue repair, whereas a prolonged presence of M1-like cells drives a FBR, characterized by scar tissue formation, presence of multinucleate giant cells, and chronic inflammation.

Different studies have shown the ability of ECM-based scaffolds to modulate the host response by increasing the ratio of M2-like to M1-like macrophages within the first 14 days post-implantation [14, 15, 67]. Further, it has been shown that these responses are in part due to

[1] Sections of this chapter to appear in *Journal of Immunology and Regenerative Medicine.*

molecular interactions between the degradation products of the ECM (cryptic peptides, growth factors, matrix bound nanovesicles (MBV), among others) and macrophages [73-76].

Macrophage activation along a broad spectrum of phenotypes involves the expression of cell surface markers, transcription factors, and activation of differential metabolic pathways (Appendix A). The activated pathways direct the release of bioactive molecules, including cytokines, chemokines, and AMP, all of which determine cellular function and sequentially drive the host immune response [10, 69, 75]. The degradation byproducts of polymeric materials of different compositions are known to elicit distinct phenotypic responses, but the specific response has not been well characterized for most materials. Characterization of the host response to polymeric materials could be determinant to understand differential clinical outcomes.

The present study evaluates the *in vitro* macrophage phenotypic profile induced by stimulation with the degradation products of P4HB as compared to the macrophage phenotype induced by degradation byproducts of other synthetic and biologic materials commonly used as surgical meshes. The immunomodulatory activity of these byproducts on macrophages activated with LPS and IFN-γ ($M_{LPS/IFN-\gamma}$) is also determined.

2.2 MATERIALS AND METHODS

2.2.1 Test articles

Common surgical polymeric materials used for tissue engineering and regenerative medicine applications are included. The source and characteristics of the surgical mesh materials under evaluation are described in Table 1.

Table 1. Composition and properties of surgical meshes

Commercial Scaffold Name	Polymer Composition	Category	*in vivo* Resorption Time	Fiber Diameter (µm)	Pore Size (mm^2)	Ref.
Phasix™	Poly-4-Hydroxybutyrate (P4HB)	Degradable Biosynthetic	12-18 months	166	0.25	[77]
Bard®	Polypropylene (PP)	Non-degradable Synthetic	NA	185.7	0.44	[25]
TIGR®	Fast Resorbing Fiber - Copolymer of Glycolide, Lactide and Trimethylene Carbonate (TMC) Slow Resorbing Fiber - Lactide and Trimethylene Carbonate	Degradable Synthetic	4 months & 36 months	10-40	1.0	[24, 78]
GORE® BIO-A®	Polyglycolic acid (PGA) & Trimethylene Carbonate (TMC)	Degradable Synthetic	6 months	3.38	NA	[24]
Strattice™	Acellular Porcine Dermis	Degradable Biologic	12 months	NA	NA	[79]

2.2.1.1 *In vitro* accelerated hydrolysis of mesh scaffolds

Phasix™ mesh was hydrolyzed with 3M HCl at 37°C using a modification of a previously established accelerated hydrolysis method [77]. Tigr® Mesh and GORE® BIO-A® were hydrolyzed with 9M NaOH at 37°C. Bard® Mesh was used as a non-degradable control, but was still subjected to all hydrolysis steps. Solubilized monomers released by the hydrolysis were neutralized to pH 7.0 with the opposite solution. The resulting solution was dialyzed with a membrane (0.1 to 0.5 Kd cut off) (Float-A-Lyzer™ G2 Dialysis Device, Fisher Scientific Cat No. 08-607-016) to remove the excess salt.

2.2.1.2 Preparation of digested ECM bioscaffold

Degradation products of Strattice™ were obtained through enzymatic digestion [80, 81]. 100 mg of pepsin (Sigma, Cat No. P7012) were mixed with 1000 mg of lyophilized Strattice™ powder in 100 ml of 0.01 M HCl. The digestion was performed for 48 hours at a constant stir.

2.2.2 Experimental design overview

Degradation products of the meshes generated by hydrolysis were used to either activate naïve murine bone marrow-derived macrophages for 24 hours, or to challenge pre-activated $M_{IFN\text{-}\gamma/LPS}$ macrophages (Figure 2). Macrophage phenotype was evaluated by immunolabeling for the markers F4/80, iNOS, Fizz1, and Arginase1. Secretion of TNF-α and IL-10 was quantified by enzyme-linked immunosorbent assay (ELISA). Gene expression of metabolic, surface markers, and transcription factors were also evaluated.

2.2.3 Gas chromatography – mass spectrometry

In collaboration with the Cambridge Polymers Group, the main degradation product of Phasix™ was determined by gas chromatography – mass spectrometry (GC-MS) and compared with the solution containing Bard® Mesh. Briefly, 1 ml of neutralized solution was filtered through a 0.45 μm PTFE syringe filter and transferred to GC autosampler vial. The samples were analyzed by an Agilent 6890GC/5973MS system, in Scan (mass spectrometer detection 50-550 m/z) or selection ion monitoring (SIM) mode with retention times selected using standards of γ-butyrolactone (GBL) and 4-hydroxybutyrate (4HB), as they are the most likely P4HB degradation

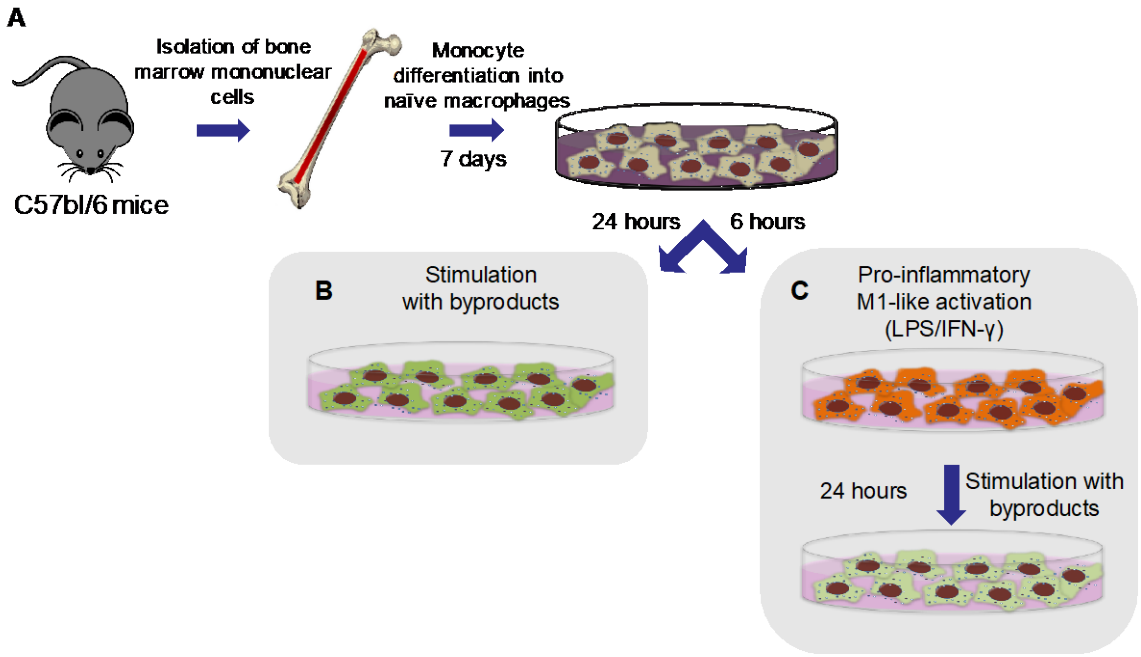

Figure 2. Macrophage differentiation and activation.

A. Primary macrophages were differentiated from mononuclear cells harvested from the bone marrow of C57bl/6 mice. B. Macrophages were exposed to degradation byproducts of the meshes or known activators of the M1-like (IFN-γ / LPS), and M2-like phenotypes (IL-4) for 24 hours. C. Macrophages were first activated to a pro-inflammatory M1-like phenotype for 6 hours, and then exposed to one of each of the degradation byproducts of the mesh scaffolds for 24 hours. The phenotype of stimulated macrophages was evaluated by immunolabeling of markers of pan-macrophages Mϕ ($F4/80^+$), pro-inflammatory M1-like macrophages ($iNOS^+$), and anti-inflammatory regulatory M2-like macrophages ($Fizz1^+$ and $Arginase1^+$).

products. The 2011 NIST/EPA/NIH spectral library database (NIST MS search 2.0g) was used for compound identification. For each peak present in the chromatogram, the mass spectrum was determined by measuring the mass spectrum at the apex of the peak and subtracting a background immediately prior to the peak onset. The resulting spectrum was screened against the mass spectral library.

2.2.4 Isolation and culture of murine bone marrow-derived macrophages (BMDM)

All procedures were approved by and performed according to the guidelines of the Institutional Animal Care and Use Committee at the University of Pittsburgh (IACUC protocol #15086460). Bone marrow-derived monocytes were obtained from female C57bl/6 mice (Jackson Laboratories, Bar Harbor, ME) and differentiated into macrophages as previously described [80, 82]. Animals were euthanized by CO_2 inhalation and subsequent cervical dislocation in accordance with the guidelines of the American Veterinary Medical Association (AVMA) Panel of Euthanasia. Following euthanasia and using an aseptic technique, the skin of the hind legs was completely removed, the coxa-femoral joint was disarticulated, and the legs harvested. The excess of muscle was removed, and after disarticulation of tarsus and stifle, tibia and femoral bones were isolated. Under sterile conditions, the ends of each bone were transected and the bone marrow flushed with medium using a 30G needle. Harvested monocytes were seeded at a concentration of $2*10^6$ cells/ml and differentiated into macrophages by culture for 7 days with macrophage-colony-stimulating-factor (MCSF)-containing media [DMEM high glucose (Gibco, Grand Island, NY), supplemented with 10% fetal bovine serum (FBS) (Invitrogen, Carlsbad, CA), 10% L929 cell supernatant, 50 μM beta-mercaptoethanol (Gibco), 100 U/ml penicillin, 100 ug/ml streptomycin, 10 mM non-essential amino acids (Gibco), and 10 mM hepes buffer]. Cells were differentiated into macrophages for 7 days at 37°C and 5% CO_2 with media changes every 48 hours.

2.2.5 Macrophage activation

Naïve macrophages were stimulated with 1.32 mg/ml of the byproducts of hydrolysis of synthetic or biosynthetic meshes, 200 μg/ml of pepsin-digested Strattice™, or the macrophage activation

controls to promote an M1-like phenotype (20 ng/ml IFNγ and 100 ng/ml of LPS) or an M2-like phenotype (20 ng/ml IL-4) for 24 hours at 37°C, 5% CO_2 [83]. In a separate experiment, macrophages were first activated toward using IFNγ and LPS for 6 hours, as described above, followed by stimulation using the byproducts of the mesh materials for 24 hours [75].

2.2.6 Immunolabeling of treated macrophages

Stimulated macrophages were fixed in 2% paraformaldehyde for 30 minutes, followed by washes with PBS. Fixed cells were then incubated for 1 hour with blocking buffer (2%v/v horse serum, 1%wt/v bovine serum albumin, 0.1%v/v triton X-100, and 0.1%v/v tween-20 in PBS) to inhibit non-specific binding of antibodies. After blocking, macrophages were incubated in primary antibodies at 4°C overnight: (1) monoclonal rat anti-murine F4/80 (CI-A3-1) (Novus Biologicals, Cat. No. NB600-404) at 1:100 dilution, (2) polyclonal rabbit anti-iNOS (Novus Biologicals, Cat. No. NB300-605) at 1:100 dilution, (3) polyclonal rabbit anti-murine Fizz1 (RELMα) (Peprotech, Cat. No. 500-P214) at 1:100 dilution, and (4) polyclonal rabbit anti-liver Arginase1 (Abcam, Cat. No ab91279) at 1:100 dilution. After washing in PBS, the macrophages were incubated in fluorophore-conjugated secondary antibodies [Alexa Fluor goat anti-rat 488 (A11006) or goat anti-rabbit 488 (Cat. No. A11034), Invitrogen] at 1:200 dilution for 1 hour at room temperature. After washing again with PBS, nuclei were counterstained with 4'-6-diamidino-2-phenylindole (DAPI) prior to imaging. Images of three 20X fields were taken for each well using a Zeus live-cell microscope, standardizing the light exposure times for based upon those set for cytokine-treated macrophages. The percent of positive cells for each marker was quantified using CellProfiler Image Analysis Software (http://www.cellprofiler.org), positive macrophages (green label) were identified by their co-localization with DAPI positive nuclei. The percent of expressing

macrophages was then determined by dividing the identified positive cells by the total number of macrophage nuclei.

2.2.7 Gene expression profile of exposed macrophages

Transcriptional activation of surface markers, metabolic markers, and transcription factors (Appendix B) was evaluated in macrophages exposed to each of the byproducts of the surgical meshes. Total RNA was extracted from stimulated macrophages with 800 μl TRIzol reagent (Ambion, Cat. No. 15596018) using cell scraper. The solution was mixed with 200 μl chloroform, vortexed for 15 seconds and centrifuged at 12,000 g for 10 minutes. The aqueous phase was transferred to a new tube and the RNA precipitated with 3M sodium acetate (1/10 of the volume) and isopropanol (1 volume), followed by centrifugation at 18,000 g for 20 minutes. RNA purification was made washing the RNA pellet in 75% ethanol with an additional centrifugation at 18,000 g for 15 minutes. The RNA pellet was air dried and re-suspended in nuclease-free water. The RNA solution was treated with DNase I to remove any residual genomic DNA. 1 μg RNA was converted in cDNA using the High Capacity cDNA Reverse Transcription Kit (Invitrogen, Cat. No. 4368814) following manufacturer instructions. Real time quantitative polymerase chain reaction (qPCR) was made using PowerUp™ SYBR® Green Master Mix (Applied Biosystems, Cat. No. A25778) to determine the levels of expression of different markers of macrophage activation. The levels of expression were normalized with the housekeeping gene *hprt1*. Results were expressed as fold change log ($2^{-\Delta\Delta Ct}$) relative to non-treated macrophages.

2.2.8 Phagocytosis

The ability of macrophages treated with byproducts of P4HB to phagocytose fluorescent latex microspheres was evaluated as previously described [73] with some modifications. Treated macrophages were rinsed with PBS and incubated with $4.55*10^7$ particles/ml of Fluoresbrite YG Microspheres 1.00 um (Polysciences, Warrington, PA) in complete media for 15 minutes at 37°C, 5% CO_2. After incubation with microparticles, macrophages were washed with PBS and harvested with Accutase® solution. Cells were centrifuged and rinsed with PBS followed by a counterstain with viability dye eFluor 780 (eBioscience, San Diego, CA) at a dilution of 1:1000 for 30 minutes on ice. The percentage of phagocytic macrophages was determined by flow cytometry.

2.2.9 Enzyme-linked immunosorbent assay (ELISA)

Specific enzyme-linked immunosorbent assays (ELISA) were used to determine the concentrations the secreted cytokines TNF-α and IL-10 in macrophages activated with LPS and IFN-γ followed by stimulation with each of the byproducts of the surgical meshes for 24 hours. Cell culture supernatants were collected and centrifuged at 1,500 g at 4°C for 10 min to remove particulate material prior to use. ELISAS were performed following specific manufacturing instructions (Mouse TNF ELISA Kit, BD OptEIA™, Cat. No. 560478; and Quantikine ELISA, mouse IL-10, R&D Systems, Cat. No. M1000B).

2.2.10 Statistical analysis

Three independent experiments were conducted. Data is presented as the mean ± standard error of the mean (SEM). Statistical differences were determined using a non-parametric ANOVA test (Kruskal-Wallis test). Differences were compared with post-hoc Dunn's test relative to non-treated macrophages. A value $p<0.05$ was considered statistically significant. Statistical analysis was performed using GraphPad Prism version 6.07 (GraphPad Software, La Jolla CA, USA).

2.3 RESULTS

2.3.1 4-hydroxybutyrate is the main degradation product of the accelerated hydrolysis of Phasix™

The product of accelerated hydrolysis of Phasix™ was confirmed by gas chromatography – mass spectrometry (GC-MS) by the Cambridge Polymers Group (Figure 3A). Using both Scan and SIM mode, a single dominant peak was observed in the sample containing the degradation products of Phasix™ (red). The peak was strongly identified as 4HB (Figure 3B) compared to the NIST mass spectrum library (Figure 3C), with a match factor of 965. No other significant peaks were observed in the chromatograms for the evaluated samples.

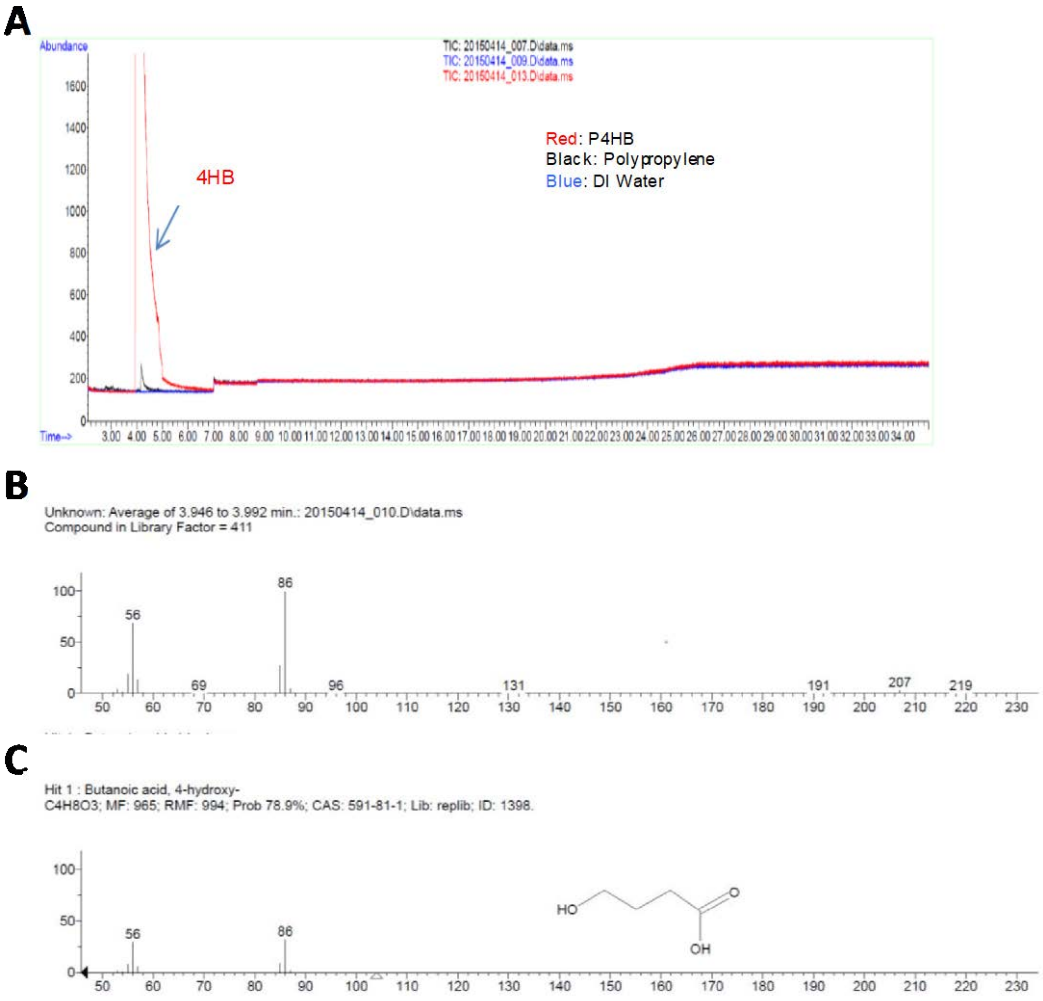

Figure 3. Gas chromatography – Mass spectrometry for degradation products of Phasix™.

A. SIM overlay of degradation byproducts of Phasix™ (red), Bard® Mesh (black), or water as a control (blue). A unique peak centered at approximately 3.9 minutes was found in the sample containing the degradation products of Phasix™. B. Measured mass spectrum of the peak found in A, corresponding to the degradation byproducts of Phasix™. C. NIST library search result showing the mass spectrum of the closest library match, corresponding to 4-hydroxybutyrate. A strong match factor of 965 was found.

2.3.2 *In vitro* macrophage response induced by degradation products of mesh scaffolds

The phenotypic profile of murine BMDM was determined by immunolabeling via the expression of the pan-macrophage marker F4/80, the pro-inflammatory, M1-like marker iNOS, and the M2-like markers Fizz1 and Arginase1. Quantitative PCR was used to determine the relative expression of markers associated with macrophage activation, metabolism, and transcription factors in comparison with non-treated macrophages.

All byproducts of the surgical meshes induced a distinctive pattern of macrophage activation (Figure 4). Exposure of the macrophages to the degradation products of all surgical meshes did not show differences in the expression of F4/80. Treatment with degradation byproducts of TIGR® and Strattice™ resulted in a phenotypic response of $iNOS^+$ cells significantly higher than non-treated macrophages (Figure 4B). All byproducts of the surgical meshes induced the transcriptional upregulation of TNF-α and downregulation of markers associated with an M2-like phenotype (Fizz1, YM1, CD206, and IL1-Ra) (Figure 4C). Degradation byproducts from Phasix™ and TIGR® induced the transcriptional activation of KLF4. The transcription factor IRF3 was upregulated by 4HB.

2.3.3 Phagocytic capability of macrophages stimulated with 4HB

Treatment of macrophages with the byproducts of Phasix™ did not affect the phagocytic activity of the cells in comparison with macrophages treated with LPS and IFN-γ, or IL-4, as shown in Figure 4D.

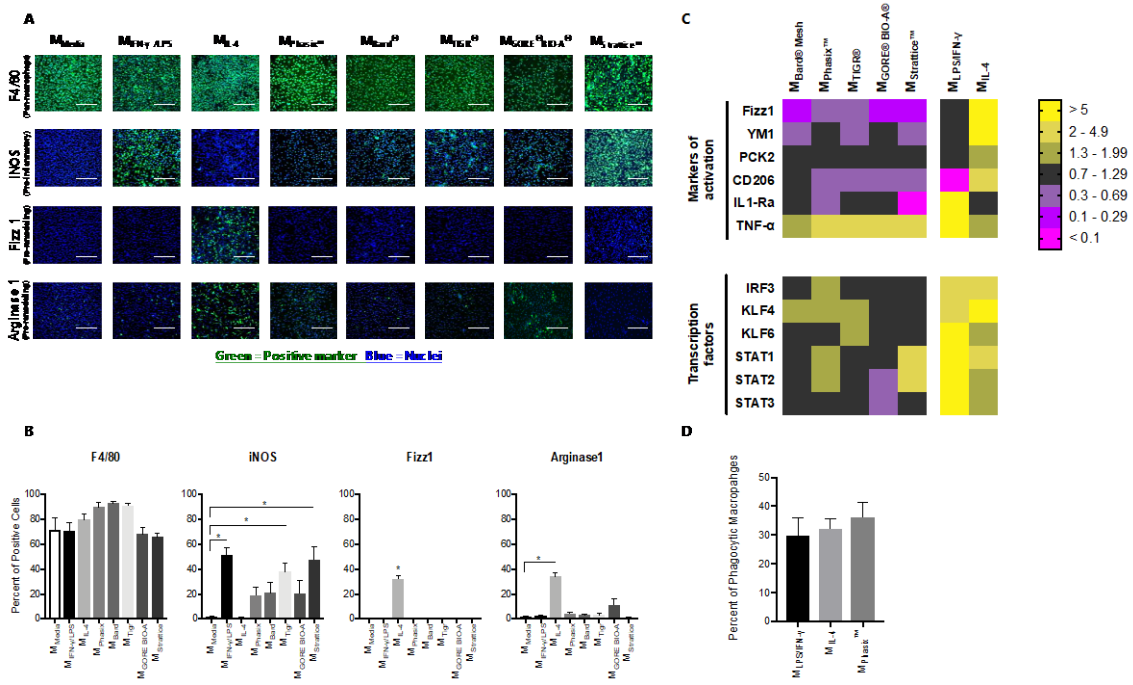

Figure 4. *In vitro* macrophage response to degradation byproducts of surgical meshes.

Primary murine BMDM were exposed to 1.32 mg/ml degradation products of Phasix™, TIGR®, GORE® BIO-A®, or Strattice™ for 24 hours. A. Activation of markers associated with pro-inflammatory (iNOS) and anti- inflammatory (Fizz1 and Arginase1) phenotypes was evaluated by immunolabeling. A general marker of macrophages (F480), was used. Known factors that are promoters of pro-inflammatory (100 ng/ml LPS and 20 ng/ml IFN- γ) or anti-inflammatory (20 ng/ml IL-4) phenotypes were included as controls. Scale bar 200 µm. B. Quantification of the response of treated macrophages in A. Images were quantified using Cell Profiler image analysis software. Values: Mean ± SEM, biologic replicates (N)=3, technical replicates=3. Differences between stimuli for each marker were evaluated using non-parametric ANOVA test, * $p<0.05$. C. Heat map of relative transcriptional activity of surface and metabolic markers, and transcription factors of macrophage activation. Data presented as fold change relative to non-treated macrophages. D. Phagocytic activity of macrophages. Values: Mean ± SEM, biologic replicates (N)=3.

2.3.4 Polymers composed of 4HB have an immunomodulatory effect upon macrophages activated with LPS and IFN-γ

When BMDM were activated with IFN-γ and LPS, followed by stimulation with the degradation products of the surgical meshes, distinctive activation patterns were seen (Figure 5). Exposure with byproducts of TIGR® and GORE® BIO-A® showed an increase in the number of cells expressing iNOS (Figure 5A). The degradation products of Phasix™ decreased the percentage of cells expressing F4/80 and increased the number of macrophages expressing Fizz1 and Arginase1, when compared with the other degradation products or the media control (Figure 5B). At the mRNA level, byproducts of Phasix™ induced the transcriptional upregulation of the surface markers Fizz1 and IL1-Ra, and the transcription factors IRF3, KLF4, and STAT3 on macrophages first activated with LPS and IFN-γ (Figure 5C). Compared to non-treated macrophages, all materials induced the expression of TNF-α in activated macrophages, as shown by the relative quantification of the mRNA and the secreted product by ELISA (Figure 5D). All byproducts of the surgical meshes also induced the secretion of IL-10 in macrophages first activated with LPS and IFN-γ as compared to non-treated macrophages.

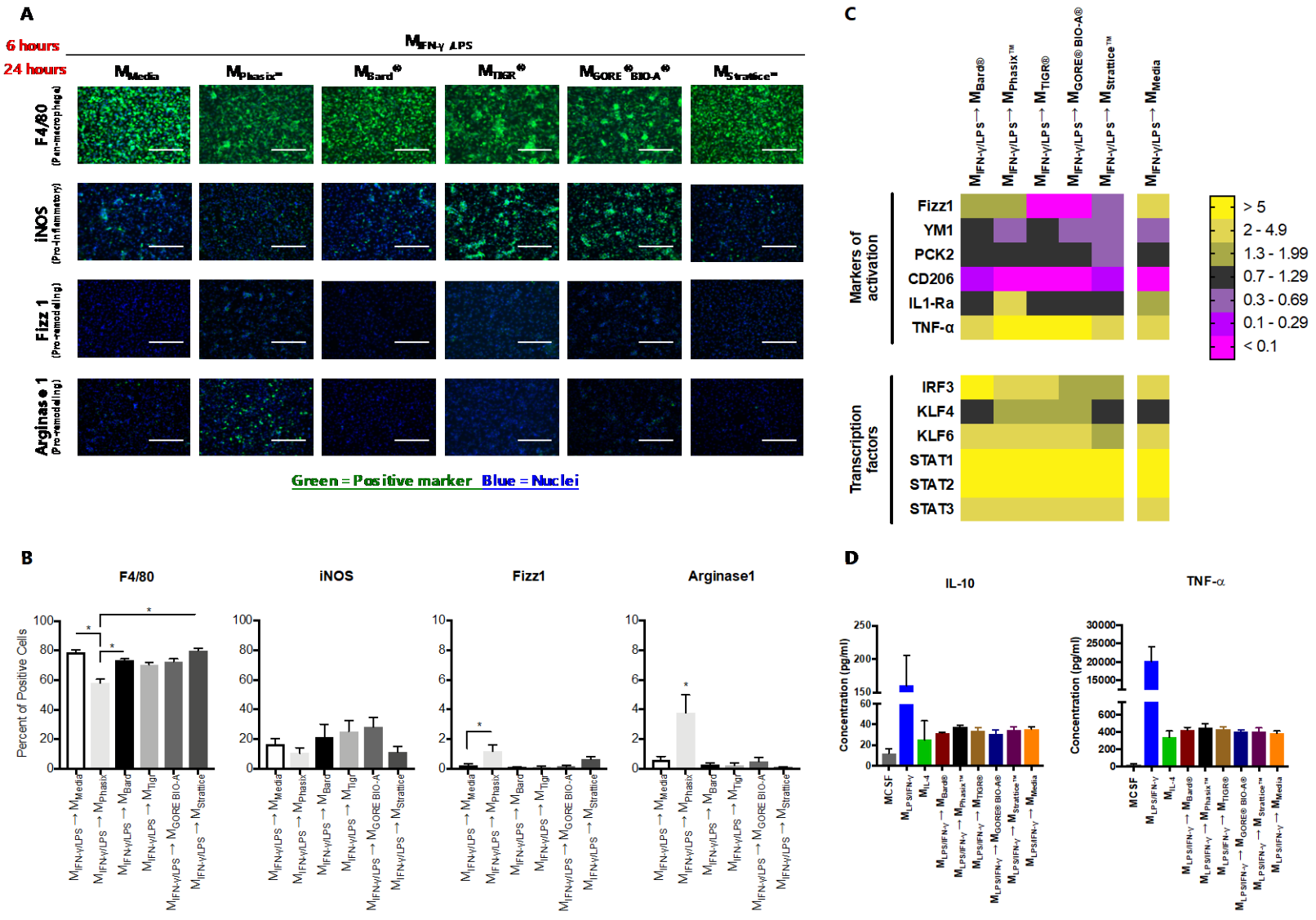

Figure 5. Effect of degradation products of mesh materials upon pro-inflammatory macrophages.

A. Degradation byproducts of P4HB have an immunomodulatory effect upon pre-activated pro-inflammatory macrophages. BMDM were challenged with 100 ng/ml LPS and 20 ng/ml IFN- γ for 6 hours to induce a pro-inflammatory phenotype, followed by exposure to 1.32 mg/ml degradation products of each of the mesh materials (Phasix™, TIGR®, GORE® BIO-A®, or Strattice™) or media alone for 24 hours. Scale bar 200 μm. B. Quantification of the response of challenged macrophages in A. Values: Mean ± SEM, biologic replicates (N)=3, technical replicates=3. Differences between stimuli for each marker were evaluated using non-parametric ANOVA test, *$p<0.05$. C. Heat map of relative transcriptional activity of surface and metabolic markers, and transcription factors of macrophage changes after LPS/IFN-γ activation and followed by stimulation with byproducts. Data presented as fold change relative to non-treated macrophages. D. Quantification of secreted cytokines IL-10 and TNF-α. Values: Mean ± SEM, biologic replicates (N)=3, technical replicates=2.

2.4 DISCUSSION

The present study evaluated the *in vitro* phenotypic pattern of murine bone marrow-derived macrophages stimulated with the degradation product of Phasix™ surgical mesh, 4HB. The macrophage phenotype induced by 4HB was compared with the activation profile induced by byproducts of other synthetic and biologic surgical meshes. The results showed a distinct activation of macrophages induced by each of the byproducts. Additional evaluation of the immunomodulatory activity of 4HB upon macrophages first activated with LPS and IFN-γ ($M_{LPS/IFN-\gamma}$) showed the ability of this SCFA to modulate the upregulation of a series of transcription factors and surface markers, modifying the LPS /IFN-γ-induced response.

The host response to biomaterials is initiated immediately after contact of the material with the host tissue. It has been well recognized that the initial cell-biomaterial interactions trigger specific molecular events of the host response, which ultimately drive downstream outcomes [23,

84, 85]. A number of cell types, from the innate and adaptive immune systems, are involved in these early events [86]. Of the many cell types involved, macrophages have received attention due to their functional plasticity and their important roles in regulating the inflammatory response and the tissue repair process following injury [87].

Macrophage plasticity moves along a broad spectrum of functional subtypes within the classically activated M1-like and the alternatively activated M2-like phenotypes [67, 87]. The plasticity of macrophages is modulated by the tissue microenvironment (i.e., tissue damage, cytokine/chemokine release, pathogens, etc.). The diverse phenotypes of macrophages are acquired by particular gene expression profiles and metabolic and functional characteristics that allow the cells to rapidly respond to the tissue's needs and perform specific functions. The present study evaluated a group of surface markers, secreted molecules, and transcription factors commonly associated with LPS/IFN-γ-induced (iNOS, TNF-α, IRF3, STAT3) or IL-4-induced (Arginase 1, Fizz1, YM1, CD206, PCK2, IL1-Ra, KLF4, IL-10) responses by either providing a positive feedback and therefore accentuating a particular function or initiating a negative response that modifies the original phenotype.

Inherent biomaterial-related factors such as the composition and the degradation products, are critical factors defining the patterns of macrophage activation. The present study used degradation byproducts of surgical meshes from different sources (synthetic, biosynthetic, and biologic) and compositions (4HB, TMC, glycolic acid, lactic acid, pepsin-digested ECM), therefore a distinct pattern of activation was expected.

The mechanisms involved in the 4HB-cell interaction and uptake are not fully understood, but they most likely involve the activation of specific G-protein coupled receptors (GPCR) and sodium-coupled membrane transporters, which are commonly used by other SCFA [88-92].

Acetate, butyrate, and propionate have been identified as endogenous ligands for the receptors GPR41, GPR43, and GPR109a, in epithelial cells, adipocytes, peripheral blood mononuclear cells, among others [93, 94], with a variety of functions that include tumor suppression [90] and regulation of energy metabolism [95]. More importantly, it has been shown that downstream events triggered by these receptors and transporters, are associated with modulation of pro-inflammatory responses [92, 96, 97], more likely through an inhibitory feedback following exposure to pro-inflammatory cytokines such as TNF-α and IL-1β [96].

The present study showed that macrophages activated with LPS and IFN-γ and then stimulated with 4HB induced a distinct pattern of expression characterized by the upregulation of important markers associated with the anti-inflammatory phenotype (Fizz1, Arginase 1, and IL1-Ra), as well as transcriptional upregulation of the transcription factor KLF4, all of which suggest an immunomodulatory effect of this 4HB upon macrophages. Stimulated macrophages were also shown to upregulate the expression of TNF-α, and the transcription factors IRF3 and STAT3. It has been suggested that after stimuli of cells with SCFA, there is a tight regulation of both pro- and anti-inflammatory responses that allow the release of ROS, but also that modulate their activation state through the activation of a negative feedback mediated by the GPCR receptors [93]. Which in turn might explain the pattern of macrophage phenotype being expressed after 4HB induction, and the associated antimicrobial activity being described in pre-clinical and clinical studies.

Although the surgical mesh material composed of polypropylene (Bard®) mesh is non-degradable, the macrophage response observed (*F4/80*$^{+high}$, *iNOS*$^{+low}$, *Fizz1*$^{-}$ *Arg*$^{-}$) and the upregulation of TNF-α and IRF4, could be produced by the presence of surfactants and detergents used during the manufacturing process.

The presence of TMC, glycolic acid and lactic acid could impact both metabolic and functional activities of exposed macrophages. Indeed, it has been shown that TMC degradation requires the release of ROS and hydrolytic enzymes to mediate its conversion into 1,3-propanediol and carbon dioxide [98, 99]; therefore, signaling pathways leading to the release of superoxide anion radicals is guaranteed to perform this function. In addition, both lactic acid and glycolic acid are endogenous intermediaries of cell pathways. In particular, lactic acid is usually increased as a consequence of metabolic reprogramming of tumor cells during the Warburg effect [100], or as a pro-inflammatory response to LPS-stimuli where the macrophages activate the glycolytic pathway. An increase in the extracellular concentration of lactic acid is sensed by macrophages through membrane receptors, which include the GPR132, and activates a signaling cascade able to abrogate the LPS-induced macrophage response. This signaling cascade acts as negative feedback to inhibit the perpetuation of the glycolytic pathway and contribute to an anti-inflammatory phenotype [101, 102] through the activation of signaling cascades mediated by the hypoxia-inducible factor 1α (HIF-1α) and the expression of Arginase 1 [102, 103].

The combined action of all three molecules (TMC, glycolic acid, and lactic acid) in the case of TIGR®, or TMC and glycolic acid in the case of GORE® BIO-A®, guarantees an increased complexity of the macrophage response. In the present study, none of the markers associated with an anti-inflammatory phenotype (Fizz1, YM1, Arginase 1, CD206, or IL1-Ra) were significantly increased after stimulation with these combined molecules. However, degradation byproducts of both TIGR® and GORE® BIO-A® induced the transcriptional activation of KLF4, which may have a downstream effect upon expression of other anti-inflammatory markers.

Finally, the use of pepsin-digested dermal ECM (Strattice™) upon the macrophages resulted in a downregulation of most of the evaluated genes/markers, with the exception of iNOS.

Previous studies have shown similar activation patterns of macrophages treated with solubilized products of dermal ECM [74]. The increased iNOS expression is not seen following treatment with ECM derived from other source tissues and therefore may be specific to the dermal tissue source. Differences in decellularization methods may be also involved in the macrophage response [14, 104].

There are several limitations to the present study. Although the markers of macrophage activation and gene expression profile provided a good source of information to determine similarities and differences between macrophages exposed to each of the byproducts of surgical meshes, inclusion of additional phenotypic and functional markers are required. The activation of transcriptionally upregulated factors, as well as their secondary products, should be investigated. Additionally, the macrophage response across different species have been shown to present variability in specific markers. For example, human macrophages exposed to IL-4 do not show increased Arginase 1 activity [105]. Therefore, future studies should investigate whether the byproducts of the surgical materials included in the present study induce similar responses in human macrophages.

2.5 CONCLUSION

Results of the present study show the ability of 4HB to modify the macrophage phenotypic response. In summary, 4HB promoted a macrophage phenotype that is distinct from classically (M1-like) and alternatively (M2-like) activated macrophages, and from the responses induced by other degradation byproducts of synthetic and biologic surgical meshes. 4HB promotes the activation of a series of transcription factors and cytokines able to modulate the macrophage

response. The findings of this study are consistent with the premise that macrophages have a remarkable functional plasticity that can be modulated by the specific molecules present within the microenvironment. The findings of this study help in understanding the factors that influence the patterns of macrophage activation and the molecular interactions of mesh materials with cells. This understanding could guide the design of meshes tailored to promote immunomodulation.

3.0 IDENTIFICATION OF THE MECHANISMS RESPONSIBLE FOR THE ANTIMICROBIAL ACTIVITY ASSOCIATED WITH THE BIOSYNTHETIC MATERIAL COMPOSED OF P4HB

3.1 INTRODUCTION

Pre-clinical studies have shown the ability of biosynthetic materials composed of P4HB to resist persistent bacterial contamination [4]. Likewise, clinical reports of hernia repair procedures using the Phasix™ surgical mesh have shown a decrease in the incidence of post-operative surgical site infections (SSI) [5-7]. The mechanisms associated with the ability of polymers of 4HB to resist bacterial contamination are, however, unknown.

Previous reports have identified the ability of other SCFA, such as butyrate and 4-phenylbutyrate, to induce upregulation of AMP through at least one of two different mechanisms: 1) entering into the nuclei and effecting as HDAC inhibitors [106-108] and therefore promoting gene expression, or 2) through signaling-transduction mechanisms mediated by MAP kinases [60, 108, 109].

The present study investigates the specific mechanisms involved in the antibacterial activity induced by polymers of 4HB. The expression of AMP in macrophages exposed to 4HB is evaluated and compared with the level induced by byproducts of other synthetic and biologic

surgical meshes. The molecular mechanisms regulating the expression of the AMP cathelicidin LL-37 in murine bone marrow-derived macrophages exposed to 4HB are investigated.

Other hydroxylated derivatives of butyrate, namely 2-hydroxybutyrate (2HB) and 3-hydroxybutyrate (3HB), are endogenous metabolites in different tissues [47, 110-112], but their ability to promote the secretion of AMP remains unknown. The potential of these hydroxylated derivatives of butyrate to control bacterial infections through promotion of endogenous upregulation of AMP is determined herein.

3.2 MATERIALS AND METHODS

3.2.1 Overview of experimental design

Four major aims were approached with the present study:

1. To determine whether the antimicrobial activity induced by 4HB was due to a direct or an indirect (cell mediated) effect, colonies of *Staphylococcus aureus* were directly exposed to the byproduct of Phasix™, 4HB, or to conditioned media produced by macrophages stimulated with 4HB for 24 hours. Growth of exposed bacteria was measured after 18 hours (Figure 6A).

2. To compare the level of expression of AMP by macrophages exposed to byproducts of different surgical mesh materials (Table 1) and hydroxylated derivatives of butyrate. Transcriptional activation of the AMP cathelicidin LL-37, and β-defensins 2, 3, and 4 was evaluated by qPCR. The number of cells expressing cathelicidin LL-37 was compared by immunolabeling (Figure 6B).

3. To determine the ability of hydroxylated derivatives of butyrate to inhibit HDAC activity in exposed macrophages. A dose response curve of HDAC activity was established for each SCFA, and the acetylation of histone 3 was evaluated by Western blot (Figure 6C).

4. To determine the transduction mechanism involved in the expression of cathelicidin LL-37 induced by 4HB in stimulated macrophages. Specific inhibitors of potential surface receptors, protein kinases, and transcription factors were used to evaluate the effects of their inhibition in the transcriptional activation of the *Cramp* gene (Figure 6D).

3.2.2 Antimicrobial activity

3.2.2.1 Preparation of bacterial inoculum

As previously described by [113], *Staphylococcus aureus* (American Type Culture Collection 29213, wound isolate) was grown in suspension overnight in a 37°C shaker. Bacteria were then diluted to $5x10^5$ CFU/ml, and 150 µl of bacterial suspension were added to each well of a 96-well microplate.

3.2.2.2 Direct antimicrobial activity

To determine the direct antimicrobial activity 1.32 mg/ml of 4HB or the vehicle control were directly mixed with the bacterial suspension. The plate was incubated at 37°C. Absorbance values were measured every hour, over a period of 24 hours, at 570 nm with a BioRad 680 Microplate Reader.

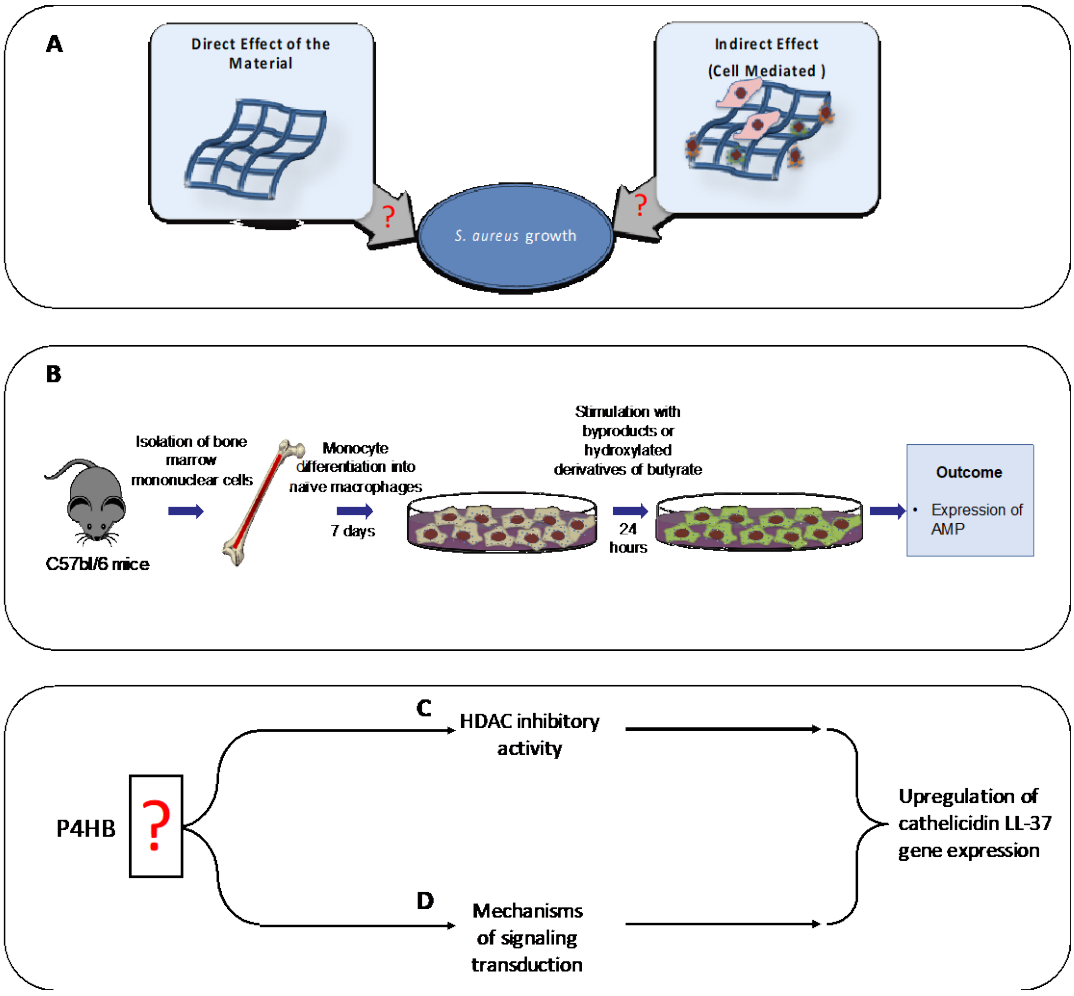

Figure 6. Experimental design overview – Mechanisms of antimicrobial activity.

A. Direct vs. indirect (cell mediated) antimicrobial effect of biosynthetic materials composed of P4HB. B. Evaluation of AMP induced by murine bone marrow-derived macrophages stimulated with byproducts of degradation of biosynthetic, synthetic, and biologic surgical scaffolds, or with hydroxylated derivatives of butyrate. C. Evaluation of inhibition of HDAC activity in macrophages exposed to byproducts of P4HB. D. Evaluation of potential membrane receptors, protein kinases, and transcription factors involved in the upregulation of the *Cramp* gene.

3.2.2.3 Indirect (macrophage-mediated) antimicrobial activity

To evaluate the indirect antimicrobial activity of 4HB, naïve macrophages were stimulated for 24 hours with 1.32 mg/ml 4HB or the vehicle control using serum-free and antibiotic-free media. The produced conditioned media was used to evaluate bacterial growth over a course of 24 hours at 37°C. Absorbance values were determined every hour at 570 nm with a BioRad 680 Microplate Reader.

3.2.3 Effects of butyrate and hydroxylated derivatives of butyrate upon murine BMDM

3.2.3.1 Monomers

Sodium butyrate (Sigma, Cat. No. B5887), butyric acid (Sigma, Cat. No. B103500), sodium 2-hydroxybutyrate (Na-2HB) (Sigma, Cat. No. 220116), 2-Hydroxybutanoic acid (Acid-2HB) (Sigma, Cat. No. CDS000492), sodium 3-hydroxybutyrate (Na-3HB) (Sigma, 54965), 3-hydroxybutyric acid (Acid-3HB) (Sigma, Cat. No. 166898), and sodium 4-hydroxybutyrate (Na-4HB) (Sigma, G-001) were used in the present study (Figure 7). The methanol containing the Na-4HB was evaporated and the SCFA was solubilized in sterile type I water.

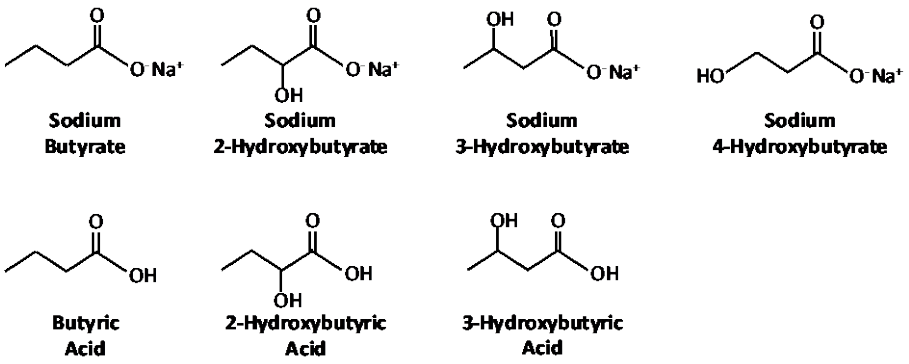

Figure 7. Chemical structure of butyrate and hydroxylated derivatives.

Butyrate and the isomers 2-hydroxybutyrate (2HB), 3-hydroxybutyrate (3HB), and 4-hydroxybutyrate (4HB) were evaluated as sodium salts or as acidic compounds.

3.2.3.2 Stimulation of BMDM with butyrate or its hydroxylated derivatives

Naïve macrophages were isolated from bone marrow and differentiated as described in section 2.2.4. Macrophages were stimulated with a series of increasing concentrations (as specified for each experiment) of the acid or sodium salt forms of butyrate or its hydroxylated derivatives (2HB, 3HB, and 4HB) for 24 hours at 37°C, 5% CO_2.

3.2.3.3 Macrophage metabolism and cell viability

Metabolism and viability of stimulated macrophages were measured using the MTT assay (Vibrant® MTT Cell Proliferation Assay Kit, V-13154, Molecular Probes) following the manufacturer instructions. Briefly, $1*10^5$ bone marrow-derived monocytes were plated and differentiated into macrophages as described in section 2.2.4. Each of the SCFA were evaluated at 0.05 mM, 0.1 mM, 0.25 mM, 0.5 mM, 1 mM, 2 mM, 4 mM, 12 mM, 24 mM, 48 mM, and 96 mM for 24 hours at 37°C, 5% CO_2. After stimulation, macrophages were washed with PBS and incubated with 100 µl of serum-free and antibiotic-free media containing 1.2 mM MTT (3-(4,5-dimethythiazol-2-yl)-2,5-diphenyltetrazolium bromide) solution for 2 hours. After the incubation period, 75 µl of media was removed from the each well and the formazan produced by reduction of the MTT was diluted with 50 µl of dimethyl sulfoxide (DMSO). Following an incubation of 10 minutes at 37°C, the concentration of formazan was determined by optical density at 540 nm. The metabolic activity of macrophages was calculated from a standard curve. Results were presented relative to untreated (media only) macrophages. Concentrations that decreased metabolic activity by more than 50% were considered cytotoxic.

3.2.4 Expression of cathelicidin LL-37 in MBMDM

The expression of cathelicidin LL-37 was evaluated by immunolabeling. Macrophages were stimulated with byproducts of the surgical mesh materials (Phasix™, Bard®Mesh, TIGR®, GORE®BIO-A®, or Strattice™), or non-cytotoxic concentrations of acid or sodium salt forms of butyrate or its hydroxylated derivatives (2HB, 3HB, and 4HB) for 24 hours. Treated macrophages were fixed in 2% paraformaldehyde for 30 minutes, followed by washes with PBS. Fixed cells were then incubated for 1 hour with blocking buffer (4%v/v horse serum, 2%w/v bovine serum albumin, 0.1%v/v triton X-100, and 0.1%v/v tween-20 in PBS) to inhibit non-specific binding of antibodies. After blocking, macrophages were incubated with the primary rabbit polyclonal antibody cathelicidin LL-37 (Abbiotec, Cat. No. 253814) at 1:100 dilution at 4°C overnight. After washing in PBS, the macrophages were incubated with fluorophore-conjugated the secondary antibody goat anti-rabbit 488 (Invitrogen, Cat. No. A11034) at 1:200 dilution for 1 hour at room temperature. After washing again with PBS, nuclei were counterstained with 4'-6-diamidino-2-phenylindole (DAPI) prior to imaging. Images of three 20X fields were taken for each well using a live-cell microscope.

3.2.5 Gene expression of antimicrobial peptides

To determine the transcriptional activation of the AMP cathelicidin LL-37, and the β-defensins 2, 3, and 4 (Appendix B), macrophages were treated with byproducts of the surgical mesh materials (Phasix™, Bard®Mesh, TIGR®, GORE®BIO-A®, or Strattice™), non-cytotoxic concentrations of sodium butyrate, or its hydroxylated derivatives (Na-2HB, Na-3HB, and Na-4HB) for 24 hours. The RNA isolation and qPCR were performed according to the protocol described in section 2.2.7.

The levels of expression were normalized with the housekeeping gene *hprt1*. Results were expressed as relative fold change log ($2^{-\Delta\Delta Ct}$) relative to non-treated macrophages.

3.2.6 HDAC inhibitory activity

3.2.6.1 Total protein isolation

Macrophages were harvested using a cell scraper and collected. After centrifugation at 3500 g for 5 min at 4°C, supernatants were removed and the cells were washed twice with 1000 µl phosphate buffered saline (PBS). The cells were then lysed with lysis buffer [150 mM NaCl, 50 mM Tris pH 8.0, 1%v/v Triton X-100, 0.5%v/v sodium deoxycholate (SDC), 0.1%v/v sodium dodecyl sulfate (SDS) and protease and phosphatase inhibitor cocktail (Thermo Fisher Scientific, Cat No. PIA32961)], incubating on ice for 1 hour, and vortexing for 30 seconds every 10 minutes. After incubation, the lysis solution was centrifuged at 14000 g for 15 minutes, and the supernatant containing the proteins was transferred to a new tube. The concentration of protein was quantified using the Pierce™ BCA Protein Assay Kit (Thermo Fisher Scientific, Cat No. 23225), following manufacturer's instructions.

3.2.6.2 HDAC activity

The Amplite™ Fluorimetric HDAC activity Assay kit *Green Fluorescence* (AAT Bioquest, Cat No. NC1484042) was used following the manufacturer's instructions to evaluate whether the hydroxylated derivatives of butyrate have an inhibitory effect on HDAC activity. Briefly, 5 ug of total protein extracts were incubated for 20 min at 37°C with increasing concentrations of each of the SCFA (0.5 mM - 96 mM). A series of increasing concentrations of sodium butyrate and 3 µM trichostatin A (TSA) were used as controls. To determine the HDAC activity, 50 µl of HDAC

Green™ Substrate working solution was added and incubated for 1 h at 37°C. Fluorescence intensity was read at Ex/Em = 490/525 nm. Percentage of HDAC inhibition was calculated relative to the non-inhibited control.

Additionally, to evaluate whether the hydroxylated derivatives of butyrate are able to directly inhibit the enzymatic activity of HDAC in naïve macrophages, cells were treated with 1 mM sodium butyrate, 4 mM of any of the hydroxylated derivatives (Na-2HB, Na-3HB, Na-4HB), or the controls 0.375 μM TSA (AAT Bioquest®, Inc) or 12.5 μM histone acetyl transferase inhibitor (HAT) (Selleckchem, Cat No. S7152) for 24 hours, followed by evaluation of the HDAC activity in the protein extracts. The results were contrasted with evaluation of the levels of acetylation of the histone H3 by western blot using the specific antibody anti-Histone H3 (acetyl K9) (Abcam, Cat No. ab61231).

3.2.7 Signaling-transduction mechanism

3.2.7.1 Transcriptional inhibition of G protein-coupled receptors (GPCR)

Hcar2 Stealth siRNA (Thermo Fisher Scientific, Cat. No. MSS234551) and SLC52A2 Stealth siRNA (Thermo Fisher Scientific, Cat. No. MSS225263) were used to inhibit the transcription of the G protein-coupled receptors GPR109a and GPR172a, respectively. These GPRs are potentially involved in the signaling cascade upregulating cathelicidin LL-37 induced by 4HB in macrophages. Liposomes (Lipofectamine™ RNAiMAX, Thermo Fisher Scientific, Cat. No. 13778030) containing the siRNA or the control (Stealth RNAi™ siRNA Negative Control Lo GC, Thermo Fisher Scientific, Cat. No. 12935-200) were prepared in Opti-MEM™ I Reduced Serum Medium (Thermo Fisher Scientific, Cat. No. 11058021) and used to transfect primary murine bone marrow-derived macrophages for 24 hours. After this period of time, cells were exposed to 1.32

mg/ml of byproducts of P4HB or the vehicle control for other 24 hours. Gene expression was used to evaluate changes in the level of cathelicidin LL-37.

3.2.7.2 Inhibition of MAP kinases and transcription factors

To determine whether the MAP kinases c-Jun N-terminal kinase (JNK), p38 and the Mitogen-activated protein kinase kinase (MEK-1,2) are involved in the activation of cathelicidin LL-37, the specific inhibitors SP600125, SB203580, and U0126, targeting each of these proteins, were used at a working concentration of 10 μM to pretreat naïve macrophages for 1 hour, before stimulating them with degradation byproducts of P4HB for 24 hours. Likewise, specific inhibitors for the transcription factors the activator protein 1 (AP-1), 10 μM SR11302, the signal transducer and activator of transcription 3 (STAT3), 20 μM STA-21, and the hypoxia inducible factor 1α (HIF-1α), 0.7 μM HIF-1α inhibitor, were used to pretreat macrophages and determine the complex(es) involved in the upregulation of this AMP induced by 4HB. Gene expression and specific immunolabeling against cathelicidin LL-37 were used to determine the effects of the inhibition upon the production of this AMP.

3.2.7.3 Evaluation of the NF-κB activity induced by 4HB

To determine the role of the nuclear factor-κB (NF-κB) in the 4HB-mediated transcriptional activation of cathelicidin LL-37, a specific inhibitor (100 μM ursolic acid) was used to pre-treat the naïve macrophages for 6 hours followed by stimulation with 4HB for 24 hours. Changes in the level of cathelicidin LL-37 expression were evaluated by immunolabeling.

3.2.8 Statistical analysis

Three independent experiments were conducted. Data is presented as the mean ± standard error of the mean (SEM). Statistical differences were determined using a non-parametric ANOVA test (Kruskal-Wallis test). Differences were compared with post-hoc Dunn's test relative to non-treated macrophages *in vitro*. The fold change gene expression relative to non-treated macrophages was analyzed using the BoostRatio Web Application for the ratio between the treatments and the control [114]. A value $p<0.05$ was considered statistically significant. Statistical analysis was performed using GraphPad Prism version 6.07 (GraphPad Software, La Jolla CA, USA).

3.3 RESULTS

3.3.1 P4HB induces an indirect (cell mediated) antimicrobial activity

Direct exposure of *S. aureus* to degradation byproducts of Phasix™ did not decrease the bacterial growth when compared with bacteria exposed to vehicle control (Figure 8A). Exposure of *S. aureus* to the conditioned media of macrophages stimulated with the byproducts of Phasix™ resulted in a 30% decrease in the bacterial growth as compared the conditioned media of macrophages stimulated with the vehicle control ($p=0.029$) (Figure 8B), suggesting an indirect antimicrobial effect of 4HB.

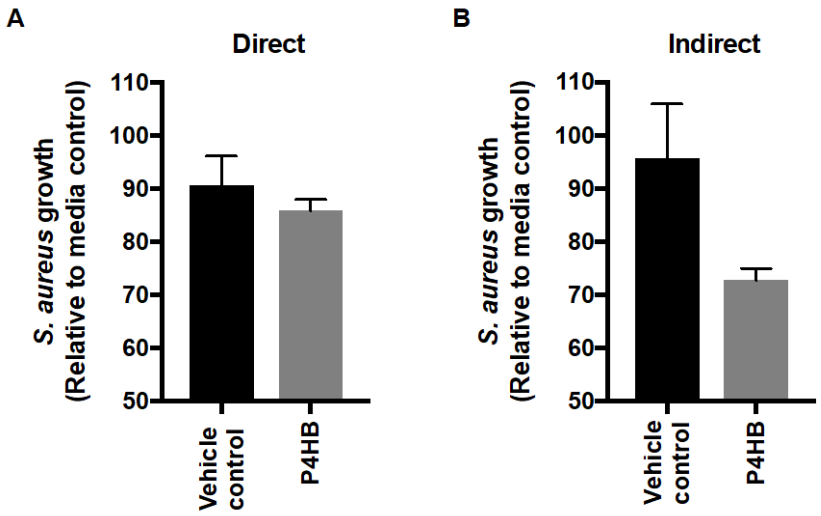

Figure 8. Direct vs. indirect antimicrobial activity.

A. Direct antimicrobial activity assay. *S. aureus* growth in the presence of degradation byproducts of Phasix™ (4HB) or vehicle control. B. Indirect antimicrobial activity assay. *S. aureus* growth in the presence of conditioned media from macrophages exposed to degradation byproducts of Phasix™ or vehicle control. Value: Mean ±standard deviation (SD), biologic replicates (N)=3, technical replicates=3.

3.3.2 P4HB induces a distinctive expression of cathelicidin LL-37

The ability of degradation byproducts of different surgical meshes (Phasix™, Bard®Mesh, TIGR®, GORE® BIO-A®, and Strattice™) to induce the secretion of the AMP cathelicidin LL-37 in stimulated macrophages was evaluated (Figure 9A). Stimulation with the byproduct of Phasix™, 4HB, significantly induced the expression of cathelicidin LL-37 when compared with non-treated macrophages (Figure 9B). Moreover, the mechanism involved in the increased expression of this AMP is through the upregulation of the *Cramp* gene, which codes for cathelicidin LL-37 (Figure 9C). Byproducts of Phasix™ and byproducts of Strattice™ induced also the transcriptional upregulation of the β-defensins 3 and 4 (Figure 9D & E).

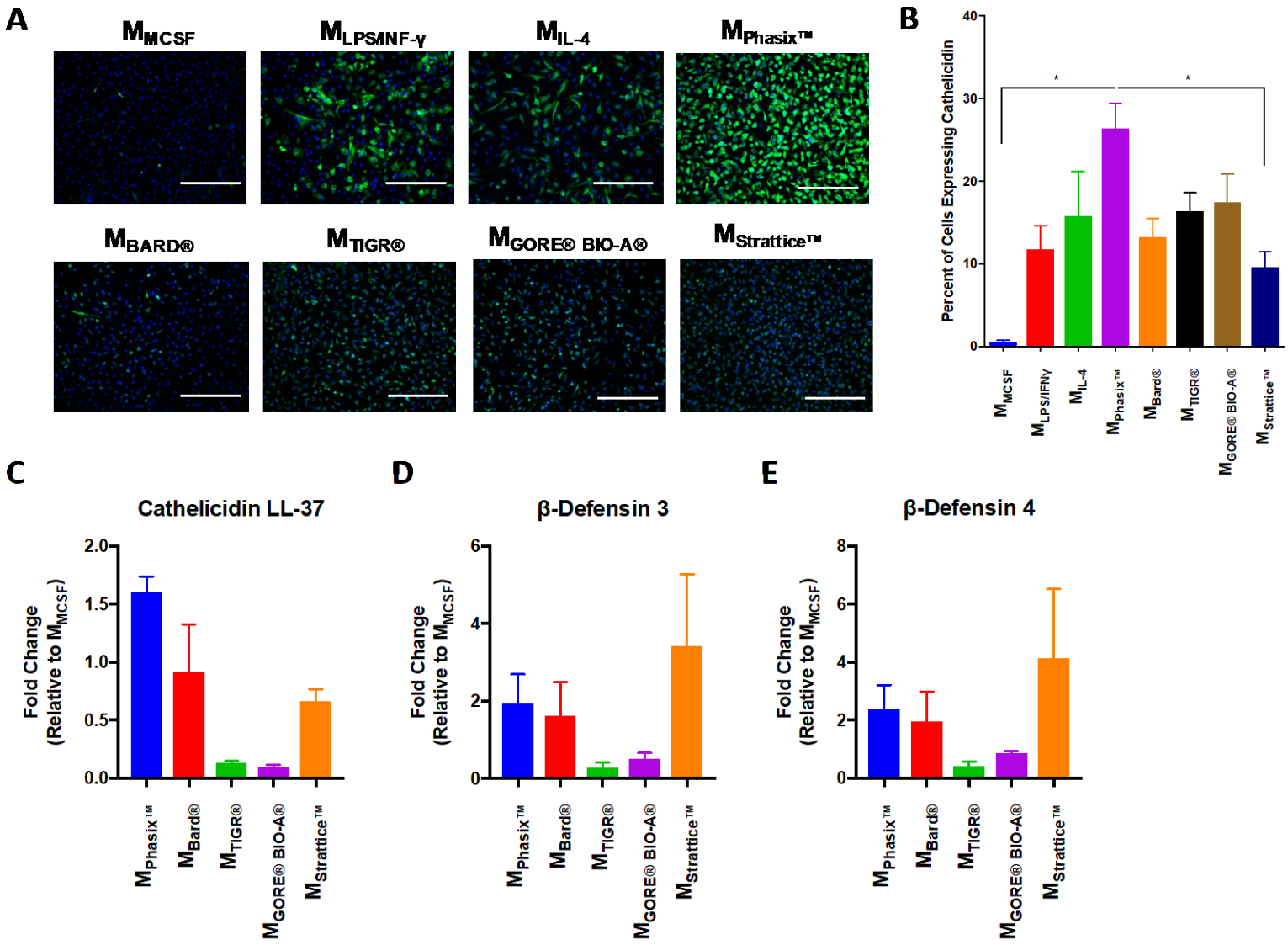

Figure 9. ***In vitro*** **expression of antimicrobial peptides induced by byproducts of surgical meshes.**

Primary murine BMDM were exposed to 1.32 mg/ml degradation products of Phasix™, TIGR®, GORE® BIO-A®, or Strattice™ for 24 hours. A. Activation of cathelicidin LL-37. Known factors that are promoters of pro-inflammatory (100 ng/ml LPS and 20 ng/ml IFN- γ) or anti-inflammatory (20 ng/ml IL-4) phenotypes were included as controls. Scale bar 200 μm. B. Quantification of the response of treated macrophages in A. Images were quantified using Cell Profiler image analysis software. Values: Mean ± SEM, biologic replicates (N)=3, technical replicates=3. Differences between stimuli for each marker were evaluated using non-parametric ANOVA test, * $p<0.05$. C-E. Relative transcriptional activity of cathelicidin LL-37 (C), β-defensin 3 (D), and β-defensin 3 (E). Data presented as fold change relative to non-treated macrophages. Values: Mean ± SEM, biologic replicates (N)=3, technical replicates=3.

3.3.3 Comparison of hydroxylated derivatives of butyrate

3.3.3.1 Sodium hydroxylated derivatives of butyrate are not associated with a cytotoxic effect upon murine bone marrow-derived macrophages

The macrophage metabolic activity and the cytotoxicity induced by sodium salt or acid forms of butyrate and its hydroxylated derivatives was evaluated. Exposure of murine bone marrow-derived macrophages to increasing concentrations of sodium butyrate, butyric acid, or the acid hydroxylated derivatives (acid-2HB and acid-3HB) induced a reduction in the cell metabolic activity by more than 50%. Concentrations higher than 2 mM of butyrate and butyric acid, and concentrations higher than 24 mM of acid-2HB and acid-3HB were associated with a cytotoxic effect. On the other hand, the sodium hydroxylated derivatives of butyrate (Na-2HB, Na-3HB, and Na-4HB) preserved the viability of stimulated macrophages at all evaluated concentrations (Figure 10).

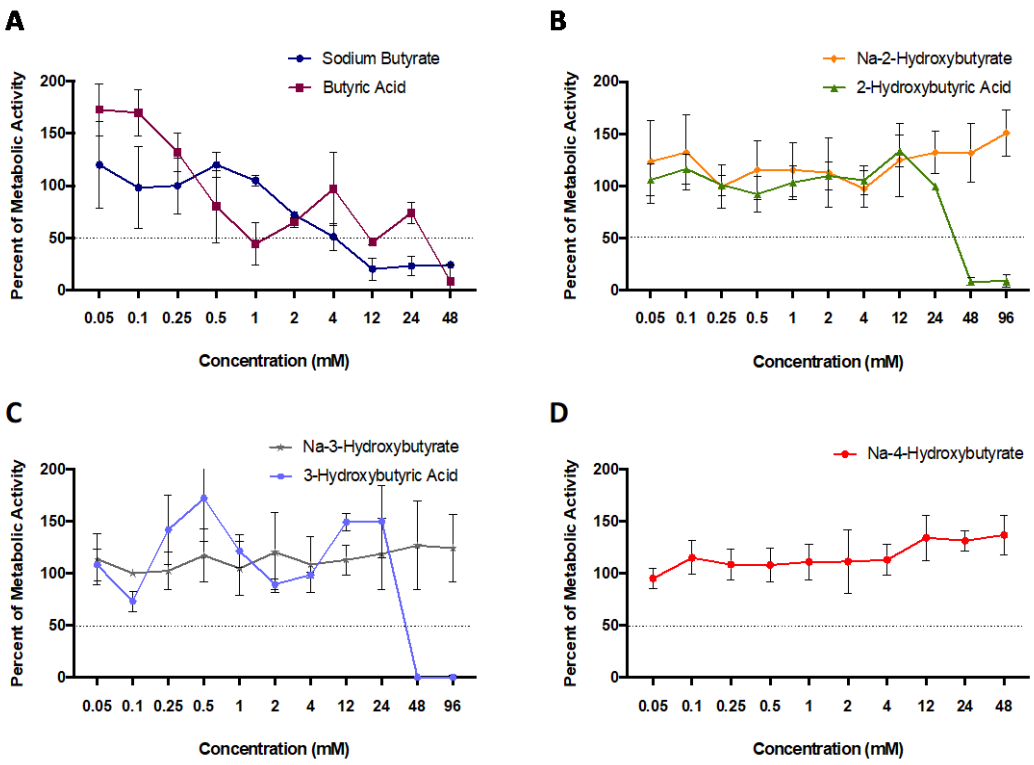

Figure 10. Dose response curves of butyrate and its hydroxylated derivatives.

A. Both sodium butyrate and butyric acid decreased the cell viability at concentrations higher than 4mM. B-D. All hydroxylated forms of butyrate in their salt forms (Na-2HB, Na-3HB, and Na-4HB) are non-cytotoxic at supra-physiologic concentrations (96 mM). Acid forms of 2HB and 3HB decreased the cell viability at concentrations higher than 24 mM. Dotted line at 50% represents the threshold of viability. Value: Mean ±SEM, biologic replicates (N)=3, technical replicates=3.

3.3.3.2 Sodium 4-hydroxybutyrate induces an increased expression of the AMP cathelicidin LL-37 in stimulated murine bone marrow-derived macrophages

The ability of hydroxybutyrate isomers to upregulate the endogenous expression of the AMP cathelicidin LL-37 in stimulated macrophages was evaluated and compared with the induction produced by sodium butyrate. All SCFA induced a distinct expression of cathelicidin LL-37 (Figure 11A). Sodium butyrate and its sodium hydroxylated derivatives (Na-2HB, Na-3HB, and

Na-4HB) induced an expression that was responsive to the dose used to stimulate the macrophages. Effective concentrations that induced significantly higher cathelicidin LL-37 expression when compared with non-treated macrophages were: between 0.5 mM to 2 mM of sodium butyrate, 2 mM of Na-2HB and Na-3HB, and between 0.5 mM to 12 mM of Na-4HB (Figure 11B). The acid counterparts of the evaluated SCFA (butyric acid, acid-2HB, and acid-3HB) were not associated with a dose response; none of the concentrations of acids induced a significantly higher expression of cathelicidin LL-37 when compared with the non-treated macrophages (Figure 11B).

3.3.3.3 Sodium 4-hydroxybutyrate induces a transcriptional activation of AMP in exposed macrophages

mRNA expression of the genes codifying for cathelicidin LL-37, β-defensin 2, β-defensin 3, and β-defensin 4, were evaluated in macrophages exposed to sodium hydroxylated derivatives of butyrate (Na-2HB, Na-3HB, and Na-4HB) and compared with non-treated macrophages. A significantly higher upregulation of the gene *Cramp* was found in macrophages treated with 2 mM Na-3HB (mean fold change: 10.62, p ratio=0.0045), and with those treated with Na-4HB at 1 mM (mean fold change: 8.14, p ratio=0.001) or 2 mM (mean fold change: 3.49, p ratio= 0.013) (Figure 12A).

Expression of β-defensin 2 was found to be modulated by sodium butyrate and Na-4HB, but not by Na-2HB and Na-3HB. The highest upregulation level was induced by 4 mM Na-4HB (mean fold change: 2.73), followed by 2 mM of either sodium butyrate (mean fold change: 2.34) or Na-4HB (mean fold change: 1.85) (Figure 12B). β-defensin 3, however, was modulated to a lower extent. Only Na-4HB at 2 mM and 4 mM induced an increase in fold induction (1.59 and

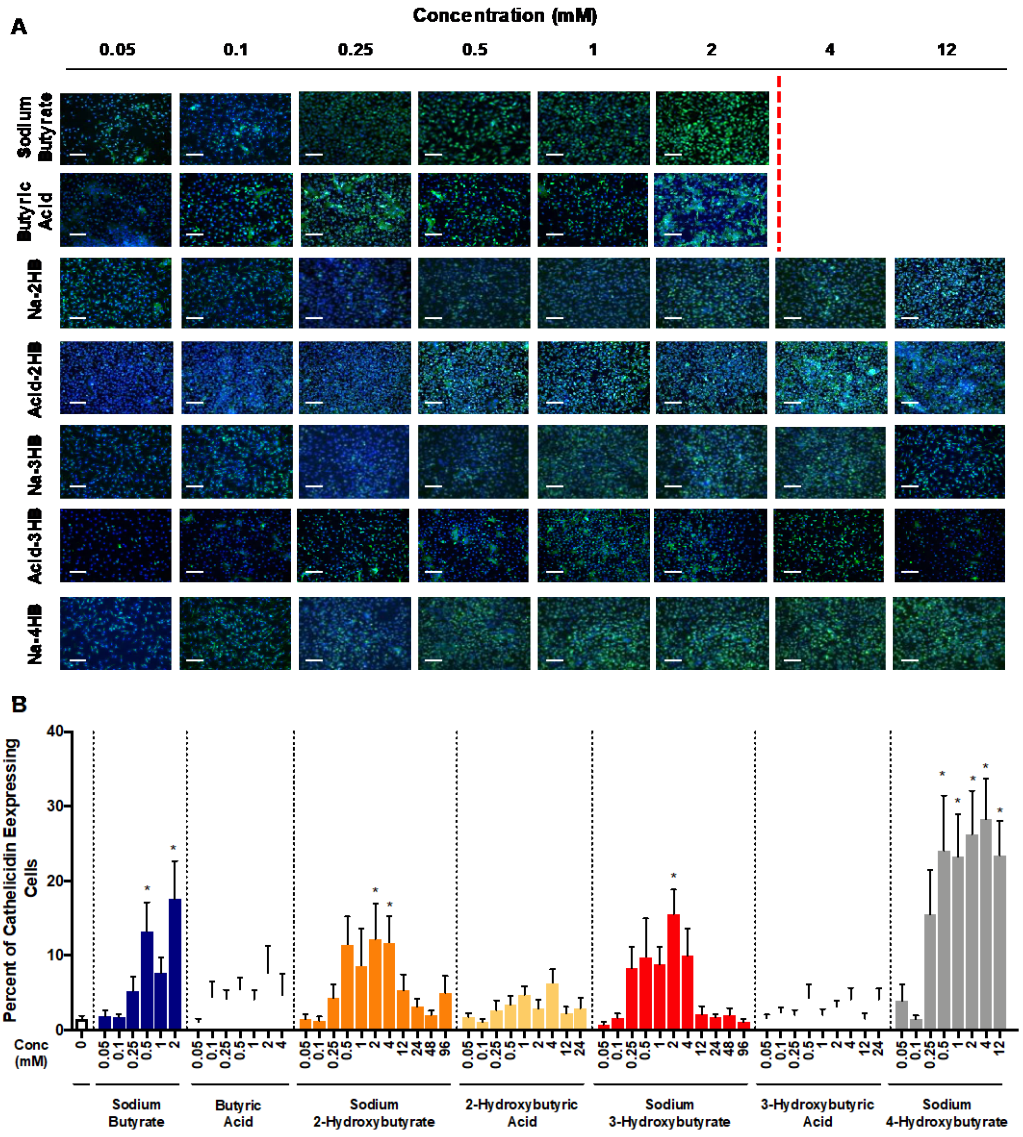

Figure 11. Expression of cathelicidin LL-37 induced by butyrate and its hydroxylated derivatives.

A. Immunofluorescence for the AMP cathelicidin LL-37. A series of increased concentrations of butyrate or its hydroxylated derivatives were used to stimulate primary murine bone marrow-derived macrophages. A dose response of expression is observed (green) for all the evaluated monomers. Biologic replicates (N)=3, technical replicates=3. Scale bar 100 μm. B. Quantification of cathelicidin LL-37 expression. Na-4HB induces the expression of cathelicidin LL-37 in amounts comparable to sodium butyrate. All hydroxylated forms have the ability to induce endogenous secretion of the AMP, with higher levels in their sodium forms than in their acid forms. Differences between concentrations for each SCFA were evaluated using non-parametric ANOVA test, *$p<0.05$ relative to non-treated macrophages. Value: Mean ±SEM, biologic replicates (N)=3, technical replicates=3.

1.62 times, respectively). None of the other sodium forms of butyrate or its hydroxylated derivatives were found to modulate the transcription of the β-defensin 3 gene (Figure 12C).

The gene codifying for β-defensin 4 was found to be upregulated by sodium butyrate and all of its hydroxylated derivatives (Figure 12D). The highest level of induction was produced by Na-4HB at both 2 mM (fold change: 2.73, p ratio=0.018) and 4 mM (fold change: 3.00, p ratio=0.024).

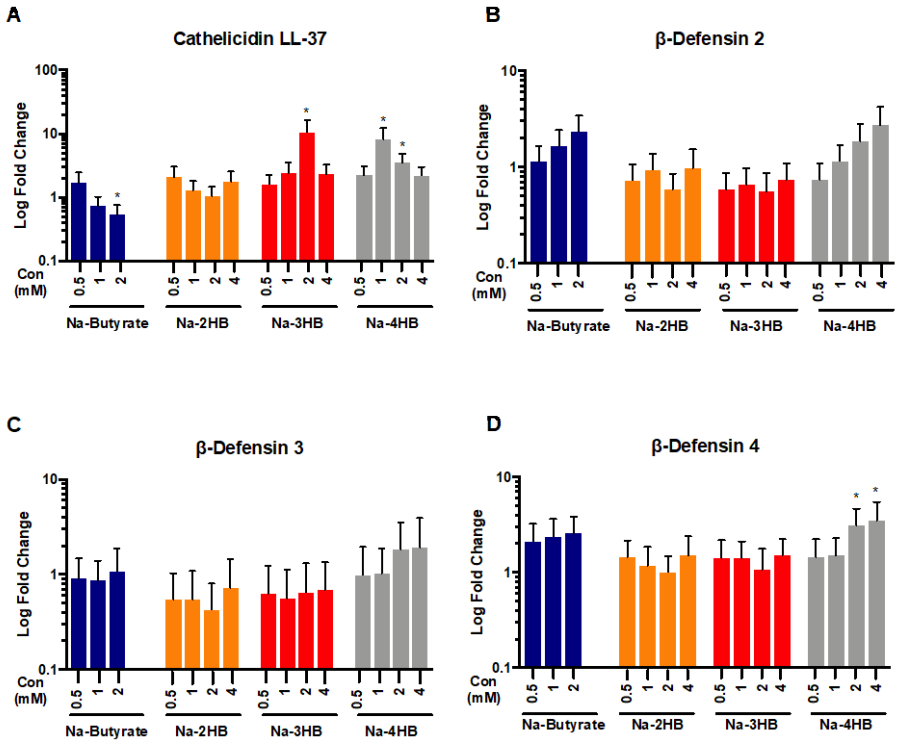

Figure 12. Gene expression of AMP induced by butyrate and its hydroxylated derivatives.

A. Na-3HB and Na-4HB induce an upregulation of the *Cramp gene* at 1 mM and 2 mM compared to non-treated macrophages. C. Expression of β-Defensin 3 is not significantly upregulated by any of the evaluated SCFA. Value: Mean ± SEM, biologic replicates (N)=3, technical replicates=3.

3.3.3.4 Sodium butyrate and its hydroxylated derivatives present a distinct HDAC inhibitory activity upon murine bone marrow-derived macrophages

The activity of sodium butyrate and its sodium hydroxylated derivatives (Na-2HB, Na-3HB, and Na-4HB) as HDAC inhibitors in primary murine bone marrow-derived macrophages was evaluated. The ability of different concentrations of these SCFA to inhibit HDAC enzymes in protein extracts was first determined. The results show a dose dependent inhibition in protein extracts incubated with sodium butyrate and Na-2HB, but not with Na-3HB or Na-4HB (Figure 13A). The half maximal inhibitory concentration (IC_{50}) was determined for sodium butyrate (3.69 ± 1.12) mM and for Na-2HB (12.51 ± 1.6) mM, using non-linear fitting regression (r^2 = 0.99 and 0.96, respectively) (GraphPad Prism).

Treatment of murine bone marrow-derived macrophages with 1 mM sodium butyrate or 4 mM of each of the sodium hydroxylated derivatives did not show an inhibition of the HDAC activity (Figure 13B). Western blot for acetyl-Histone 3, at the lysine 9 further confirmed that none of the treatments at the working concentrations had an effect upon the level of acetylation (Figure 13C), validating the results obtained with the dose response evaluation.

3.3.4 4HB induces transcriptional activation of cathelicidin LL-37 through a signaling-transduction mechanism

The signal-transduction mechanism involved in the transcriptional upregulation of the antimicrobial peptide cathelicidin LL-37 induced by the byproduct of Phasix™ (4HB) was evaluated. Transcriptional inhibition of two potential membrane receptors showed that decreasing GPR109a, but not GPR172a, reduced the 4HB-mediated cathelicidin LL-37 transcription in

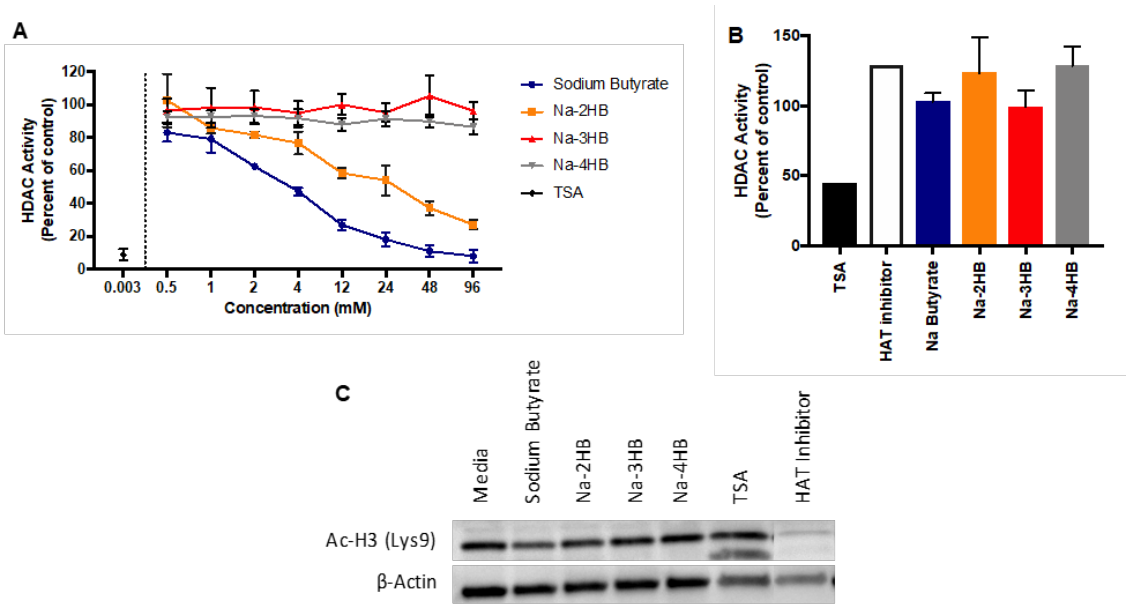

Figure 13. Differential HDAC inhibition induced by sodium butyrate and its hydroxylated derivatives.

A. HDAC activity in macrophage-derived protein extracts induced by increasing concentrations (0.5 mM to 96 mM) of sodium butyrate or each of the hydroxylated derivatives (Na-2HB, Na-3HB, and Na-4HB). 0.003 mM trichostatin A (TSA) or non-treated extracts were used as controls. HDAC activity is presented as a percent normalized to non-treated protein extracts. A dose-dependent inhibition was found in protein extracts treated with sodium butyrate (IC_{50} 3.69 ± 1.12) mM and for Na-2HB (IC_{50} 12.51 ± 1.6), but not with Na-3HB and Na-4HB. B. Murine bone marrow-derived macrophages were treated with 1mM sodium butyrate or 4mM of one of the hydroxylated derivatives (Na-2HB, Na-3HB, or Na4HB) for 24 hours. Non-treated macrophages, 0.375 μM TSA, or 12.5 μM HAT inhibitor were used as controls. HDAC activity of treated macrophages was determined and presented as a percent normalized to non-treated macrophages. At the concentrations evaluated, none of the SCFA induced an HDAC inhibitory activity. C. Representative western blot for acetyl (lys9)-histone 3, of three independent experiments.

BMDM (Figure 14A). The use of specific inhibitors targeting the MAP kinases JNK, p38, and MEK 1,2, showed that p38 and, to a lower extent, JNK are required to induce the upregulation of cathelicidin LL-37 in macrophages stimulated with the byproduct of Phasix™, 4HB, as shown in the relative mRNA quantification (Figure 14B) and the protein level (Figure 14C). A synergistic effect from the MAP kinases was additionally seen since the combined inhibition of these proteins completely abolished the expression of cathelicidin LL-37 (Figure 14C).

Results of the present study showed that besides the requirements of a 4HB cell membrane receptor and the activation of p38, the expression of cathelicidin LL-37 mediated by 4HB in macrophages requires the specific activation of NF-κB as shown in Figure 14D, and when this nuclear transcription factor becomes is inhibited, the level of cathelicidin LL-37 secretion is blocked.

In summary, the evaluation of the pattern of protein activation during a period of time of 24 hours after cell stimulation with 4HB showed an early activation by phosphorylation of p38 (with maximum activation between 1 and 3 hours), and a sequential activation of the subunit p65 of the NF-κB protein (between 3 and 9 hours, and a maximum activity at 6 hours post induction). The activation pathway is then followed by the increased level of cathelicidin LL-37 between 9 and 24 hours (Figure 14E).

The specific inhibition of the transcription factors HIF-1α, AP-1, and STAT3 showed that only blocking AP-1 decreased expression of cathelicidin LL-37 in macrophages treated with 4HB (Figure 14 F & G).

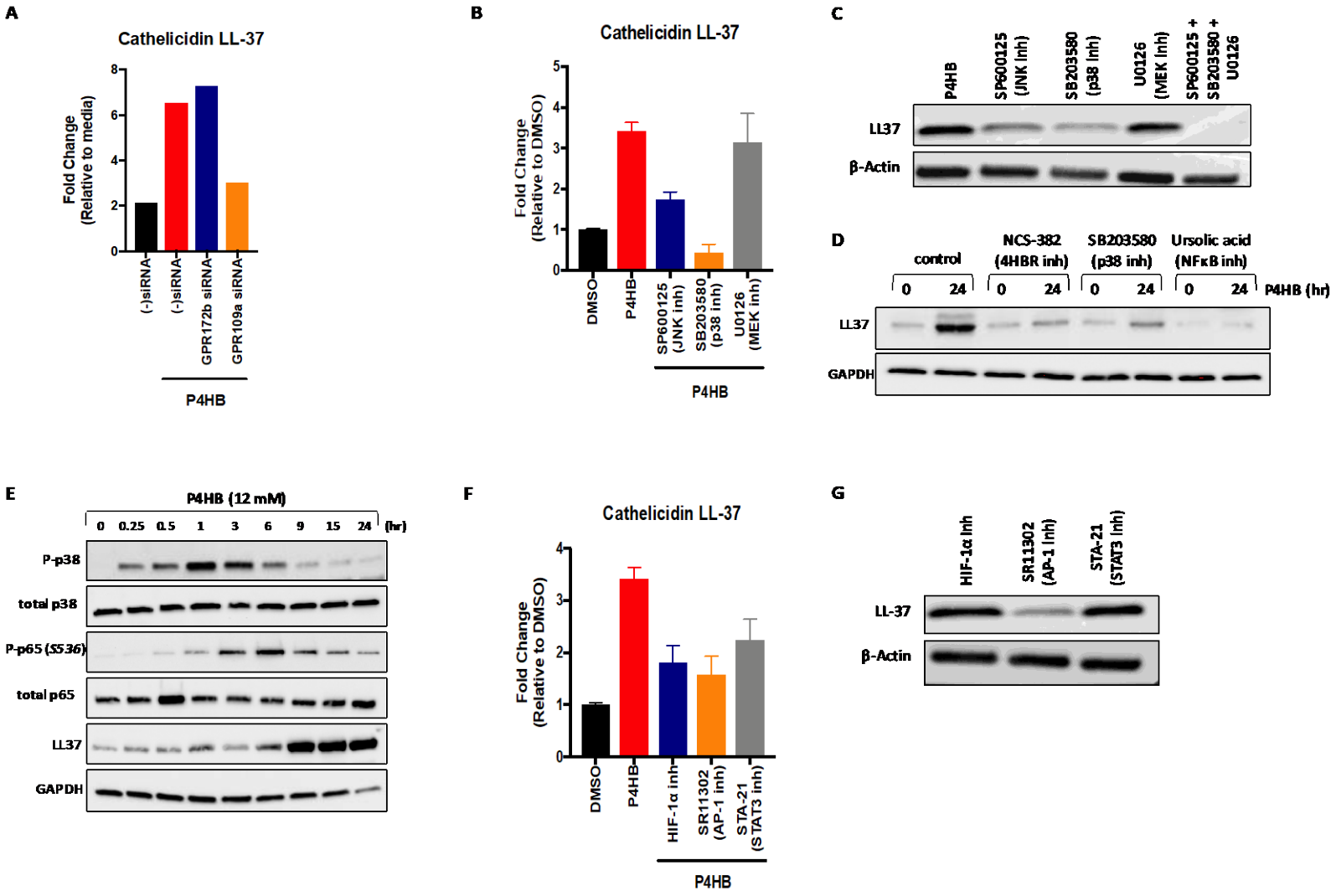

Figure 14. Signal-transduction mechanism involved in the upregulation of cathelicidin LL-37 mediated by 4HB.

A. RNA expression level of the *camp* gene codifying for cathelicidin LL-37. Specific siRNA inhibitors for GPR109a and GPR172a show association of the former in the AMP expression. B-C. Inhibitors targeting the MAP kinases p38, JNK, and MEK showed the association of these proteins with the expression of cathelicidin LL-37 mediated by 4HB. P38 and to a lower extent JNK are required for the expression of cathelicidin LL-37, by gene expression (B) and protein level (C). D. Specific inhibitors targeting 4HB receptors, p38, and NF-κB confirm the association of these molecules with the production of this AMP. E. Protein activation was evaluated over a time period of 24 hours. An earlier activation of the MAP kinase p38 (0.5 to 3 hours), was followed by activation of NF-κB (3 to 9 hours), and finally concluded in cathelicidin LL-37 expression between 9 and 24 hours. F-G. Specific inhibitors targeting the transcription factors AP-1, HIF-1α, and STA-21, suggest that only AP-1 is involved in the secretion of cathelicidin LL-37 induced by 4HB, gene expression (F) and protein level (G).

3.4 DISCUSSION

The present study evaluated the mechanisms by which 4HB promotes antibacterial activity in murine bone marrow-derived macrophages. This study showed that 4HB-mediated antimicrobial protection occurs via endogenous upregulation of AMP. The 4HB-induced expression of cathelicidin LL-37 is independent of a direct HDAC inhibitory activity of 4HB. Instead, it seems to be associated with a cell signaling mechanism that involves an activation cascade through the MAP kinases p38 and JNK, and the NF-κB pathways (Figure 15).

The present study compared the effect of sodium butyrate and its hydroxylated derivatives (Na-2HB, Na-3HB, and Na-4HB) upon HDAC activity and the expression of AMP in murine bone marrow-derived macrophages. The results showed a distinct HDAC inhibitory activity associated with sodium butyrate and Na-2HB in a concentration-dependent fashion, whereas Na-3HB and Na-4HB were not associated with HDAC inhibition even at high millimolar concentrations. Sodium butyrate showed more inhibition than Na-2HB. The present study also showed that the hydroxylated derivatives of butyrate differentially modulate the macrophage expression of the AMP cathelicidin LL-37, and to a lesser degree the β-defensins 2 and 4 *in vitro*. Na-4HB induced the greatest level of endogenous secretion of these AMP; amounts comparable to those induced by sodium butyrate. Less induction of AMP expression was induced by Na-3HB, and the least by Na-2HB. The present study also showed preservation of cell viability when exposed to a wide range of physiologic and supra-physiologic concentrations of the hydroxylated derivatives of butyrate, which contrasted with the cytotoxic effect induced by sodium butyrate.

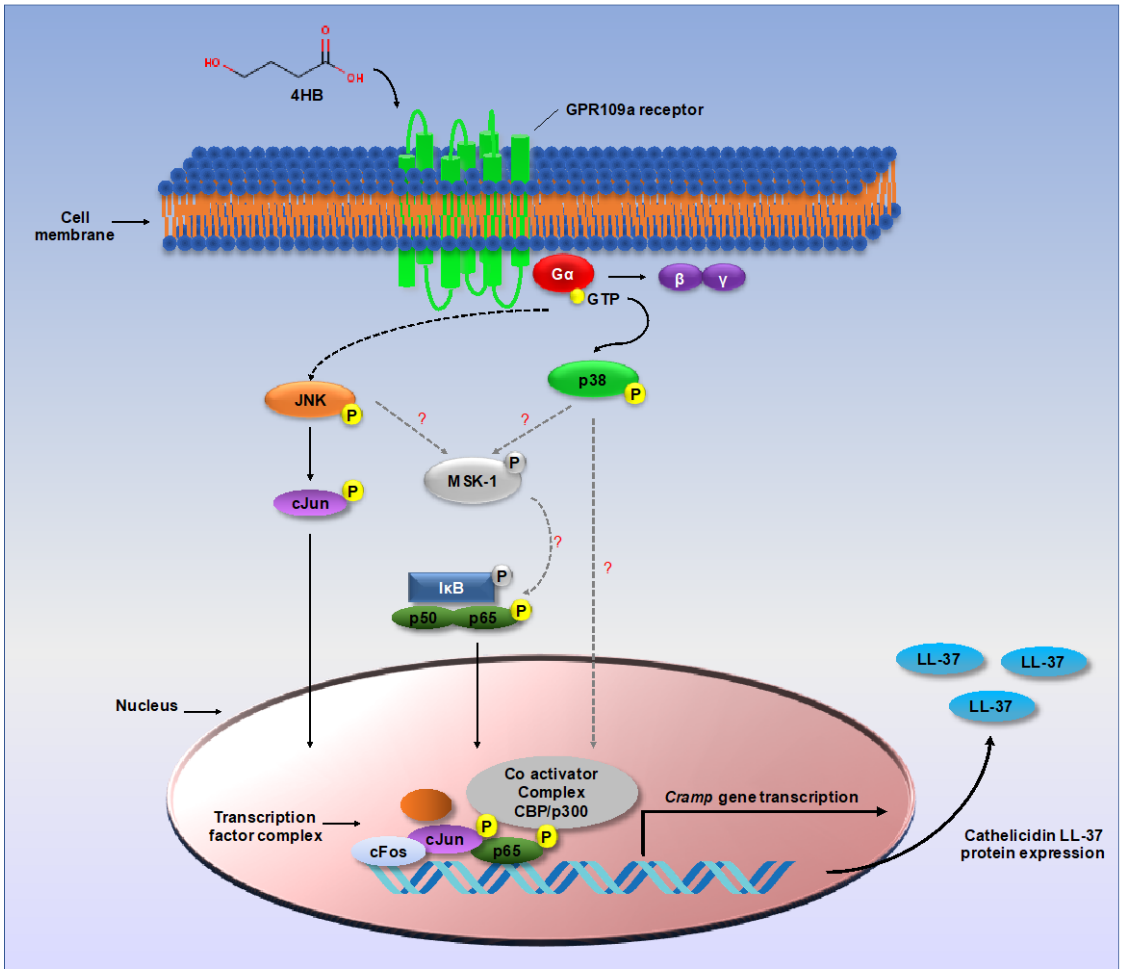

Figure 15. Proposed molecular mechanism of 4HB-mediated transcriptional activation of cathelicidin LL-37.

Transcriptional upregulation of cathelicidin LL-37 in macrophages exposed to 4HB requires a specific ligand-receptor activation modulated by the G-protein coupled receptor GPR109a. After activation, an intracellular signaling cascade promotes the sequential phosphorylation and activation of the MAP Kinases, p38 and JNK. Although the mechanisms of NF-κB phosphorylation have not been evaluated in the present model, its activation occurs downstream from p38, and is essential for the AMP transcriptional response. Once translocated to the nuclei, the transcriptional factors AP-1 (cFOS/c-Jun subunits) and p65 participate in the transcriptional activation of cathelicidin LL-37 mediated by 4HB.

Different SCFA have been associated with a weak HDAC inhibitory activity when compared to potent inhibitors such as trichostatin A [106]. Variables such as concentration, cell type, specific HDAC groups and subgroups, the ability of the molecule to enter into the nuclei, among others, are determinant in this activity [93]. Sodium butyrate is a known inhibitor of HDAC classes I and II in a broad spectrum of cell types. This molecule has been shown to induce apoptosis among different epigenetic effects [115]. Evaluation of sodium butyrate in the present study confirms the HDAC inhibitory activity induced by this molecule in exposed macrophages, and its cytotoxic effect when used at high concentrations. The present study also shows the AMP induction by Na-2HB is associated with HDAC inhibition. Although the results of this study show that Na-3HB and Na-4HB did not have a HDAC inhibitory activity in treated macrophages, these molecules have been clearly shown to inhibit HDAC activity in other body systems. For example, Shimazu *et al.,* 2013 showed that physiologic circulatory concentrations of 3HB (higher than 1 mM) during prolonged exercise or starvation have a direct HDAC inhibitory activity upon human embryonic kidney 293 (HEK293) cells *in vitro,* and whole kidney *in vivo,* in a dose dependent manner. The study reported that the major targets of acetylation were lysine 9 and 14 of histone 3, and that the inhibited HDAC belonged to classes I and II, with a generalized effect of protection against oxidative stress [116]. Similarly, Klein *et al*., 2009 have shown a heterogeneous HDAC inhibitory response induced by 4HB in different regions of the rat brain. Whereas a significant acetylation was found in the cerebellum, the hippocampus, and brain stem, other regions like the temporal and parietal cortex were shown to be unresponsive to 4HB. Of particular interest, only those regions that were responsive express class IV HDAC, suggesting that this subgroup is the target of 4HB [48].

The lack of HDAC inhibitory activity associated with Na-4HB and its ability to upregulate the expression of AMP further supports the requirement of specific surface receptors at the cell level to trigger the transcriptional activation of AMP. It is hypothesized herein that the presence of the hydroxyl group at the carbons -2 and -3 provide a less stable molecular interaction, which results in a lower endogenous AMP induction. In fact, the presence of the 4-hydroxyl group has been shown to play a key role in high affinity interactions between 4HB and $GABA_A$ receptors in the brain [50]. Other ligand-receptor interactions, in particular those associating SCFA with the GPR109a, suggest that the carboxylic group of the fatty acids is the anchor point to trigger a receptor-mediated response [117]. Other derivatives of butyrate which have chemical modifications in the carbon -4, but have a preserved carboxylic group, such as sodium 4-phenylbutyrate, have been shown to induce an effective transcriptional activation of AMP in epithelial cells and macrophages [60, 109, 118].

The present study evaluated the signal-transduction mechanism by which 4HB induced the expression of cathelicidin LL-37. When evaluating potential GPCR associated with macrophages, a high mRNA expression of GPR109a and GPR172a, was seen in naïve macrophages. From those, the transcriptional inhibition of GPR109a was shown to have an inhibitory effect on the expression of cathelicidin LL-37, suggesting that, at least partially, this receptor is involved in the molecular mechanism activating the AMP in 4HB-stimulated macrophages.

GPCR-mediated activation of MAP Kinases following stimulation with SCFA has already been described for a variety of cell types [119]. The specific set of proteins involved (JNK, p38, or MEK1,2, and specific downstream transcription factors), however, seem to be differentially activated depending upon the molecule triggering the response and the type of cell involved [107,

120, 121]. Results of the present study showed that activation of JNK and p38 are required to induce the transcriptional activation of cathelicidin LL-37 in 4HB-stimulated macrophages.

Additionally, phosphorylation of the NF-κB protein was necessary to induce the AMP response in 4HB-treated cells. Importantly, phosphorylation of the p65 subunit of NF-κB did not occur before three hours of stimuli, whereas LPS- or TNF-α-induction of the NF-κB pathway are usually associated with a rapid (5 min to 60 min) phosphorylation [122]. The delayed NF-κB response in the present study suggests that activation of p65 could be part of a secondary response that depends upon the development of a prior response within the cell. Given the pattern of macrophage activation described in Chapter 2.0 of the present dissertation, it could be hypothesized that either transcriptional activation of IRF3 or secreted TNF-α from 4HB-stimulated macrophages, are a requirement for the subsequent activation of NF-κB.

A second hypothesis explaining the delayed phosphorylation of NF-κB relies in a transactivation mechanism of p65 mediated by the MAP kinases. It has been previously shown that non-canonical activation of the p65 subunit can occur through phosphorylation mediated by the mitogen- and stress-activated kinase 1 (MSK1) (Figure 15), which is a downstream molecule of JNK and p38 [123].

Others have shown, however, that under TNF-α induction, transactivation of p65 is p38-independent. In this particular case, activation of the MAP Kinase is required to further induce the co-activator complex CBP/p300 (Figure 15), which stabilizes the interaction of p65 at the promoter domain of the gene being transcribed, but does not influence phosphorylation of p65 [124]. Within the present study, it is still unknown what is the molecular association between p38 and p65. The use of an inhibitor of p38 significantly decreased, but not abolished, cathelicidin LL-37 secretion. On the other hand, inhibition of NF-κB completely blocked the production of this AMP, which

suggests that NF-κB is not being directly phosphorylated by a downstream element of p38. Future studies to confirm these mechanisms are warranted.

Transcriptional activation of cathelicidin LL-37 has been shown to be a complex process that involves the activation of several transcriptional factors and *cis*-elements at both the 5'-UTR and 3'-UTR regions of the *Cramp* gene [125]. Specific domains for NF-κB, nuclear factor NF-IL-6, granulocyte macrophage-colony stimulating factor (GM-CSF), CCAAT/enhancer binding protein (C/EBP), GATA transcription factors, and interferon regulatory element-δ (IRE-δ) have already been identified [126]. Moreover, upregulation of cathelicidin LL-37 has been shown to be modulated by the transcription factor specificity protein-1 (Sp1) after induction with double-stranded RNA [127], STAT3 and HIF-1α when mediated by entinostat [128], and the cAMP-response element binding protein (CREB) and AP-1 after stimulation with butyrate [107, 125]. The present study showed that 4HB-stimulation of macrophages induced cathelicidin LL-37 expression through a mechanism that requires the complex factors AP-1 and NF-κB, which are consistent with the molecular pathways being activated. Furthermore, it was shown that 4HB-mediated cathelicidin upregulation in macrophages is independent of STAT3 or HIF-1α.

A number of important clinical implications are derived from the results of the present study. Both p38 and NF-κB are known targets of a broad number of nonsteroidal anti-inflammatory drugs (NSAIDs) [129]. In fact, a number of studies associate the use of NSAIDs with a stronger progression of infections [130-132]. An understanding of the mechanisms involved in the endogenous upregulation promoting resistance to bacterial infection, and the inhibitory role of NSAIDs, will help clinical practitioners to determine alternative anti-inflammatory cocktails that do not inhibit the potential of implanted polymers composed of 4HB.

There are several limitations to the present study. Although two potential GPCR were evaluated, additional membrane receptors (GPR41 and GPR43) and sodium-coupled transporters (Slc5a8) could be contributing to the 4HB-associated effect in macrophages. Direct molecular interactions between the kinases and additional intermediaries of the activation cascade need to be further investigated.

3.5 CONCLUSION

The present study showed the ability of 4HB to induce antimicrobial resistance through the promotion of an endogenous upregulation of AMP in exposed macrophages. The mechanisms of AMP secretion are independent of a direct HDAC inhibitory activity, which has been commonly associated with SCFA. 4HB instead promoted a specific molecular activation cascade that resulted in the increased expression of cathelicidin LL-37. The increased expression of AMP as well as the ability to preserve the viability of the cells suggest that 4HB may be used in many applications, such as functionalization of biomaterials or as a cargo molecule for drug delivery. 4HB has the advantage of promoting bacterial resistance without the risk of adverse effects on the cells.

4.0 COMPARATIVE HOST MACROPHAGE RESPONSE TO SURGICAL MESHES USED FOR VENTRAL HERNIA REPAIR[2]

4.1 INTRODUCTION

The use of surgical mesh materials for ventral hernia repair has become commonplace, largely in response to the documented decrease in the incidence of hernia recurrence compared to repair without the use of a surgical mesh [133-135]. However, all meshes elicit a host tissue response that is dependent, in part, upon the material(s) from which the implant is manufactured, the design and degradability of the material, and host variables such as age, body mass index, smoking history, and co-morbidities, among others [12, 136-140].

At the cellular level, one of the major determinants of the downstream outcome is the phenotype of the innate immune response, especially the macrophage component of the innate response (Figure 1, adapted from [8, 9]). A persistent pro-inflammatory (M1-like) macrophage phenotype is typically associated with dense fibrosis and scar tissue formation and, if the implanted material is non-degradable, the well described foreign body response (FBR) [13, 15, 21]. In contrast, a regulatory, pro-remodeling (M2-like) macrophage phenotype within the first 14 days

[2] Sections of this chapter to appear in *Journal of Immunology and Regenerative Medicine.*

post-implantation is predictive of the deposition of less dense, organized and site appropriate connective tissue [14].

The initiators of a pro-inflammatory vs. a pro-remodeling macrophage response are not fully understood but with respect to biomaterials, synthetic and non-degradable biomaterials typically induce a pro-inflammatory response, while naturally occurring, degradable materials typically induce a pro-remodeling response [15, 16, 141]. Neither of these phenotypes is exclusive and in reality, the ratio of cells with their respective phenotype defines and determines the microenvironmental milieu and associated tissue response [14, 15, 142].

The objective of the present study is to characterize the host response induced by a subset of surgical meshes composed of synthetic, biosynthetic, and biologic sources.

4.2 MATERIALS AND METHODS

4.2.1 Experimental Design Overview

The effects of selected synthetic, biosynthetic, and biologic surgical meshes upon macrophage activation were evaluated *in vivo*. Three synthetic surgical mesh devices: 1) Bard® Mesh, 2) TIGR® Matrix Surgical Mesh, 3) GORE® BIO-A® Tissue, one biosynthetic mesh device: 4) Phasix™ Mesh, and one biologic mesh device: 5) Strattice™ Reconstructive Tissue Matrix, were used in the present study (Table 1) [24, 25, 77-79].

A rat abdominal bilateral partial thickness defect was used to evaluate the host response to the implanted surgical mesh devices [14, 143]. The histologic appearance, macrophage phenotype,

and cathelicidin LL-37 expression were evaluated at 3, 7, 14, 21, and 35 days after surgery (Figure 16).

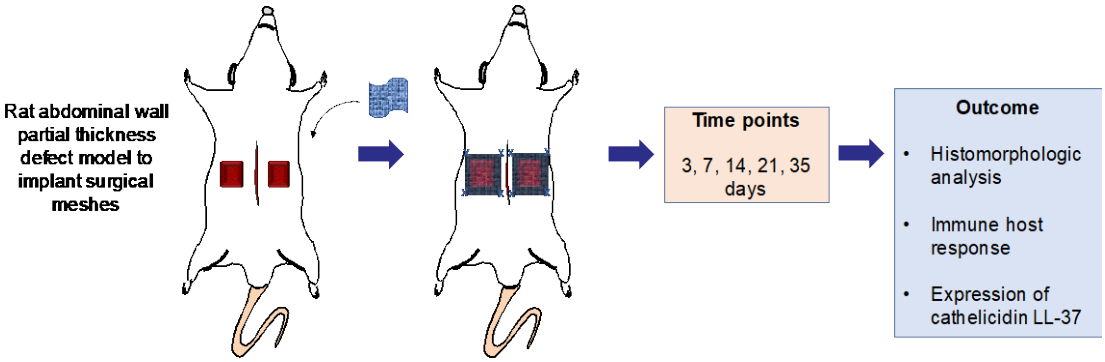

Figure 16. Experimental design overview.

In vivo evaluation of the host response to biomaterials. The test articles were evaluated in a Sprague–Dawley rat partial thickness abdominal wall defect model. A 1.5 cm x 1.5 cm test article was implanted following surgical removal of the external and internal oblique muscles. The animals were sacrificed and materials harvested at 3, 7, 14, 21, and 35 days post-surgery. Explanted specimens were used for histomorphologic analysis quantifying cellularity, vascularity, foreign body multinucleate giant cells, and cell thickness around the implanted mesh materials. Immunolabeling using antibodies specific for markers of macrophage phenotype [Pan-Mϕ ($CD68^+$), M1-like ($CD68^+CD86^+$), and M2-like ($CD68^+CD206^+$)] were used to determine the potential immunomodulatory effect of the tested materials upon macrophages.

4.2.2 Scanning Electron Microscopy

Surface characteristics of the surgical meshes were evaluated by scanning electron microscopy (SEM) (Figure 17). Strattice™ scaffold was fixed in aqueous glutaraldehyde solution (2.5% v/v) for 30 minutes, followed by immersion in a series of progressively greater concentrations of ethanol (30%, 50%, 70%, 90%, and 100%). The scaffold material was then dried in 100% hexamethyldisilazane (HMDS) (Sigma-Aldrich, MW, USA) for 3 minutes. All other evaluated surgical mesh materials did not require fixation or dehydration steps. The surgical mesh materials

were mounted onto aluminum stubs and sputter coated with gold/palladium alloy (thickness: 4.0 nm). The meshes were imaged with a scanning electron microscope (JEOL JSM6330f, JEOL, Peabody, MA) at a 3.0 kV accelerating voltage.

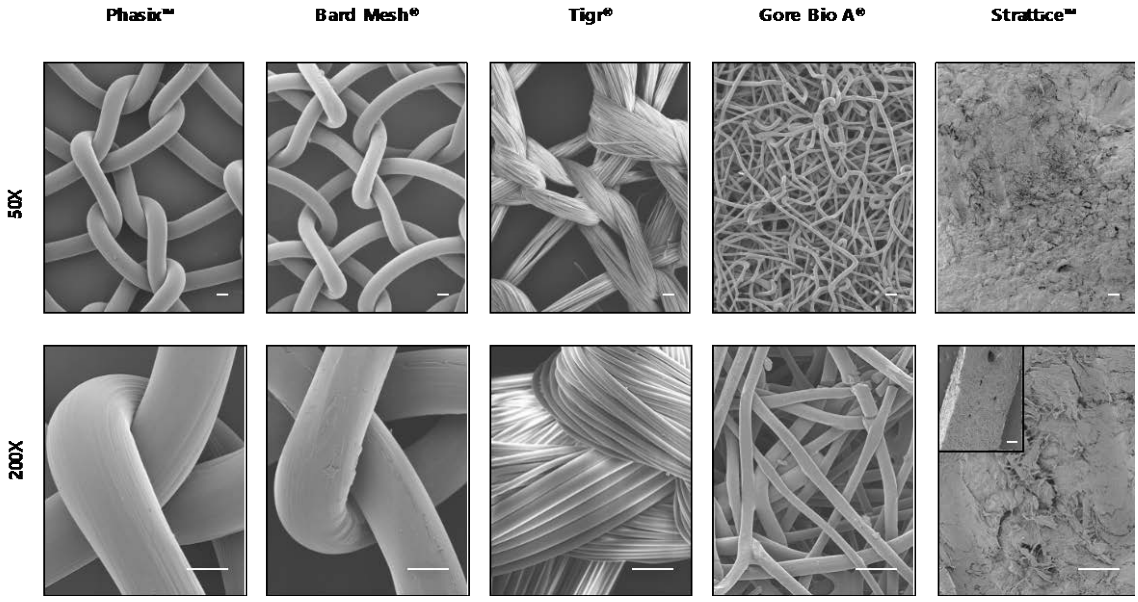

Figure 17. Scanning electron microscopy of surgical mesh materials.

SEM images of each mesh device at 50x magnification (upper row, scale bar 100 μm) and 200x magnification (bottom row, scale bar 100 μm). Inset represents the cross-section of the biologic scaffold 50x magnification (scale bar 200 μm).

4.2.3 Surgical model and mesh implantation

The host response to the implanted surgical meshes was evaluated using a previously described rat abdominal wall partial thickness defect model [143, 144]. Animal procedures were approved by and performed according to the guidelines of the Institutional Animal Care and Use Committee at the University of Pittsburgh (IACUC protocol #15127009). Sixty Sprague–Dawley rats were randomly divided into six separate groups. Each rat was anesthetized and maintained at a surgical plane of anesthesia with 2% isoflurane in oxygen. The surgical site was prepared in sterile fashion

using a betadine (providone-iodine) solution followed by placement of sterile drapes. Bilateral paramedian skin incisions were made to provide access to the muscular abdominal wall. Defects measuring 1 cm x 1 cm were created in the exposed musculature (external and internal oblique muscles), leaving the underlying peritoneum and transversalus fascia intact. The defects were then either repaired with one of the test articles or left unrepaired (n=4 for each group at each time point). Each mesh was sutured to the adjacent abdominal wall musculature with 4–0 Prolene non-absorbable suture at each corner to secure the mesh and allow for partial mechanical loading of the test article, and to allow for identification of the implant boundaries at the time of euthanasia and explanation. A minimal amount of suture material was used to avoid eliciting a host response to the suture material that would obscure the host response to the mesh material itself. The skin was closed using absorbable 4–0 Vicryl suture. The animals were recovered from anesthesia on a heating pad and allowed normal activity and diet for the remainder of the study period.

4.2.4 Test article collection

At 3, 7, 14, 21, and 35 days post implantation, 2 animals in each group were euthanized by CO_2 inhalation and subsequent cervical dislocation in accordance with the guidelines of the American Veterinary Medical Association (AVMA) Panel of Euthanasia. Following euthanasia and using sterile technique, the skin was gently dissected and reflected, and the test specimens and surrounding tissue were collected and immersed in 10% Neutral Buffered Formalin (NBF) for subsequent histologic evaluation.

4.2.5 Quantitative Histomorphologic Analysis

A quantitative scoring system (Table 2) was used to evaluate the host response to the implanted surgical meshes at each time point. The NBF-preserved specimens were embedded in paraffin prior to being cut into 5 μm thick sections and mounted onto glass slides. The specimens were deparaffinized with xylene immersion followed by exposure to a graded series of ethanol solutions (100%, 95%, 75%) [15]. Sections were stained with hematoxylin and eosin (H&E) (Sigma-Aldrich, USA) following manufacturer instructions. Stained slides were dehydrated using a graded series of ethanol solutions (75%, 95%, 100%) prior to cover-slipping. A total of 3 low magnification (100x) and 3 high magnification (400x) images were acquired for each H&E section at the mesh-tissue interface. The criteria used to quantitatively evaluate the histomorphology of the specimens included: total cellular infiltration, vascularization, number of multinucleate foreign body giant cells (MNGC), and cell layer thickness around the implanted surgical mesh. The total number of cells per field of view (FOV) was quantified using CellProfiler Image Analysis Software (http://www.cellprofiler.org). All other scoring criteria were quantified by three independent blinded observers.

Table 2. Quantitative Histomorphologic Analysis

Image Magnification	Category	Description
Low magnification (100x)	Cellularity	Number of cells at the mesh-tissue interface per FOV
	Vascularity	Number of blood vessels per FOV
High magnification (400x)	Multinucleate foreign body giant cells	Number of foreign body giant cells per FOV
	Cell layer thickness	Number of cell layers of dense cellular accumulation immediately adjacent to mesh fibers per FOV

4.2.6 Immunolabeling of tissue sections

The macrophages within each FOV were identified and quantified by immunofluorescence. Antigen retrieval of tissue sections was facilitated with citrate buffer (10 mM citrate, pH 6.0) at 95-100˚C for 20 minutes. The blocking solution, consisting of 2%v/v normal horse serum (Hyclone), 1%wt/v bovine serum albumin (Sigma), 0.1%v/v Triton X-100 (Sigma), and 0.1%v/v Tween-20 (Sigma) in PBS, was applied for 1 h. Primary antibodies against the pan-macrophage marker CD68 (mouse anti-rat CD68, clone ED1, Abd Serotec) and the M1-like, pro-inflammatory macrophage marker CD86 (rabbit anti-human CD86, clone EP1158Y, Abcam) were used at 1:150 dilution, the M2-like, pro-remodeling macrophage marker CD206 (goat anti-human CD206, polyclonal, Santa Cruz) was used at 1:100 dilution, incubating overnight at 4˚C. Sections were washed and incubated with the following fluorescently conjugated secondary antibodies diluted in blocking solution for 1 hour at room temperature: donkey anti-mouse Alexa Fluor-594 (1:200 dilution, Invitrogen), donkey anti-rabbit PerCPCy5.5 (1:300 dilution, Santa Cruz), and donkey

anti-goat Alex Fluor-488 (1:200 dilution, Invitrogen). Nuclei were labeled with DAPI and slides coverslipped with fluorescent mounting medium (Dako). Three multispectral epifluorescent images were acquired for each slide at the mesh-tissue interface (Nuance multispectral imaging system, CRi Inc.).

Macrophages were defined as CD68 positive co-localized with nuclei. The total number of cells co-expressing CD68 with CD86 and/or CD206 was quantified for each image using CellProfiler Image Analysis Software (http://www.cellprofiler.org). The subpopulation of macrophages $CD68^{+}CD206^{+}CD86^{+}$ was denoted as "triple-labeled". The M1-like subpopulation was calculated by subtracting the number of triple-labeled $CD68^{+}CD206^{+}CD86^{+}$ cells from the $CD68^{+}CD86^{+}$ cells, to remove double counted cells. Likewise, the M2-like subpopulation of macrophages was calculated by subtracting the number of triple-labeled $CD68^{+}CD206^{+}CD86^{+}$ cells from the $CD68^{+}CD206^{+}$ cells. A ratio of the number of M2-like to M1-like cells (($CD68^{+}CD206^{+}$):($CD68^{+}CD86^{+}$)) was calculated for each field. The ratio was obtained dividing the number of M2-like macrophages by the number of M1-like macrophages.

4.2.7 Statistical analysis

Quantification of histomorphologic criteria and immunolabeling are presented as the mean ± the standard error of the mean (SEM) from four biologic replicates. Data normality was evaluated using the Kolmogorov-Smirnov test for each mesh device at each time point. Statistical differences between the mesh materials at each time point were determined using a non-parametric ANOVA test (Kruskal-Wallis test). The pattern of differences was evaluated with post-hoc Dunn's multiple comparison test. A value $p<0.05$ was considered statistically significant. Statistical analysis was performed using GraphPad Prism version 7.0c (GraphPad Software, La Jolla CA, USA).

4.3 RESULTS

4.3.1 Macroscopic assessment

All animals survived to the intended time point. All implanted surgical meshes were integrated with surrounding tissue. By day 35, all implanted materials remained largely intact and were easily identified during necropsy. None of the implanted test articles induced edema at the implant site.

4.3.2 Histomorphologic quantification

The host tissue remodeling response was quantified from H&E stained images (Figure 18) with respect to vascularization, total number of infiltrating cells, presence of MNGC, and cell thickness around the implanted material. At each of the evaluated time points, non-parametric test indicated that the level of vascularization per FOV around the implanted surgical meshes remained comparable (Figure 19A). After 35 days of implantation, the number of vessels found at the mesh-tissue interface ranged between 6 to 12 per 100x FOV.

The acute host response (days 3 and 7) to all materials was characterized by a dense infiltration of mononuclear cells. TIGR® mesh showed greater infiltration of mononuclear cells compared with the other meshes at all time points (Figure 19B). Differences in the number of MNGC between the surgical meshes were evident as early as day 7 post-implantation. By day 7, quantification of these cells showed (2.5 ± 1.4) MNGC around Phasix™, (2.3 ± 1.3) MNGC around Bard® Mesh, (2.5 ± 1.5) cells around GORE® BIO-A®, (8.5 ± 4.9) cells around TIGR®, and (0.4 ± 0.2) cells around Strattice™. These values remained similar by day 35 for each of the

meshes, as shown in Figure 19C. Further analysis indicated that there were significant differences in the number of MNGC between Strattice™ and TIGR® mesh at 7, 14, 21, and 35 days (Figure 19C).

The number of cell layers in the area of dense accumulation immediately adjacent to TIGR®, GORE® BIO-A®, and Strattice™ remained constant at all time points. Phasix™ mesh showed an increased cell-layer thickness around the fibers at day 7 compared with GORE® BIO-A®, that decreased over time. For all the other time points (days 14 to 35), the cell-layer thickness around the implanted material remained similar between the meshes (Figure 19D).

4.3.3 Spatiotemporal analysis of macrophage phenotype

The spatiotemporal distribution of phenotypically distinct macrophages at the material-tissue interface was characterized by immunolabeling. The co-expression of the pan-macrophage cell surface marker CD68 with the pro-inflammatory (M1-like) CD86 marker and/or the pro-remodeling (M2-like) scavenger receptor CD206 was determined (Figure 20). As shown in the defect control (i.e., no implanted material), earlier time points (days 3 and 7) were associated with a pro-inflammatory response at the wound site, with marked infiltration of $CD86^+$ macrophages. The response transitioned into a pro-remodeling reaction by day 14, when an increased population of $CD206^+$ macrophages was observed (green). A resolution phase without prolonged macrophage response was found at day 35 in normal tissue.

All implanted surgical meshes induced a macrophage response that, although variable in phenotype remained active for the 35 days of evaluation. Infiltrated macrophages were localized

at the biomaterial-tissue interface and in close proximity to the mesh fibers of Phasix™, Bard® Mesh, TIGR® and GORE® BIO-A®, and at the periphery of the Strattice™ scaffold (Figure 20).

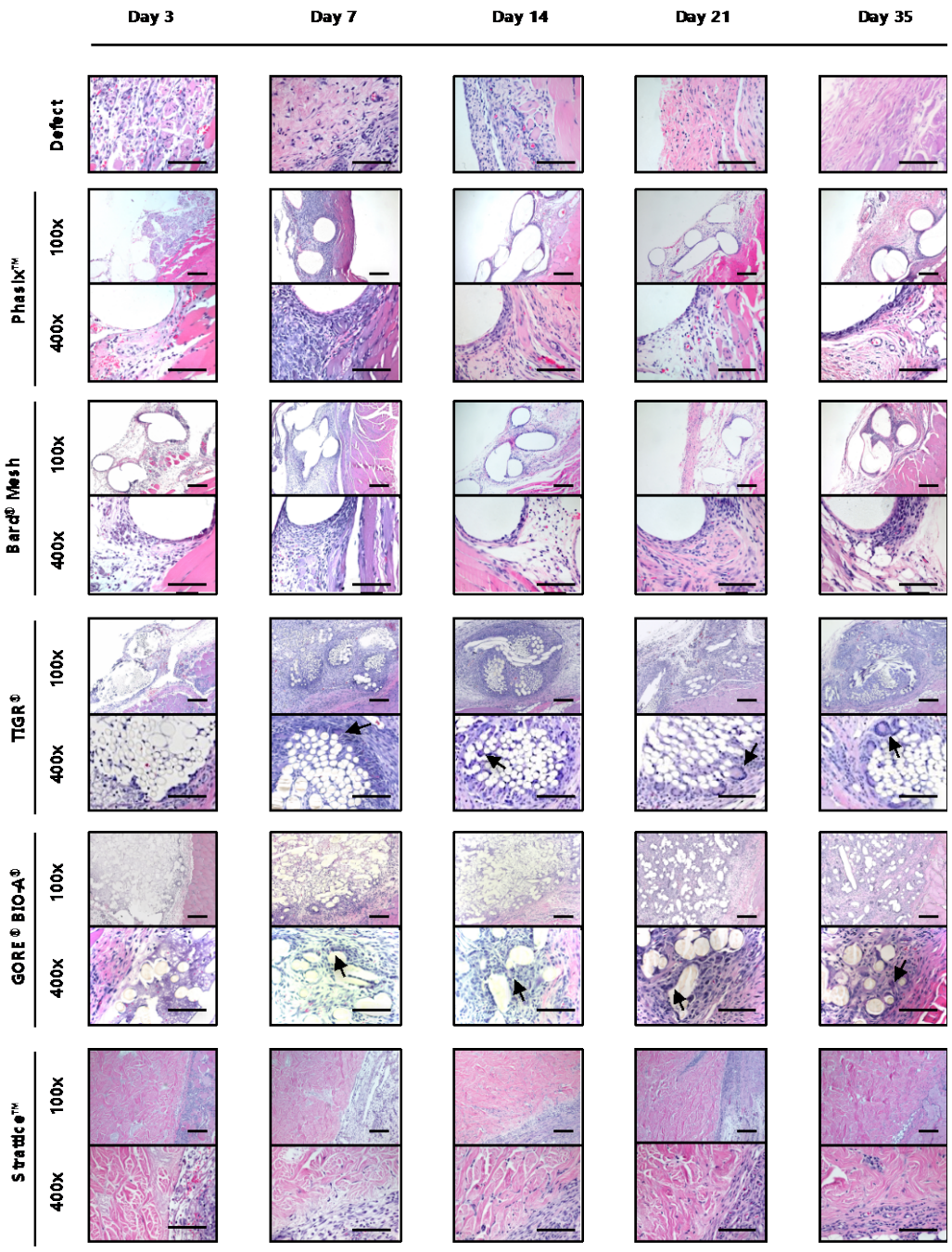

Figure 18. Histologic appearance implanted surgical meshes.

Representative hematoxylin and eosin stained histologic cross sections of each mesh at 3, 7, 14, 21, and 35 days post-implantation, showing the cell response to implanted surgical meshes: Phasix™ Mesh, Bard® Mesh,

TIGR®, GORE® BIO-A®, and Strattice™. Low magnification images (100x, upper, scale bar 200 µm) show the levels of vascularization and cellular infiltration. High magnification images (400x, bottom, scale bar 100 µm) show the MNGC and the cellular thickness at the margins of the implanted materials.

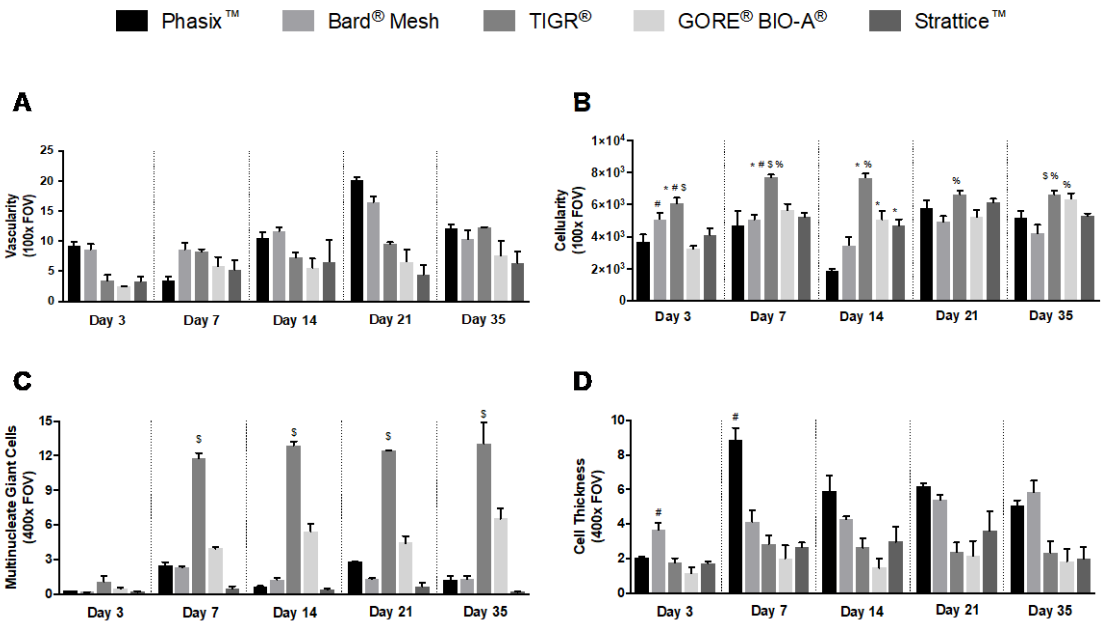

Figure 19. Quantification of histomorphologic profile of explanted mesh materials.

A. Number of blood vessels per 100x Field of view (FOV). B. Number of cells at the mesh-tissue interface in a 100x FOV. C. Number of formed multinucleate giant cells per 400x FOV. D. Number of cell layers of dense cellular accumulation immediately adjacent to the mesh fibers per 400x FOV. Values: Mean ± SEM, biologic replicates (N)=4, technical replicates=3. Differences between the implanted mesh devices for each criteria were evaluated using non-parametric ANOVA test. Statistical significance was determined by $p<0.05$, * as different from Phasix™, % as different from Bard® Mesh, # as different from GORE® BIO-A®, and % as different from Strattice™.

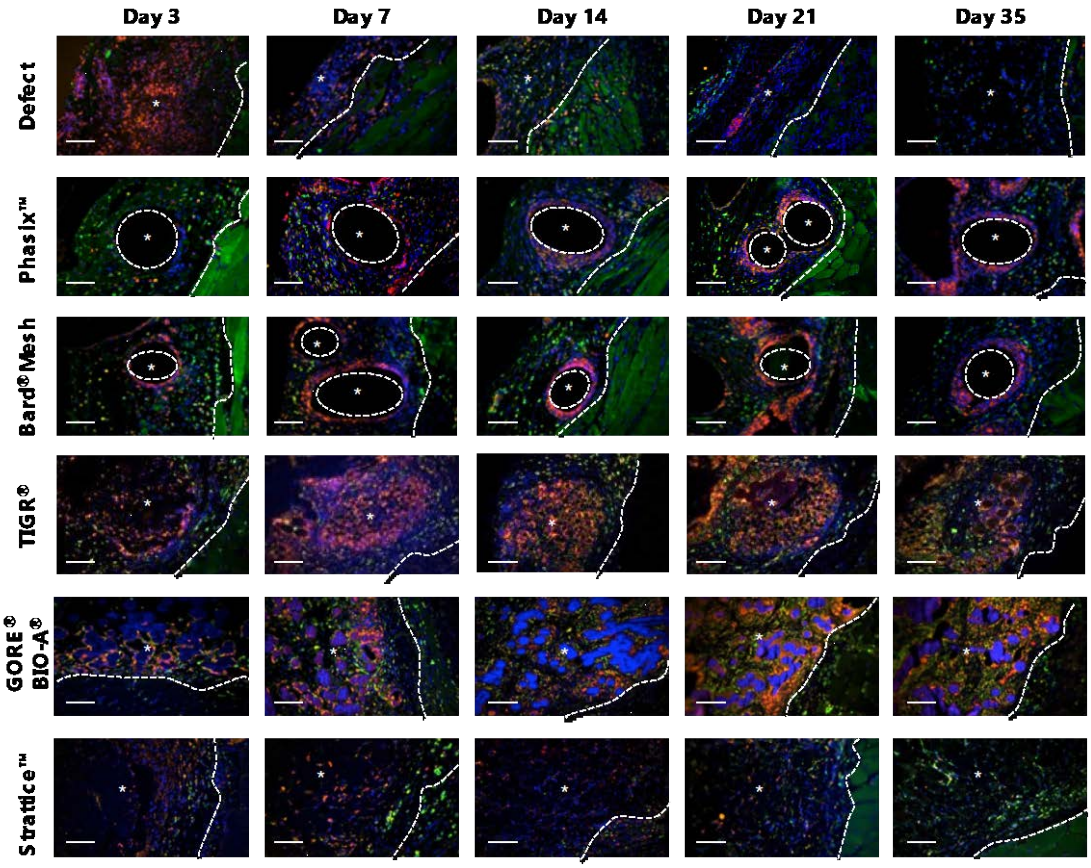

Figure 20. Biosynthetic scaffolds composed of P4HB modulate an early anti-inflammatory phenotype of macrophages.

Immunolabeling of implanted mesh materials or defect alone controls. Red: $CD68^{+}$ (pan macrophages), Green: $CD206^{+}$(pro-remodeling macrophages), Orange: $CD86^{+}$ (pro-inflammatory macrophages), Blue: DAPI. Earlier time points were characterized by a pro-inflammatory acute host response surrounding the implanted synthetic materials and the defect alone in contrast with a markedly pro-remodeling population of macrophages surrounding the Phasix™ mesh device. Scale bar 100 μm.

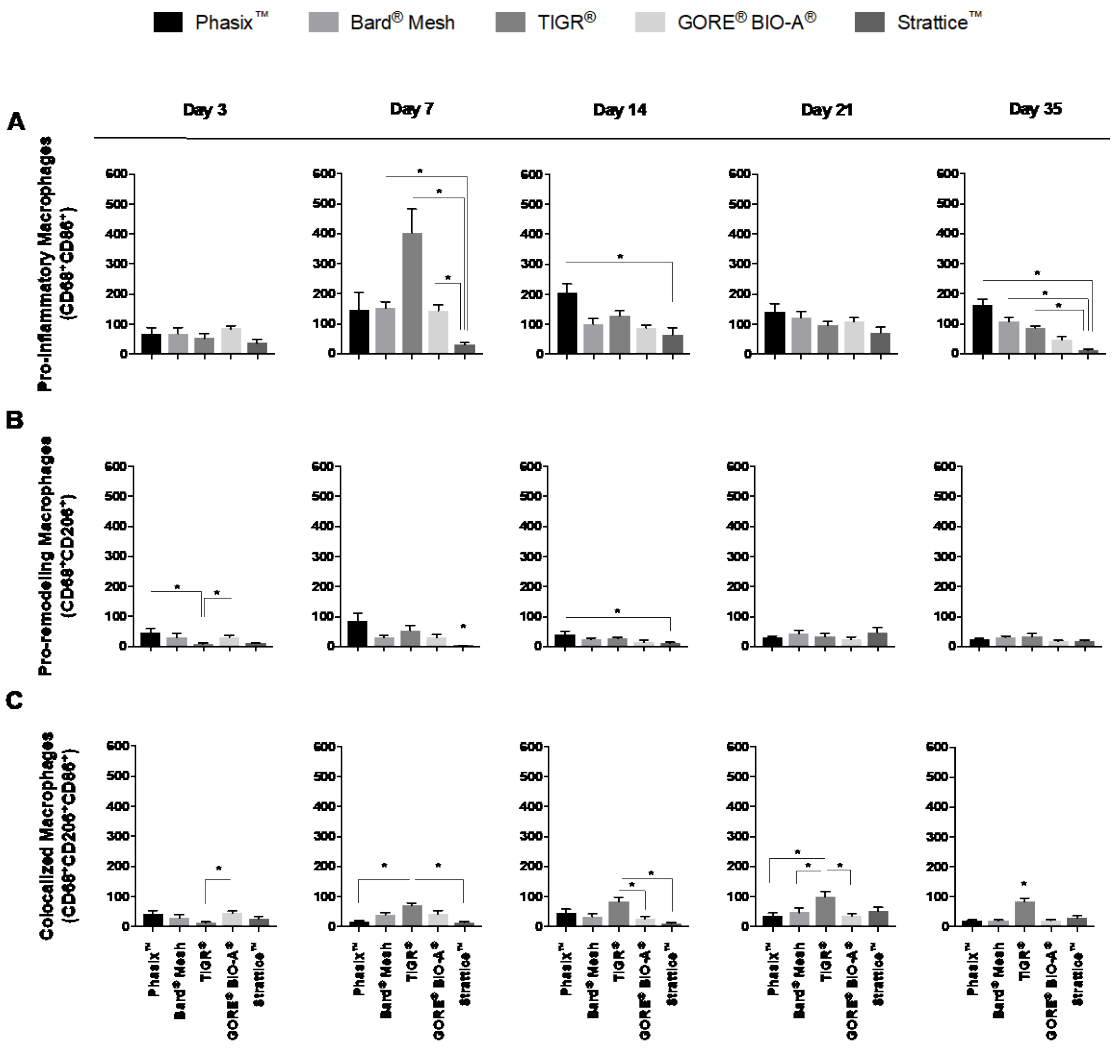

Figure 21. Quantification of macrophage subpopulations at the mesh-tissue interface.

Images were quantified using Cell Profiler image analysis software. A. Number of pro-inflammatory M1-like macrophages $CD68^{+}CD86^{+}$, per 200x FOV. B. Number of pro-remodeling m2-like $CD68^{+}CD206^{+}$, per 200x FOV. C. Number of triple-labeled $CD68^{+}CD206^{+}CD68^{+}$ macrophages, per 200x FOV. Values: Mean ± SEM, biologic replicates (N)=4, technical replicates=3. Differences between the implanted mesh devices for each criteria were evaluated using non-parametric ANOVA test at 3, 7, 14, 21, and 35 days. Statistical significance was determined by $p<0.05$.

Day 3: By 3 days, the population of pro-inflammatory (M1-like) macrophages, recognized as $CD68^+CD86^+$ cells, was similar among the implanted materials (Figure 21A, Day 3). However, the pro-remodeling (M2-like) subpopulation of macrophages, identified as $CD68^+CD206^+$, showed variability among the materials. Macrophages with an M2-like phenotype were in greatest number around Phasix™ (46.5 ± 13.2 cells), with fewer cells around Bard® Mesh (31.8 ± 12.8 cells), GORE® BIO-A® (30.5 ± 7.5 cells), Strattice™ (10.8 ± 2.8 cells), and the least number of M2-like macrophages around TIGR® (7.2 ± 3.9 cells). Statistical analysis of the M2-like macrophages at this time point showed differences between the materials. The differences were particularly found between Phasix™ and GORE® BIO-A® with TIGR®, respectively, as indicated in Figure 21B, Day 3. Likewise, quantification of triple-labeled $CD68^+CD206^+CD86^+$ macrophages showed the greatest number around GORE® BIO-A® (44.5 ± 6.2 cells), with fewer cells around Phasix™ (42.5 ± 10.9 cells), Bard® Mesh (30.2 ± 8.9 cells), Strattice™ (25.4 ± 8.2 cells), and the least number of triple-labeled cells around TIGR® (12.7 ± 2.4 cells). Statistical analysis showed differences for this subpopulation of macrophages between the implanted materials, as indicated in Figure 21C, Day 3. Differences observed in the subpopulations of macrophages for each of the implanted materials was reflected in the ratio of M2-like:M1-like macrophages. Analysis of the M2-like:M1-like ratio at day 3 showed a differential response among the materials. The ratio was higher for Phasix™ (4.44 ± 3.33) than for TIGR® (0.13 ± 0.03) (Figure 22A).

Day 7: The macrophage response at 7 days was distinct among the evaluated meshes. A predominant pro-inflammatory response was seen at the interface of the implanted TIGR® material, whereas all the other materials were characterized by a mixed population of macrophages (Figure 20, column 2). Macrophages with an M1-like phenotype were in the greatest number

around TIGR® (404.3 ± 78.6 cells), with fewer M1-like cells around Bard® Mesh (152.5 ± 20.8 cells), Phasix™ (147.5 ± 55.8 cells), GORE® BIO-A® (143.3 ± 19.7 cells), and the least number of M1-like macrophages around Strattice™ (31.0 ± 7.1 cells) (Figure 21A, Day 7). Statistical differences were found between Strattice™ compared to either TIGR, Bard® Mesh, and GORE® BIO-A®. The number of pro-remodeling M2-like macrophages was lower around the implanted Strattice™ scaffold compared to the other materials (Figure 21B, Day 7). At day 7, the number of cells co-expressing $CD68^{+}CD206^{+}CD86^{+}$ also presented differences between the materials. The number of this subtype of macrophages was higher around TIGR® (70.3 ± 9.6 cells) when compared to Strattice™ (13.7 ± 3.8 cells) and Phasix™ (15.7 ± 5.1 cells) (Figure 21C, Day 7). Statistical analysis of the M2-like:M1-like ratio at day 7 showed differences between the implanted meshes. The M2-like:M1-like ratio was higher around Phasix™ (2.06 ± 1.09 cells) than around TIGR® (0.12 ± 0.02 cells) and Strattice™ (0.08 ± 0.02 cells), respectively (Figure 22B).

Day 14: By day 14, the macrophage response remained a mixture of M1-like and M2-like cells for all materials (Figure 20, column 3). The number of macrophage subtypes varied among the implanted materials. Phasix™ showed a higher number of both pro-inflammatory M1-like (205.0 ± 29.1) and pro-remodeling M2-like (41.1 ± 10.3) macrophages compared with Strattice™ (66.1 ± 23.2 and 11.4 ± 3.6, respectively) (Figure 21A & Figure 21B, Day 14). Likewise, TIGR® presented an increased subpopulation of cells co-expressing $CD68^{+}CD206^{+}CD86^{+}$ (84.5 ± 13.9) when compared with Strattice™ (11.2 ± 3.8) and GORE® BIO-A® (26.6 ± 7.5), respectively (Figure 21C, Day 14). At this time point, the ratio of M2-like:M1-like macrophages did not show differences between the surgical materials (Figure 22C).

Day 21: After 21 days, the macrophage response to the implanted surgical meshes persisted as a mixture of phenotypic subtypes. The number of pro-inflammatory and pro-remodeling macrophages were similar among the materials (Figure 21A & Figure 21B); and therefore no differences were observed between the M2-like:M1-like ratios (Figure 22D). In contrast, TIGR® was associated with an increased number of macrophages co-expressing $CD68^{+}CD206^{+}CD86^{+}$ (99.5 ± 16.7) compared with either Phasix™ (35.9 ± 8.3), GORE® BIO-A® (35.5 ± 6.6), and Bard® Mesh (47.1 ± 15.7) (Figure 21C, Day 21).

Day 35: A mixed macrophage activation profile continued by day 35 at the interface of all implanted materials (Figure 20, column 5). A significant change was observed for the number of M1-like macrophages associated to each of the implanted materials. In particular, the number of pro-inflammatory macrophages decreased at the periphery of Strattice™ (12.8 ± 2.7 cells) compared with either Phasix™ (163.7 ± 18.1 cells), Bard® Mesh (108.5 ± 13.5 cells), and TIGR® (86.8 ± 7.1 cells) (Figure 21A, Day 35). At this time point, however, no differences were observed between the pro-remodeling M2-like macrophages (Figure 21B, Day 35), and as a consequence, an increased M2-like:M1-like ratio was associated to Strattice™ (1.86 ± 0.57) compared with Phasix™ (0.18 ± 0.05) and Bard® Mesh (0.36 ± 0.12), respectively (Figure 22E). The number of triple-labeled $CD68^{+}CD206^{+}CD86^{+}$ macrophages also presented differences between the meshes. TIGR® continued with increased values of this subpopulation of cells (83.7 ± 11.6 cells), as observed since day 7, that by day 35 were significantly higher compared with each of the other materials: Bard® Mesh (19.3 ± 3.5 cells), GORE® BIO-A® (19.5 ± 3.2 cells), Phasix™ (19.3 ± 3.3 cells), and Strattice™ (29.2 ± 6.1 cells) (Figure 21C, Day 35).

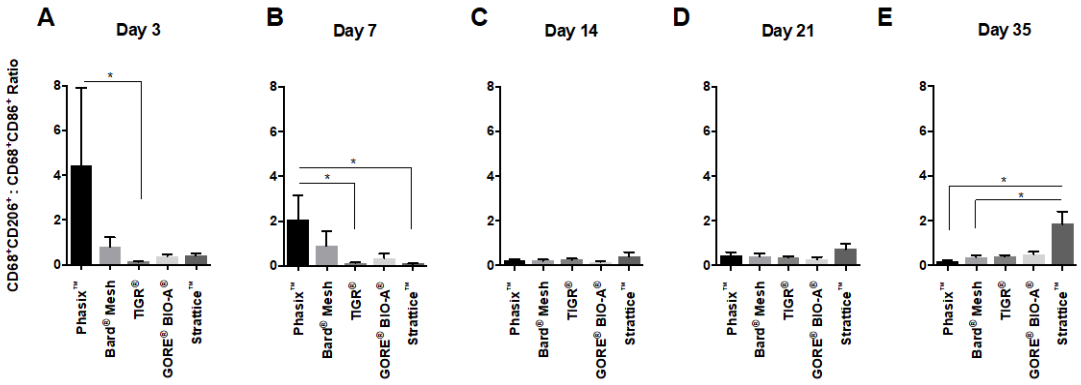

Figure 22. Quantification of M2-like:M1-like ratio of macrophages.

Ratio of M2-like:M1-like around mesh fibers at A. 3 days, B. 7 days, C. 14 days, D. 21 days, and E. 35 days. Images were quantified using Cell Profiler image analysis software. *In vivo*, Phasix™ mesh device modulates an earlier transition of pro-inflammatory to anti-inflammatory macrophages compared to synthetic mesh materials. Values: Mean ± SEM, biologic replicates (N)=3, technical replicates=3. Differences between surgical meshes were evaluated using non-parametric ANOVA test, *p<0.05.

4.3.4 Expression of cathelicidin LL-37 around implanted surgical meshes

The secretion of the AMP cathelicidin LL-37 around implanted surgical meshes was evaluated (Figure 23). Immunolabeling results showed an increase in the expression of this AMP following muscle injury compared to non-injured muscle, as seen in the images of native muscle vs. defect alone (Figure 23A & Figure 23B). Immunolabeling at the interface of the implanted surgical meshes showed an increased expression of cathelicidin LL-37 by the cells localized immediately around the fibers of Phasix™, Bard® Mesh, TIGR®, and GORE® BIO-A®. The least expression was shown in cells infiltrating the Strattice™ scaffold. Quantification of the number of cells expressing cathelicidin LL-37 showed that Phasix™ presented the highest number of cells around the mesh fiber at all time points, when compared to all the other surgical meshes or the defect

alone (Figure 23C). Moreover, statistical analysis showed that these numbers were different when compared with GORE® BIO-A® and Strattice™ at almost all evaluated time points.

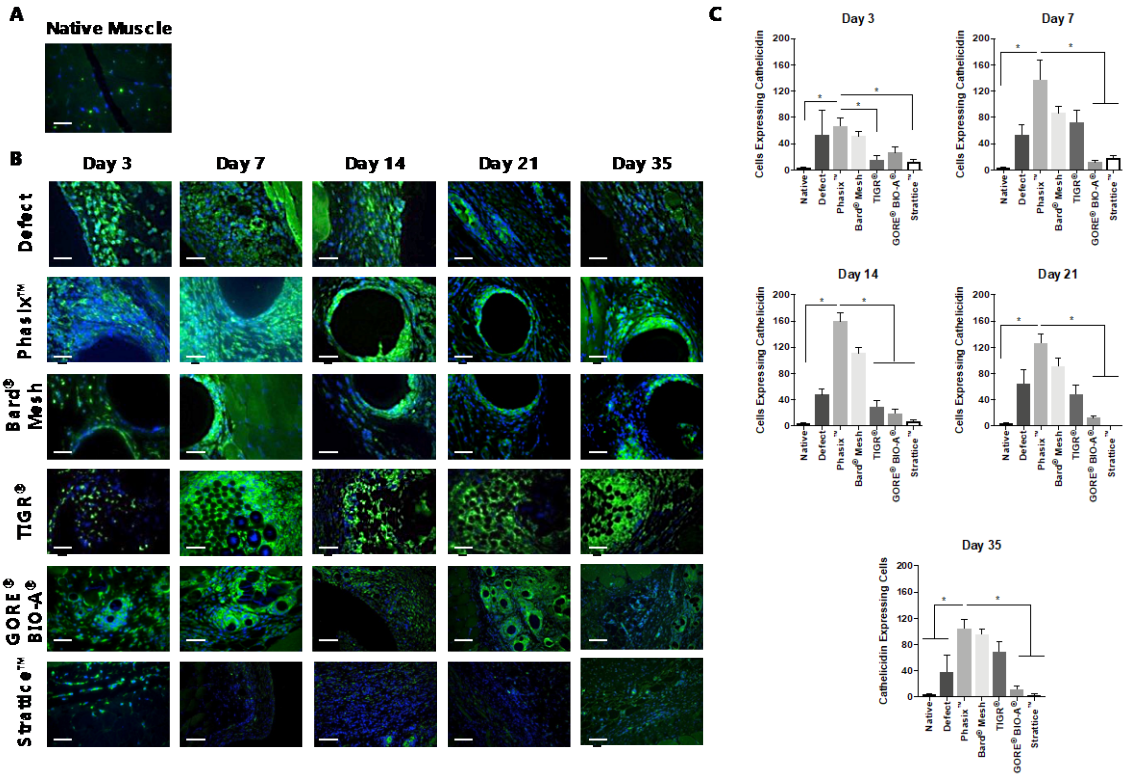

Figure 23. ***In vivo*** **cathelicidin LL-37 expression (green) around fibers of synthetic, biosynthetic and biologic scaffold materials.**

A. Basal expression of cathelicidin LL-37 in native muscle. B. Immunolabeling of cathelicidin LL-37 surrounding the mesh fibers or the defect alone control. Increased expression of the antimicrobial peptide is associated with the tissue repair process, as evidenced in the defect alone samples. Scale bar 50 µm. C. Quantification of cells expressing cathelicidin LL-37. Values: Mean ± SEM, biologic replicates (N)=3, technical replicates=3. Differences between surgical meshes were evaluated using non-parametric ANOVA test, *$p<0.05$.

4.4 DISCUSSION

Macrophages are the most abundant cell type involved in the host response to implanted biomaterials [84, 145]. Once thought to function primarily or exclusively as a phagocyte in response to infectious agents, foreign materials, and/or damaged tissue, and to occasionally combine with neighboring cells to form multinucleate giant cells as part of the foreign body reaction [18, 21] at sites of chronic inflammation, the plasticity of macrophages and their essential role in diverse physiologic processes is now recognized [10, 146].

Macrophages have antigen-presenting functions that link the innate and adaptive arms of the immune system [147], participate in fetal and post-natal development [148, 149], tissue homeostasis [150, 151], and even tissue and organ regeneration [152-155]. Macrophages show remarkable diversity with respect to their phenotype and secretome and play a crucial role in mitigating, not promoting, inflammation [156]. The macrophage phenotype induced within the first 14 days following implantation of a biomaterial has been associated with downstream tissue remodeling and clinical outcome [14, 15].

The present study showed a distinctive temporal macrophage phenotype response to five different surgical meshes that differ in composition and degradability. The Bard® surgical mesh is a non-degradable mesh composed of the synthetic material polypropylene and elicited a dominant foreign body response, as shown by the increased cell-layer thickness accumulation (Figure 18).

The two degradable synthetic surgical meshes, TIGR® and GORE® BIO-A®, elicited an M1-like response with the TIGR® mesh showing a more robust pro-inflammatory response and accumulation of multinucleate giant cells than GORE® BIO-A®. The cause for the more

pronounced M1-like response to the TIGR® mesh is unknown but may be related to composition, knit pattern, degradation rate, and/or the degradation by-products, among other variables [19, 134, 157]. TIGR® mesh is composed of multifilament fibers that have different degradation rates depending upon the presence or absence of glycolide. The fast resorbing co-polymer is formed by glycolide, lactide, and trimethylene carbonate (TMC), and is hydrolyzed within the body in four months. The slow resorbing co-polymer, formed by lactide and TMC, takes three years to degrade [158]. In contrast, GORE® BIO-A® is a mesh composed of monofilament fibers of a co-polymer of glycolide and TMC, with an *in vivo* degradation time of 6 months [159].

Strattice™ is a slowly degradable biologic mesh composed of porcine dermal extracellular matrix (ECM). Most biologic meshes composed of ECM that is not chemically cross-linked are associated with a more favorable M2-like:M1-like ratio than synthetic meshes. However, tissue processing methods, including residual decellularization agents and preservatives can markedly influence the host response toward a pro-inflammatory state [104, 160]. Strattice™ has previously been shown to cause a more dominant pro-inflammatory response than other biologic surgical meshes [14, 159].

Phasix™ is a slowly degradable biosynthetic surgical mesh. The term biosynthetic in the present context is defined as a naturally occurring (i.e., biologic origin) monomer or polymer manufactured by synthetic methods. Hydroxylated and non-hydroxylated forms of butyrate are naturally occurring molecules that belong to the group of short chain fatty acids. Butyrate is produced in abundant amounts by bacteria in the gastrointestinal tract to protect against chronic inflammation [55, 161], whereas 4-hydroxybutyrate (4HB) is produced in various tissues as a neurotransmitter [51] and with protective effects against stress and ischemia [52]. Other hydroxylated isoforms of butyrate are modulators of metabolism during ketosis and insulin-

resistance [110, 111]. The ability to knit the polymeric form of 4-hydroxybutyrate provides the potential to create a surgical mesh with predictable mechanical properties. One of the hypothesized physiologic functions of 4HB, which is the hydrolytic degradation product of Phasix™, is the activation of an M2-like, or regulatory macrophage phenotype. Results of the present study show the increased presence of $CD206^{+}$ macrophages immediately adjacent to Phasix™ mesh fibers at early post-implantation time points. Previous studies have shown that the presence of M2-like macrophages in the early post-implantation period biomaterials portends a favorable tissue remodeling outcome [14-16]. The present study lasted 35 days but a 52-week animal study and 18-month clinical data show favorable outcomes [3, 7].

The present study also showed the ability of a 4HB polymeric surgical mesh to modulate the endogenous upregulation of cathelicidin LL-37 in a clean soft tissue environment. The results showed robust expression of cathelicidin LL-37 with Phasix™ and highlight the importance of cathelicidin LL-37 during normal wound healing, as has been previously reported [40-43]. The stronger and more prolonged response obtained with the addition of 4HB can potentially provide for an improved clinical outcome.

It is clear from the results presented herein that the host response to different surgical mesh materials is distinctive. It has been suggested that the host response to biomaterials is the single most important determinant of the clinical outcome [162]. Although other variables in surgical mesh properties such as strength, degradability and cost are important considerations, the host response will largely determine functionality, the incidence of complications and other metrics of success vs. failure.

There are several limitations to the present study. Only a single marker (CD86 or CD206) were used to determine the phenotype of macrophages present at the mesh-tissue interface. These

have been used to identify macrophages pushed to a pro-inflammatory ($CD86^+$) activation state or an anti-inflammatory and regulatory activation state ($CD206^+$) by non-physiologic amounts of cytokines, LPS+IFN-γ and IL-4, respectively [10]. Additional characterization of the phenotypic profile of the subpopulations of macrophages, by using other surface, metabolic, and secreted markers would represent a more comprehensive characterization of phenotype. In addition, these meshes represent only a small subset of biosynthetic, synthetic and biologic meshes. Therefore conclusions may not extend to other meshes within these three groups.

4.5 CONCLUSION

Results of the present study are consistent with the premise that the phenotypic profile of macrophages interacting with implanted materials in the early post-operative period (within the first 14 days) are predictive of long term outcomes (months or years after implantation). Further, it appears that 4HB, the degradation product of Phasix™, increases the M2-like/M1-like ratio and facilitates robust cathelicidin LL-37 expression. A more complete understanding of the factors influencing the patterns of macrophage activation, and the molecular interactions of mesh materials with cells will influence the design of meshes tailored to promote site appropriate tissue repair.

5.0 COMPARATIVE RESISTANCE OF SURGICAL MESH MATERIALS TO DELIBERATE BACTERIAL CONTAMINATION IN A RAT SUBCUTANEOUS IMPLANT MODEL

5.1 INTRODUCTION

The design and composition of biomaterials for hernia repair have evolved considerably during the past several decades. Large pore size (type I meshes, greater than 75 μm pore size), monofilament, degradability, and mesh characteristics that promote host tissue integration are among the features now considered desirable [134, 157]. Modifications of mesh design and composition continue in an attempt to improve clinical outcomes, but the incidence of surgical site infection (SSI) remains problematic [163]. The risk of SSI following hernia repair depends on a number of factors including the type of material implanted, the repair technique utilized, the anatomic location of the hernia, and patient co-morbidities, among others. For example, post-surgical infection rates after inguinal hernia repair range from 0 to 6 percent [164], while infection rates following ventral hernia repair range from 3 to 22 percent [163, 165]. High infection rates have also been associated with incisional hernia repair procedures [166]. Complications from SSI are associated with increased morbidity, hospital length of stay, and cost. It is estimated that SSI is responsible for additional annual hospital charges of approximately $1.6 billion in the United

States alone. *Staphylococcus aureus*, a facultative anaerobic Gram-positive pathogen, is the most commonly reported cause of surgical mesh contamination [166, 167].

The use of metallic meshes to reinforce hernia repair achieved widespread use by 1946 [168], but the high incidence of post-operative complications including seroma formation, infection, and non-resolving drainage resulted in their use being abandoned by 1970 [169]. Synthetic mesh devices replaced metallic meshes but the challenges of infection, foreign body reaction, and encapsulation persist. Modifications of the physical properties of synthetic mesh materials have been made to diminish the foreign body reaction and subsequent encapsulation [141, 170], and biomaterials derived from biologic sources (e.g., extracellular matrix) are now commonly used in contaminated surgical fields [171-173]. A number of antimicrobial mesh coatings and synthetic-biologic hybrids have been developed and are being investigated for their ability to confer resistance to bacterial contamination [174] and modulate the host response after implantation [15, 16].

Each material has advantages and disadvantages. While synthetic meshes have highly tunable properties, can retain their tensile strength indefinitely (if non-degradable), and have successfully reduced some of the complications associated with metallic meshes, they are associated with intra-abdominal adhesion formation, enteric fistulas, and SSI [175]. Biologic materials, on the other hand, typically degrade and are replaced by host tissue, and provide a natural source of AMP which help to resist SSI [176]. However, the composition and processing of biologic materials are variable, the mechanical properties are not as tunable as those of synthetic materials, and the manufacturing is costly [177]. A new group of biodegradable biosynthetic meshes has recently become available for clinical use. Biosynthetic materials, which consist of naturally occurring molecules that can be manufactured by methods similar to synthetic materials,

have shown biocompatibility in different medical applications [3, 178-180]; but their ability to resist SSI has not yet been evaluated.

The objective of the present study is to determine the ability of five surgical mesh devices to resist deliberate contamination with a clinical strain of *S. aureus* in a rat model. The mesh devices investigated included a biosynthetic surgical mesh, three synthetic mesh surgical meshes, and a biologic graft.

5.2 MATERIALS AND METHODS

5.2.1 Experimental design

The surgical meshes Phasix™, Bard® Mesh, TIGR® Matrix Surgical Mesh, GORE® BIO-A® Tissue Reinforcement, and Strattice™ Reconstructive Tissue Matrix were implanted in a rat dorsal subcutaneous model for 14 days. Three inoculation levels of *S. aureus* were investigated: $1x10^4$ CFU, $1x10^6$ CFU, or $1x10^8$ CFU in 100 µl sterile PBS. A non-contaminated control group was included for each test article, and a sham-operated control group was also included. Six animals were used per test article at each inoculation level. Histologic evaluation and quantification of persistent bacterial contamination were conducted (Figure 24).

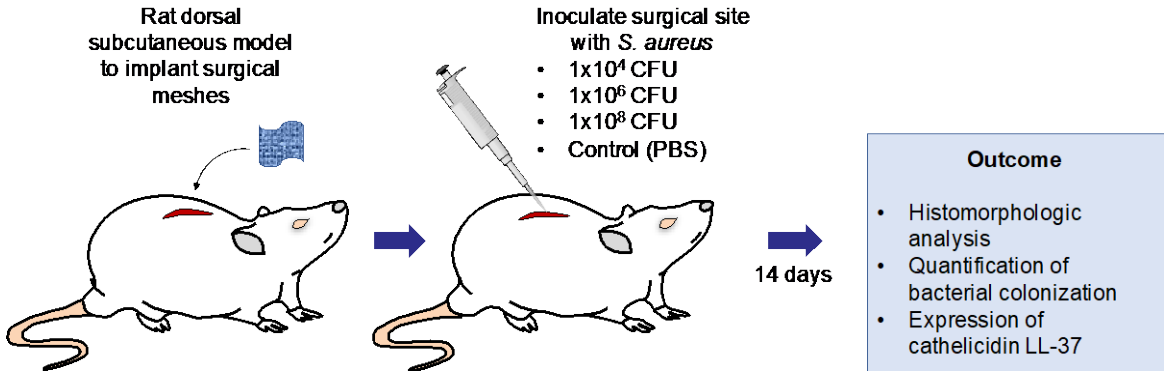

Figure 24. Experimental design overview.

A rat dorsal subcutaneous model was used to study surgical meshes characterized as synthetic (BARD® Mesh, TIGR®, and GORE® BIO-A®), biosynthetic (Phasix™ Mesh), or biologic (Strattice™ Reconstructive Tissue Matrix). After implantation, one of three different concentrations of a clinical isolate of *Staphylococcus aureus* was inoculated on the mesh material, or PBS was used as negative control. Sham-operated animals without mesh were used as a second control. The test devices were explanted after 14 days. The histologic characteristics of the harvested tissues were evaluated, and the amount of bacteria colonizing the meshes was quantified.

5.2.2 Preparation of Bacterial Inoculum

Single colonies of a clinical isolate *S. aureus* (ATCC 25923) were cultured in tryptic soy broth (Soybean-Casein Digest Medium) (BD, USA) overnight at 37°C with constant shaking. *S. aureus* concentration was calculated based on optical density and compared to a predetermined growth curve for the bacterial strain. $1x10^4$ CFU, $1x10^6$ CFU, or $1x10^8$ CFU *S. aureus* were obtained by diluting the cultured bacteria in 100 µl sterile PBS.

5.2.3 Surgical model, mesh implantation, and bacterial inoculation

All procedures were approved by and performed according to the guidelines of the Institutional Animal Care and Use Committee at the University of Pittsburgh (IACUC protocol #14020360).

Anesthesia was induced with 2.5-4% isoflurane, and surgical plane anesthesia was maintained with 0.5-4% isoflurane throughout the procedure. The surgical site was prepared by clipping the fur over the entire dorsal region, and cleaning the operative site with three alternating scrubs of providone-iodine surgical scrub and 70% isopropyl alcohol solutions. A final scrub with 70% isopropyl alcohol was applied and allowed to dry, followed by placement of sterile surgical drape(s) over the entire field. A 1 cm incision was made over the dorsal midline and a 2.0 cm x 3.0 cm subcutaneous pocket was created on one side of the midline (Figure 25A). Each animal received one sterile 2.0 cm x 3.0 cm test article implanted into the dorsal subcutaneous pocket (Figure 25B). Briefly, the mesh device was folded over itself to minimize contact with the skin during the implantation. Once positioned in the pocket, the test article was unfolded again. Following implantation, the surgical site was inoculated with one of the S. aureus preparations: $1.0x10^4$ CFU, $1.0x10^6$ CFU, or $1.0x10^8$ CFU in 100 µl sterile PBS (Figure 25C), designated as low, medium, and high inoculation levels, respectively. Non-contaminated test articles were injected with 100 µl sterile PBS. Following placement of the test article and the designated inoculum, the skin was closed with a continuous 4-0 VICRYL™ suture. For the sham-operated group, the inoculum was injected into the dorsal subcutaneous pocket without any implanted material, followed by skin closure as described above. Each animal was recovered from anesthesia, returned to its cage and allowed free access to food and water ad libitum. Rats were given Buprenex® (0.06 mg/kg subcutaneously) and Baytril® (5 mg orally) at the time of surgery and for 3 days post-surgery.

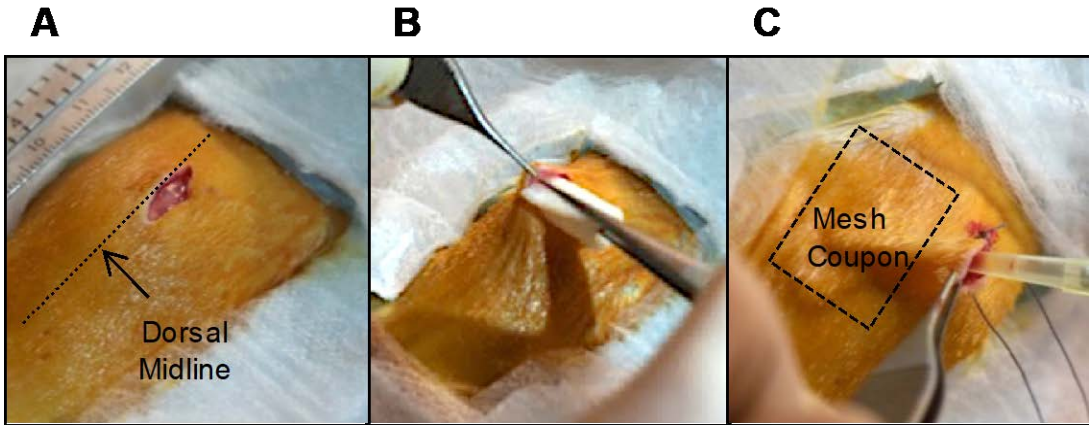

Figure 25. Surgical model of dorsal subcutaneous mesh implantation in a rat.

A. A 1 cm incision was made along the dorsal midline. B. A 2 cm x 3 cm subcutaneous pocket was bluntly dissected and a 2.0 cm x 3.0 cm mesh device implanted. C. After the mesh device was implanted, the pocket was injected with $1.0x10^4$ CFU, $1.0x10^6$ CFU, or $1.0x10^8$ CFU of a clinical isolate of *Staphylococcus aureus* suspended in 100 µl of sterile PBS. Sterile PBS was used as non-inoculation control. No-mesh controls were used at the different inoculum levels. After performing the injection, the incision was closed with suture.

5.2.4 Test article collection

At 14 days post implantation, animals were euthanized by CO_2 inhalation and subsequent cervical dislocation in accordance with the guidelines of the AVMA Panel of Euthanasia. Following euthanasia and using sterile technique, the skin was gently dissected and reflected, the specimens and surrounding tissue were collected. Using a sterile razor blade, 100 mg of the collected specimens were used for *S. aureus* quantification, as described below. The remaining specimen material was immersed in 10% NBF for subsequent histologic evaluation.

5.2.5 Qualitative histologic assessment

Fixed specimens were embedded in paraffin prior to being cut into 5 μm thick sections, and mounted onto glass slides. The specimens were deparaffinized with xylene immersion followed by exposure to a graded series of ethanol solutions (100%, 95%, 75%). Sections were stained with hematoxylin and eosin (H&E) and tissue gram stain (Sigma-Aldrich, USA) following manufacturer instructions. Stained slides were dehydrated using a graded series of ethanol solutions (75%, 95%, 100%) prior to cover-slipping. A total of 3 images were acquired for each H&E and gram stained section at the mesh/tissue interface. The criteria used to evaluate the histomorphology of the specimens included: organization of the tissue surrounding the implanted mesh devices, cellular infiltration, granulation tissue formation, and the presence of Gram-positive bacterial colonies.

5.2.6 Quantification of *Staphylococcus aureus*

100 mg of the explanted specimen (mesh and adjacent tissue) was taken from the lateral edge near the center of the mesh (Figure 26), immersed in 5 ml sterile PBS, and homogenized for 30 seconds at room temperature to dissociate adherent bacteria. 1:1,000 and 1:10,000 dilutions were prepared from the homogenized PBS solution. Undiluted and diluted solutions were plated on tryptic soy agar plates. The plates were incubated at 37°C for 24 h and *S. aureus* colonies quantified for each specimen.

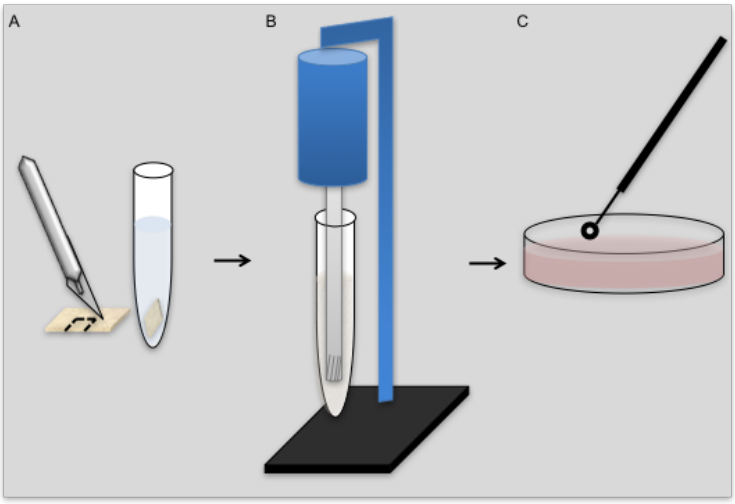

Figure 26. Quantification of *S. aureus* in explanted devices.

A. Explanted specimens were consistently cut as depicted, and 100 mg immersed in 5 ml sterile PBS. B. Dissociation of the adhered bacteria was made by homogenization for 30 seconds. C. Serial dilutions of the homogenized solution were plated on tryptic soy agar plates and incubated at 37°C for 24 h.

5.2.7 Statistical analysis

Quantification of *S. aureus* CFU is presented as the mean ± the standard error of the mean (SEM). Statistical differences between the mesh materials at each inoculation level were determined using a one-way non-parametric ANOVA test (Kruskal-Wallis test). The pattern of differences was evaluated with Dunn's multiple comparison test. A value $p<0.05$ was considered statistically significant. Statistical analysis was performed using GraphPad Prism version 6.07 (GraphPad Software, La Jolla CA, USA).

5.3 RESULTS

5.3.1 Macroscopic assessment

All animals survived the 14 days of study. All non-contaminated mesh materials were integrated with surrounding tissue, and were easily identified during necropsy. Animals receiving Strattice™ mesh showed clear signs of infection such as swelling and accumulation of purulent material at low ($1x10^4$ CFU), medium ($1x10^6$ CFU) and high ($1x10^8$ CFU) inoculation levels. Animals implanted with BARD® mesh showed these same signs of infection at medium ($1x10^6$ CFU) and high ($1x10^8$ CFU) inoculation levels. Animals implanted with BARD® Soft mesh, TIGR®, and GORE® BIO-A®, showed a macroscopic purulent exudate only at the highest ($1x10^8$ CFU) inoculation level. Likewise, the animals that received the Phasix™ mesh showed purulent exudate at the highest ($1x10^8$ CFU) inoculation level only, but the appearance was of less severity (decreased macroscopic purulent exudate) compared to the other explanted mesh devices. The no-mesh control groups showed edema and accumulation of purulent material at the highest ($1x10^8$ CFU) inoculation level.

5.3.2 Qualitative histologic assessment

At 14 days post implantation, all devices showed robust host mononuclear cell infiltration (Figure 27). Accumulation of host cells was localized around the fibers of synthetic (BARD® TIGR®, and GORE® BIO-A®) and biosynthetic (Phasix™) meshes, and along the margins of the Strattice™ mesh. For all meshes, the highest ($1x10^8$ CFU) inoculation level of *S. aureus* was associated with granulation tissue and necrosis surrounding the implanted device and a large number of

polymophonuclear (PMN) cells, characteristic of an active bacterial infection. H&E images from Strattice™ mesh showed an increased degradation of the mesh material compared to the non-contaminated control, and increased cellular infiltration within the device at the different bacterial inoculation levels ($1x10^4$ CFU, $1x10^6$ CFU, and $1x10^8$ CFU). The no-mesh control groups showed the prevalence of polymorphonuclear cells at the medium ($1x10^6$ CFU) and highest ($1x10^8$ CFU) inoculation levels.

The gram-stained sections showed no signs of bacterial contamination among the non-contaminated controls (Figure 28). Consistent with the macroscopic observations, the presence of Gram-positive bacteria was identified in both BARD® and Strattice™ mesh devices at all bacterial inoculation levels. Specimens containing BARD® Soft mesh did not show histologic evidence of bacterial colonization at low ($1x10^4$ CFU) and medium ($1x10^6$ CFU) inoculation levels; however, robust bacterial colonization was present around the mesh fibers at the highest ($1x10^8$ CFU) inoculation level. Phasix™ showed areas of bacterial colonization around the mesh fibers only at the highest level ($1x10^8$ CFU) of *S. aureus* inoculation. The no-mesh control groups showed the presence of Gram-positive bacteria at the highest ($1x10^8$ CFU) inoculation level.

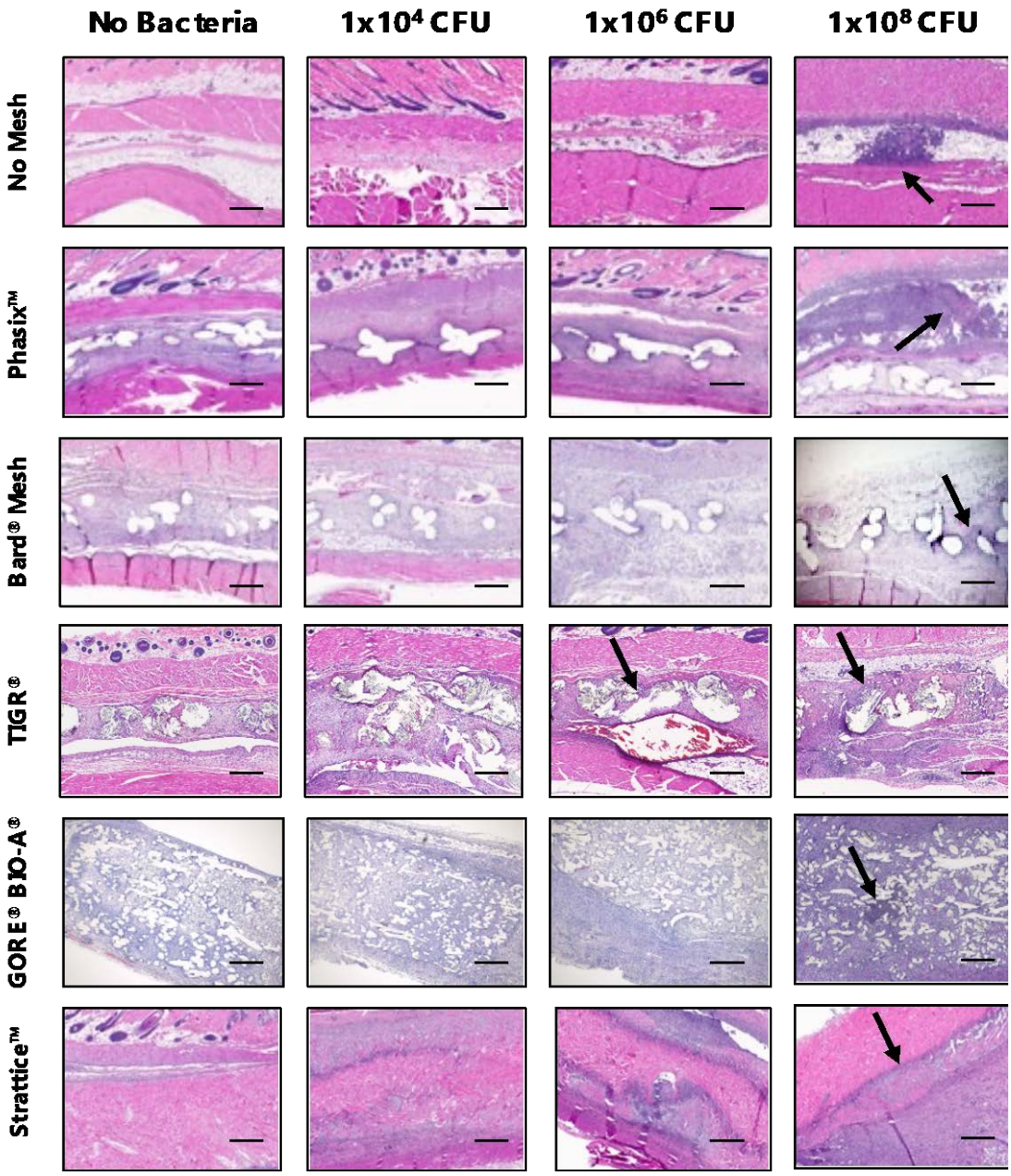

Figure 27. Histologic appearance of mesh devices after 14 days of *in vivo* implantation.

Representative hematoxylin and eosin stained histologic cross sections of each mesh/inoculation level were imaged at 40x magnification. Black arrows show necrotic tissue and granulation tissue formed as a consequence of the bacterial infection. Scale bar represents 500 µm.

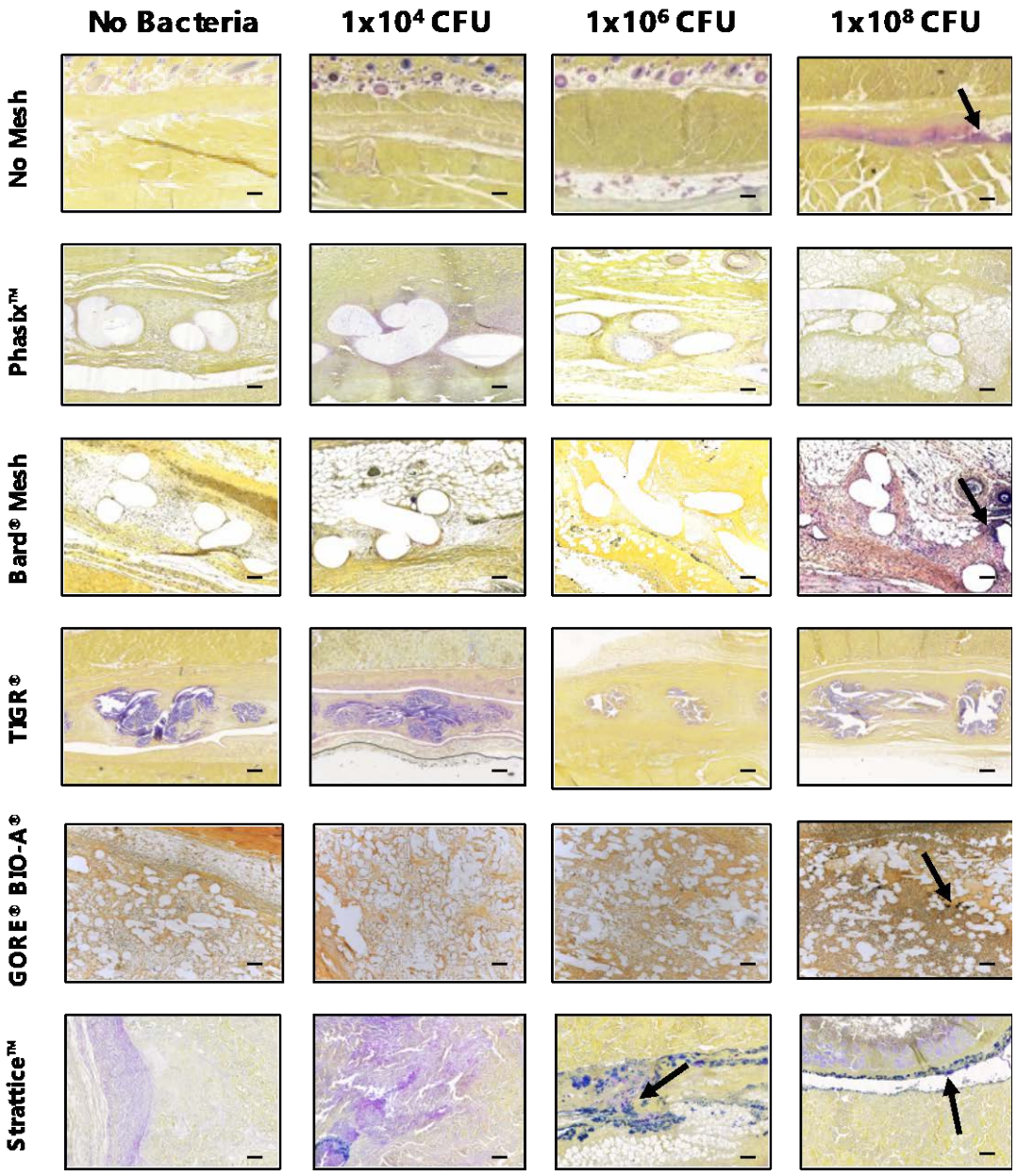

Figure 28. Gram staining oh histologic sections.

Gram stained histologic cross sections were imaged at 100x magnification. Black arrows indicate the areas that were positive for bacterial colonies. Scale bar represents 100 µm.

5.3.3 Quantification of *Staphylococcus aureus*

Quantification of bacteria within the explanted meshes at 14 days showed differences in the amount of viable *S. aureus* between the groups (Figure 29). The non-contaminated controls had undetectable levels of bacterial contamination, and the Kruskal-Wallis test showed no differences between the meshes (statistic=3.968, p=0.5540). For animals inoculated with a low level ($1x10^4$ CFU) of *S. aureus*, Strattice™ showed the greatest number of bacteria (1.32 ± 0.6) x 10^6 CFU, fewer bacteria was associated to BARD® Mesh (5.5 ± 3.4) x 10^5 CFU, TIGR® (7.5 ± 2.4) x 10^4 CFU, Phasix™ (7.2 ± 7.1) x 10^4 CFU, and the no-mesh control (1.2 ± 1.0) x 10^4 CFU, and the least number of bacteria was associated with GORE® BIO-A® (8.3 ± 6.5) CFU. Statistical analysis indicated significant differences between the number of bacterial colonies in GORE® BIO-A® compared with Strattice™, BARD® Mesh, and TIGR®.

At the medium ($1x10^6$ CFU) inoculation level, quantification of the *S. aureus* showed the greatest numbers for Strattice™ (1.6 ± 0.5) x 10^6 CFU and BARD® (1.6 ± 1.2) x 10^6 CFU, fewer number of bacteria for TIGR® (3.0 ± 1.0) x 10^5 CFU and the no-mesh control (1.8 ± 0.2) x 10^5 CFU, and the lowest number of bacteria associated with Phasix™ (8.5 ± 4.3) x 10^4 CFU and GORE® BIO-A® (8.0 ± 5.1) x 10^4. Statistical analysis showed that either Phasix™ and GORE® BIO-A® were significantly more resistant to bacterial contamination than Strattice™ and BARD®, respectively.

Data at the highest inoculation level ($1x10^8$ CFU) showed the greatest numbers of bacteria associated with BARD® Mesh (4.3 ± 0.4) x 10^6 CFU, TIGR® (4.2 ± 0.6) x 10^6 CFU, Strattice™ (3.7 ± 0.8) x 10^6 CFU from, and the no-mesh control (3.5 ± 0.6) x 10^6 CFU, a fewer number associated with GORE® BIO-A® (2.3 ± 1.7) x 10^6, and the lowest number of bacteria associated with Phasix™ (1.3 ± 0.7) x 10^6 CFU.

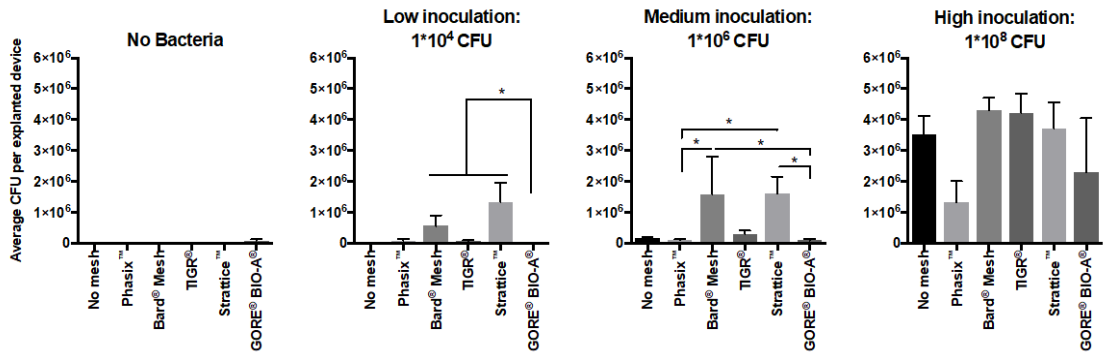

Figure 29. Quantification of colonizing *S. aureus* in explanted specimens 14 days post implantation.

Significance represents differences in the number of CFU between the mesh materials at each inoculation level. Values: Mean ± SEM, biologic replicates (N)=6. Differences between surgical meshes were evaluated using non-parametric ANOVA test, *$p<0.05$.

5.3.4 Cathelicidin LL-37 expression around implanted mesh devices with bacterial contamination

Expression of cathelicidin LL-37 was evaluated in the contaminated field of Phasix™, BARD® Mesh, or the no-mesh control. Immunolabeling images showed an increased secretion of this AMP around the Phasix™ fibers at all the bacterial inoculation levels (Figure 30).

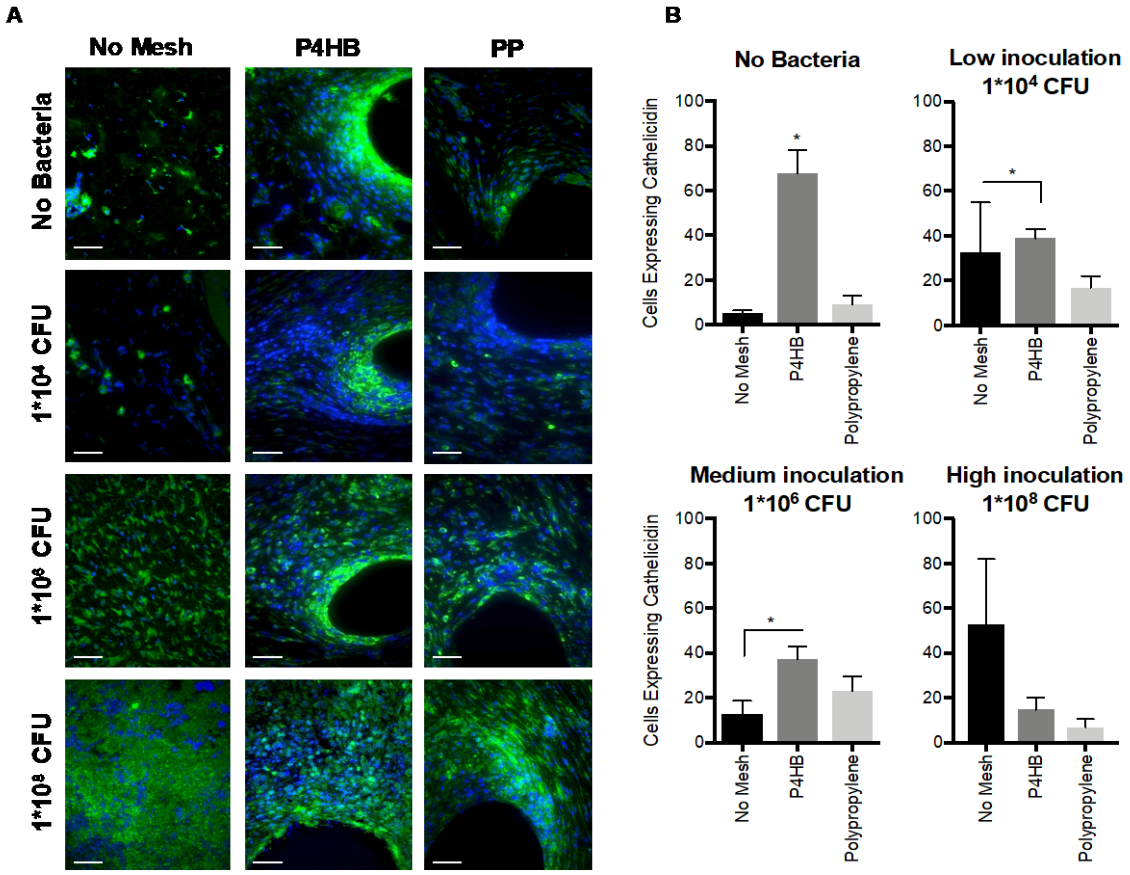

Figure 30. Cathelicidin LL-37 expression around implanted mesh devices with bacterial contamination.

A. Representative images of cathelicidin LL-37 expressed (green) around the fibers of P4HB and PP at each bacterial inoculation level. Scale bar 50 μm. B. Quantification of the number of cells expressing cathelicidin LL-37 at each inoculation level. Values: Mean ± SEM, biologic replicates (N)=3, technical replicates=3. Differences between surgical meshes were evaluated using non-parametric ANOVA test, *$p<0.05$.

5.4 DISCUSSION

The present study used a rat model of subcutaneous implantation to determine the ability of five surgical meshes to resist deliberate *S. aureus* contamination at three different inoculation levels. The test articles included three synthetic devices (BARD® Mesh, TIGR®, and GORE® BIO-A®), a biosynthetic device (Phasix™ Mesh), and a biologic mesh (Strattice™ Reconstructive Tissue Matrix). Results showed that Phasix™ and GORE® BIO-A® were more resistant to bacterial contamination than the polypropylene-derived mesh material (BARD®) and the biologic mesh (Strattice™) at low and medium inoculation levels. In addition, at the highest inoculation level, Phasix™ was associated with the lowest number of bacteria compared with all the other groups, suggesting a greater resistance to deliberate bacterial contamination.

Although various factors contribute to the development of SSI after hernia repair procedures [167, 181], the physical and chemical properties of surgical mesh materials are of obvious importance. The inherent characteristics of surgical mesh materials influence the adherence of bacteria to the mesh surface, the formation of bacterial biofilms, and the ability of the host to appropriately respond to and control bacterial contamination [182]. For example, it has been shown that monofilament woven/knitted materials are more resistant to bacterial contamination than multifilament structures [183].

The ability of a mesh material to degrade under physiological conditions is another factor influencing bacterial adherence and persistence of bacterial contamination. Synthetic non-degradable polymers like polypropylene are known to produce a host response characterized by increased cellular infiltration and production of pro-inflammatory signals that result in a foreign response to the implanted material [15, 184]. The fibrous tissue encapsulation response may impose a barrier that inhibits bacterial clearance. In contrast, degradable materials may provide a

temporary substratum for bacterial attachment, but this is progressively diminished as degradation of the mesh material occurs [140, 182]. The chemical composition of Phasix™ combined with its degradation properties may contribute to the high resistance to bacterial contamination for this mesh material.

The presence of innate antimicrobial peptides (AMP) has been demonstrated in some biologic derived materials like small intestinal submucosa (SIS) and urinary bladder matrix (UBM), which are capable of eliciting antimicrobial activity during the process of ECM degradation [113]. However, studies have shown that differences in tissue processing, such as applied detergents and chemical solutions, can affect the inherent properties of the ECM mesh materials [104]. Given the variable composition and processing methods of biologic mesh materials, further studies are required to fully evaluate the potential ability of biologic meshes to resist bacterial contamination.

There are limitations to the present study. The *in vivo* model involved a subcutaneous implant into a non-injury site (i.e., healthy tissue). The human clinical scenario would likely involve placement of a mesh as part of a ventral abdominal hernia repair. Selection of the model is a critical factor for consideration, and requires an understanding that there is no animal model that fully recapitulates the events involved in wound healing following SSI [185]. Confounding results have been found in studies comparing surgical mesh materials in contaminated environments in rat versus rabbit models [4], with materials being more susceptible to persistent bacterial contamination in one species than in the other. Physiological differences (i.e., host immune response) between rodents and rabbits, and susceptibility of each species to the bacterial inoculum employed, should be further studied to clarify the genesis of these differences.

Further analysis of the evaluated devices in a model of contamination in abdominal hernia repair would be of interest. However, since the degradation time of the surgical meshes included in this study exceeds one year, a long-term study would be required to determine whether their complete resorption correlates with bacterial clearance. It is important to note however, that an increased degradation rate was histologically observed for Strattice™ following bacterial inoculation compared to the non-contaminated control. Strattice™ degradation might be accelerated by the presence of bacterial enzymes and acidification of the microenvironmental pH as a result of the host immune response, among other factors. Finally, these devices represent only a small subset of synthetic, biosynthetic, and biologic devices, therefore generalized conclusions cannot be made for these three main groups based on the results found herein and only device-specific and comparative conclusions are valid.

6.0 DISSERTATION SUMMARY

The work presented in this dissertation characterized the host macrophage response to a biomaterial composed of poly (4-hydroxybutyrate) as a mode of understanding the early events associated with the surgical mesh material, which could explain the beneficial clinical outcome and decreased surgical site infection incidences reported for P4HB. The phenotypic spatiotemporal pattern of macrophages exposed to 4HB was evaluated. The immunomodulatory activity induced by 4HB upon exposed macrophages that were first activated with LPS-IFN-γ was identified. Additionally, the 4HB-mediated endogenous upregulation of AMP in stimulated macrophages was evaluated. The cellular and molecular mechanisms by which 4-hydroxybutyrate drives these modulatory effects were also investigated. Finally, a rat model of a partial thickness abdominal wall defect and a rat model of deliberate contamination in a subcutaneous tissue pocket were used to evaluate the host macrophage response and the expression of cathelicidin LL-37 in the presence of P4HB surgical mesh. The major findings of each aim are outlined below.

6.1 MAJOR FINDINGS

Specific aim 1: Determine the phenotypic response of macrophages following exposure to degradation byproducts of P4HB.

Sub Aim 1.1: Compare the phenotypic response of macrophages exposed to degradation byproducts of a subset of biosynthetic, synthetic, and biologic surgical mesh materials.

- Oligomeric and monomeric forms of 4HB are capable of inducing a rapid murine macrophage phenotype activation within the M1-like and M2-like spectrum, producing an expression pattern ($F4/80^{+high}/iNOS^{+low}/Arg^{+low}/Fizz1^{-}$). Transcriptional activation of TNF-α, IRF3, and KLF4 was also observed.
- Degradation byproducts of P4HB have immunomodulatory properties upon primary murine macrophages already committed to a pro-inflammatory phenotype (i.e., $M_{LPS/IFN-\gamma}$). In particular, inducing upregulation of Arginase 1, Fizz1, IL1-Ra, and KLF4.
- Four additional materials, commonly used in hernia repair applications, were characterized. Biomaterial composition (i.e., TMC+PLA+PGA vs. P4HB) induces a differential effect on the phenotypic activation pattern of exposed macrophages.

Specific aim 2: Identify the mechanisms responsible for the antimicrobial activity associated with the biosynthetic material composed of P4HB.

Sub Aim 2.1: Determine the direct and indirect (macrophage-mediated) antimicrobial effect of degradation byproducts of P4HB.

Sub Aim 2.2: Compare the expression of AMP of macrophages exposed to degradation byproducts of a subset of biosynthetic, synthetic, and biologic surgical mesh materials.

- P4HB exerts resistance to bacterial contamination using an indirect (cell-mediated) mechanism. Specifically, the mechanism occurs by promoting endogenous upregulation of antimicrobial peptides.

- 2HB, but not 3HB and 4HB, is a HDAC inhibitor in murine bone marrow-derived macrophages.
- Degradation products of P4HB induce an upregulation of cathelicidin LL-37 through a signaling-transduction mechanism. The key proteins identified in the transcriptional activation process were GPR109a, JNK, P38, NF-kB, and AP-1.
- Hydroxylated derivatives of butyrate differentially induce expression of cathelicidin LL-37.

Specific aim 3: Evaluate the spatiotemporal pattern of host tissue response to biosynthetic materials composed of P4HB implanted in a rat partial thickness abdominal wall defect model.

Sub-Aim 3.1: Compare the resistance to deliberate bacterial contamination of biosynthetic, synthetic, and biologic surgical mesh materials implanted in a rat subcutaneous model.

- Characterization of the spatiotemporal distribution of macrophages suggests the ability of P4HB to mitigate the acute pro-inflammatory response in a pre-clinical model.
- Four additional materials, commonly used in hernia repair applications, were characterized.
- Implanted P4HB induce upregulation of cathelicidin LL-37 when compared to other synthetic and biologic scaffolds.
- Implanted P4HB materials showed a higher resistance to deliberate bacterial contamination in an *in vivo* animal model compared to the other evaluated materials.

6.2 CONCLUSION

The work described in the present dissertation shows the effects of 4-hydroxybuturate upon the phenotypic activation of macrophages. 4HB promoted a pro-remodeling, regulatory phenotype and increased expression of AMP in subjected macrophages. The associated molecular mechanism involves transcriptional activation of cathelicidin LL-37 through MAP-kinase and NF-κB pathways.

In vivo, P4HB mitigates the acute, pro-inflammatory host response and provides an increased resistance to bacterial contamination. The results of this work expand the understanding of the biologic activity of 4HB in cells of the immune system and show its potential to promote a constructive tissue remodeling effect for regenerative medicine applications.

The described molecular mechanism has important clinical implications. The main proteins driving the activation of cathelicidin LL-37 expression, induced by 4HB, are direct targets of non-steroidal anti-inflammatory drugs (NSAID). Therefore, current post-surgical anti-inflammatory treatments might be reducing the potential of implanted surgical meshes composed of P4HB. Understanding of mechanisms involved in the endogenous upregulation promoting resistance to bacterial infection, and the inhibitory role of NSAIDs, may help clinical practitioners to determine alternative anti-inflammatory cocktails that do not inhibit the potential of implanted polymers composed of 4HB.

APPENDIX A

MACROPHAGE PHENOTYPIC MARKERS

Table 3. Description of macrophage phenotypic markers

Name	Description
Arginase 1	In murine macrophages, arginase 1 expression is induced by IL-4, microbes and microbial products, hypoxia, or lactic acid [186]. The activity of the metabolic enzyme arginase limits the availability of L-arginine to synthesize nitric oxide (NO), thus reducing the secretion of reactive nitrogen species. The enzyme arginase hydrolyses L-arginine into ornithine and urea. Further downstream pathways from this secretion promote cellular proliferation and tissue repair [187]. A number of different molecular mechanisms and associated transcription factors have been shown to regulate the transcriptional activation of arginase 1. Specific domains at the promoter have been recognized for PPARγ, PPARδ, STAT6, KLF4, C/EBPβ, PU.1, IRF8, and AP-1 [105, 188].
CD206	Identified as the mannose receptor C type 1 from the lectin family. It is a scavenger receptor that mediates endocytosis and phagocytosis processes. CD206 recognizes mannose N-linked glycoproteins that compose the coating of many pathogens [189]. Expression of the CD206 receptor is known to be induced by IL-4 and other anti-inflammatory cytokines [75, 153]. CD206 further induce inhibit pro-inflammatory signals mediated by Th1 cells [153].
CD68	CD68 is a marker restricted to monocytes and macrophages, and therefore has been widely used as a pan-macrophage marker [190]. It is a glycosylated type I transmembrane protein with functions as scavenger receptor and antigen processing protein [191].

Table 3 (continued)

Name	Description
CD86	The cluster of differentiation 86 (CD86) is a costimulatory receptor involved in regulation of the innate immune response and inflammation [192, 193]. Activation of CD86 in macrophages induces the expression of pro-inflammatory cytokines, such as IL-6, via activation of the NF-κB transcription factor [194].
F4/80	F4/80 is a transmembrane glycoprotein constitutively expressed by murine macrophages. The levels of expression are higher in macrophages than in monocytes. Although F4/80 is not indispensable for monocyte differentiation, its expression in macrophages is required to induce T cell differentiation [195].
Fizz1	Protein found in inflammatory zone 1 (Fizz1) is also identified as resistin-like molecule α (RELM-α) [196]. Fizz1 regulates the expression of the Th2 cytokines, IL-4 and IL-13.
IL1-Ra	Interleukin 1- receptor antagonist (IL1-Ra) is a soluble inhibitor secreted by immune cells to regulate pro-inflammatory events. IL1-Ra is a high affinity competitor of the interleukins 1 α and β (IL-1α and IL-1β) blocking the response mediated by the interleukin 1 receptor 1 (IL1-R1) [197].
iNOS	Induced nitric oxide synthase (iNOS) is regulated via transcriptional mechanisms induced by the pro-inflammatory cytokines IL-1β, IFN-γ and TNF-α, microbial products such as LPS, and hypoxia. iNOS is a competitor of argines 1. iNOS metabolizes arginine to NO and citrulline, therefore promoting the production of reactive nitrogen species [187].
IRF3	Interferon regulatory factor 3 (IRF3) is an important transcription factor mediating viral and bacterial infections [198]. Activation of IRF3 has been associated with downstream secretion of interferon 1β (IFN-1β) and interleukin-6 (IL-6), ultimately leading to NO production [199].
KLF4	Kruppel-like factor 4 (KLF4) is a transcription regulator required for both monocyte differentiation into macrophages [200] and IL-4-induced macrophage activation [201]. Binding of KLF4 to the promoter of the *arginase* gene is required for its transcriptional activation [202].
KLF6	Kruppel-like factor 6 (KLF6) is another transcription factor of the Kruppel-like family of zinc finger proteins. KLF6 activation is induced by LPS and IFN-γ, and has been shown to be inhibited by IL-4 and IL-13. KLF6 modulates the activity of NF-κB, stabilizing the pro-inflammatory response in activated macrophages [203].

Table 3 (continued)

Name	Description
PCK2	Phosphoenolpyruvate carboxykinase 2 (PCK2) is localized in the mitochondria. In glucose-limited microenvironments, PCK2 catalyzes the conversion of glutamine into phosphoenolpyruvate [204].
STAT1	Signal transducers and activators of transcription-1 (STAT1). STAT1 plays an important role in the activation of signaling cascades induced by toll-like receptors (TLR) [205] and interferon receptors [206]. STAT1 mediates the secretion of iNOS, MCP-5, and IP-10, through an IFN-β-activated signaling cascade [207].
STAT2	It has been suggested that STAT1 and STAT2 are functionally redundant; upon activation, STAT1 and STAT2 form a heterodimer to mediate the transcriptional activation of IFN-1 (α & β)-induced genes [208]. It has been shown that human monocyte differentiation into macrophages requires STAT1-induced STAT2 activation [209].
STAT3	After pro-inflammatory responses, macrophages activate additional signaling cascades towards resolution of the pro-inflammation. Activation of STAT3 is required to mediate this resolution phase. STAT3 induces an indirect IL-10 secretion through upregulation of IFN-1 [210].
TNF-α	Tumor necrosis factor α (TNF-α) is a pro-inflammatory cytokine responsible of multiple pro-inflammatory effects, such as T cell activation, histamine release, among others [211]. TNF-α expression is essential to protect against intracellular pathogens. TNF-α has an inhibitory effect on arginase 1 secretion, thus preventing the alternative activation of macrophages (M2-like response) [186].
YM1	YM1 is a chitinase-like secretory lectin [196, 212]. YM1 secretion is strongly induced by IL-4 and IL-13 stimuli through a signal transduction mediated by STAT6 [213].

APPENDIX B

PCR PRIMER SEQUENCES

Table 4. PCR murine primer sequences

mRNA	Primer sequence	Accession number	Ref.
YM1	F: 5'-GGATGGCTACACTGGAGAAA-3' R: 5'-AGAAGGGTCACTCAGGATAA-3'	NM_009892.3	[68]
CD206	F: 5'-GCAGACTGCACCTCTGCCGG-3' R: 5'-TGCTGCTTGCAGCTTGCCCT-3'	NM_008625.2	[68]
Fizz1	F: 5'-CCCTCCACTGTAACGAAG-3' R: 5'-GTGGTCCAGTCAACGAGTAA-3'	NM_020509.3	[68]
TNF-α	F: 5'-CCACCACGCTCTTCTGTCTA-3' R: 5'-AGGGTCTGGGCCATAGAACT-3'	NM_013693.3	[75]
IRF3	F: 5'-GATGGCTGACTTTGGCATCT-3' R: 5'-ACCGGAAATTCCTCTTCCAG-3'	NM_016849.4	[75]
IL1-Ra	F: 5'-GTGAGACGTTGGAAGGCAGT-3' R: 5'-GCATCTTGCAGGGTCTTTTC-3'	NM_031167.5	[75]
KLF4	F: 5'-GCCACCCACACTTGTGACTA-3' R: 5'-CAGTGGTAAGGTTTCTCGCC-3'	NM_010637.3	[75]
KLF6	F: 5'-CACGAAACGGGCTACTTCTC-3' R: 5'-ACACGTAGCAGGGCTCACTC-3'	NM_011803.2	[75]
STAT1	F: 5'-TCCCGTACAGATGTCCATGAT-3' R: 5'-CTGAATATTTCCCTCCTGGG-3'	NM_001357627.1	[75]
STAT2	F: 5'-CGCTTGGAGAATTGGAAGTT-3' R: 5'-GCTGTCAAGGTTCTGCAACA-3'	NM_019963.2	[75]

Table 4 (continued)

mRNA	Primer sequence	Accession number	Ref.
STAT3	F: 5'-CTCAGCCCCGGAGACAGT-3' R: 5'-CTGCTCCAGGTAGCGTGTGT-3'	NM_213659.3	[75]
PCK2	F: 5'-GTACTGGGAAGGCATTGACC-3' R: 5'-AGTTTGGATGTGCACAGGGT-3'	NM_028994.3	[75]
Cramp	F: 5'-CTTCAACCAGCAGTCCCTAGACA-3' R: 5'-TCCAGGTCCAGGAGACGGTA-3'	NM_009921.2	[214]
β-Defensin 2	F: 5'-AAGTATTGGATACGAAGCAG-3' R: 5'-TGGCAGAAGGAGGACAAATG-3'	NM_010030.1	[215]
β-Defensin 3	F: 5'-GCATTGGCAACACTCGTCAGA-3' R: 5'-CGGGATCTTGGTCTTCTCTA-3'	NM_013756.2	[215]
β-Defensin 4	F: 5'-GCAGCCTTTACCCAAATTATC-3' R: 5'-ACAATTGCCAATCTGTCGAA-3'	NM_019728.4	[215]
Hprt1	F: 5'-TGATCAGTCAACGGGGGACA-3', R: 5'-TTCGAGAGGTCCTTTTCACCA-3'	NM_013556.2	[216]

BIBLIOGRAPHY

1. Williams, S.F., S. Rizk, and D.P. Martin, *Poly-4-hydroxybutyrate (P4HB): a new generation of resorbable medical devices for tissue repair and regeneration.* Biomed Tech, 2013. **58**(5): p. 439-452.

2. Martin, D.P. and S.F. Williams, *Medical applications of poly-4-hydroxybutyrate: a strong flexible absorbable biomaterial* BIochemical Engineering Journal, 2003. **16**: p. 97-105.

3. Deeken, C.R. and B.D. Matthews, *Characterization of the Mechanical Strength, Resorption Properties, and Histologic Characteristics of a Fully Absorbable Material (Poly-4-hydroxybutyrate-PHASIX Mesh) in a Porcine Model of Hernia Repair*. ISRN Surg, 2013. **2013**: p. 238067.

4. Jacobsen, G. and C. DuCoin, *Biodegradable Meshes in Abdominal Wall Surgery*, in *Hernia Surgery: Current Principles*, Y.W. Novitsky, Editor. 2016, Springer International Publishing: Switzerland. p. 71-78.

5. Plymale, M.A., et al., *Ventral hernia repair with poly-4-hydroxybutyrate mesh.* Surg Endosc, 2017.

6. Buell, J.F., et al., *Initial Experience With Biologic Polymer Scaffold (Poly-4-hydroxybuturate) in Complex Abdominal Wall Reconstruction.* Ann Surg, 2017. **266**(1): p. 185-188.

7. Roth, J.S., et al., *Prospective evaluation of poly-4-hydroxybutyrate mesh in CDC class I/high-risk ventral and incisional hernia repair: 18-month follow-up.* Surg Endosc, 2017.

8. Witte, M.B. and A. Barbul, *General Principles of Wound Healing.* Surgical Clinics of North America, 1997. **77**(3): p. 509-528.

9. Naranjo, J.E., et al., *Regenerative Medicine: lessons from Mother Nature.* Regenerative Medicine, 2016. **11**(8): p. 767–775.

10. Mantovani, A., et al., *The chemokine system in diverse forms of macrophage activation and polarization.* Trends Immunol, 2004. **25**(12): p. 677-86.

11. Tatara, A.M., D.P. Kontoyiannis, and A.G. Mikos, *Drug delivery and tissue engineering to promote wound healing in the immunocompromised host: Current challenges and future directions.* Adv Drug Deliv Rev, 2017.

12. Londono, R. and S.F. Badylak, *Factors Wich Affect the Host Response to Biomaterials*, in *Host Response to Biomaterials The impact of Host Response on Biomaterial Selection*, S.F. Badylak, Editor. 2015, Elsevier: USA. p. 1-10.

13. Anderson, J. and S. Cramer, *Perspectives on the Inflammatory, Healing, and Foreign Body Responses to Biomaterials and Medical Devices*, in *Host Response to Biomaterials The impact of Host Response on Biomaterial Selection*, S.F. Badylak, Editor. 2015, Elsevier: USA. p. 13-36.

14. Brown, B.N., et al., *Macrophage phenotype as a predictor of constructive remodeling following the implantation of biologically derived surgical mesh materials.* Acta Biomater, 2012. **8**(3): p. 978-87.

15. Wolf, M.T., et al., *Macrophage polarization in response to ECM coated polypropylene mesh.* Biomaterials, 2014. **35**(25): p. 6838-49.

16. Faulk, D.M., et al., *ECM hydrogel coating mitigates the chronic inflammatory response to polypropylene mesh.* Biomaterials, 2014. **35**(30): p. 8585-95.

17. Ibrahim, A.M., et al., *Properties of meshes used in hernia repair: a comprehensive review of synthetic and biologic meshes.* J Reconstr Microsurg, 2015. **31**(2): p. 83-94.

18. Sheikh, Z., et al., *Macrophages, Foreign Body Giant Cells and Their Response to Implantable Biomaterials.* Materials (Basel), 2015. **8**(9): p. 5671-5701.

19. Kalaba, S., et al., *Design Strategies and Applications of Biomaterials and Devices for Hernia Repair.* Bioact Mater, 2016. **1**(1): p. 2-17.

20. Falagas, M.E. and S.K. Kasiakou, *Mesh-related infections after hernia repair surgery.* Clin Microbiol Infect, 2005. **11**(1): p. 3-8.

21. Klopfleisch, R. and F. Jung, *The pathology of the foreign body reaction against biomaterials.* J Biomed Mater Res A, 2017. **105**(3): p. 927-940.

22. Wang, Y., et al., *Foreign Body Reaction to Implantable Biosensors: Effects of Tissue Trauma and Implant Size.* J Diabetes Sci Technol, 2015. **9**(5): p. 966-77.

23. Hachim, D., et al., *Shifts in macrophage phenotype at the biomaterial interface via IL-4 eluting coatings are associated with improved implant integration.* Biomaterials, 2017. **112**: p. 95-107.

24. Deeken, C.R. and S.P. Lake, *Mechanical Properties of the Abdominal Wall and Biomaterials Utilized for Hernia Repair.* Journal of the Mechanical Behavior of Biomedical Materials, 2017. **74**: p. 411-427.

25. Deeken, C.R., et al., *Physicomechanical evaluation of polypropylene, polyester, and polytetrafluoroethylene meshes for inguinal hernia repair.* J Am Coll Surg, 2011. **212**(1): p. 68-79.

26. Perez-Kohler, B., et al., *Bacterial adhesion to biological versus polymer prosthetic materials used in abdominal wall defect repair: do these meshes show any differences in vitro?* Hernia, 2015.

27. Yuan, R., et al., *Low-grade inflammatory polarization of monocytes impairs wound healing.* J Pathol, 2016. **238**(4): p. 571-83.

28. Schultz, G.S., et al., *Dynamic reciprocity in the wound microenvironment.* Wound Repair Regen, 2011. **19**(2): p. 134-48.

29. Bueno-Lledo, J., et al., *Predictors of mesh infection and explantation after abdominal wall hernia repair.* Am J Surg, 2017. **213**(1): p. 50-57.

30. Batoni, G., G. Maisetta, and S. Esin, *Antimicrobial peptides and their interaction with biofilms of medically relevant bacteria.* Biochim Biophys Acta, 2015.

31. Costerton, J.W., P.S. Stewart, and E.P. Greenberg, *Bacterial Biofilms: A Common Cause of Persistent Infections.* Science, 1999. **284**(5418): p. 1318-1322.

32. Duplantier, A.J. and M.L. van Hoek, *The Human Cathelicidin Antimicrobial Peptide LL-37 as a Potential Treatment for Polymicrobial Infected Wounds.* Front Immunol, 2013. **4**: p. 143.

33. Wong, T.W. and N.A. Ramli, *Carboxymethylcellulose film for bacterial wound infection control and healing.* Carbohydr Polym, 2014. **112**: p. 367-75.

34. Jamal, M., et al., *Bacterial biofilm and associated infections.* J Chin Med Assoc, 2018. **81**(1): p. 7-11.

35. McCloskey, A.P., B.F. Gilmore, and G. Laverty, *Evolution of antimicrobial peptides to self-assembled peptides for biomaterial applications.* Pathogens, 2014. **3**(4): p. 791-821.

36. Kasetty, G., et al., *Anti-endotoxic and antibacterial effects of a dermal substitute coated with host defense peptides.* Biomaterials, 2015. **53**: p. 415-25.

37. Zasloff, M., *Inducing endogenous antimicrobial peptides to battle infections.* Proc Natl Acad Sci U S A, 2006. **103**(24): p. 8913-4.

38. Wang, G., *Human antimicrobial peptides and proteins.* Pharmaceuticals (Basel), 2014. **7**(5): p. 545-94.

39. Vandamme, D., et al., *A comprehensive summary of LL-37, the factotum human cathelicidin peptide.* Cell Immunol, 2012. **280**(1): p. 22-35.

40. Silva, J.P., et al., *Improved burn wound healing by the antimicrobial peptide LLKKK18 released from conjugates with dextrin embedded in a carbopol gel.* Acta Biomater, 2015. **26**: p. 249-62.

41. Ramos, R., et al., *Wound healing activity of the human antimicrobial peptide LL37.* Peptides, 2011. **32**(7): p. 1469-76.

42. Winter, J. and M. Wenghoefer, *Human Defensins: Potential Tools for Clinical Applications.* Polymers, 2012. **4**(4): p. 691-709.

43. Koczulla, R., et al., *An angiogenic role for the human peptide antibiotic LL-37/hCAP-18.* J Clin Invest, 2003. **111**(11): p. 1665-72.

44. Stock, U.A., et al., *Patch augmentation of the pulmonary artery with bioabsorbable polymers and autologous cell seeding.* J Thorac Cardiovasc Surg, 2000. **120**(6): p. 1158-67; discussion 1168.

45. Odermatt, E.K., et al., *MonoMax Suture: A New Long-Term Absorbable Monofilament Suture Made from Poly-4-Hydroxybutyrate.* International Journal of Polymer Science, 2012. **2012**: p. 1-12.

46. Meur, S.L., et al., *Poly(4-hydroxybutyrate) (P4HB) production in recombinant Escherichia coli: P4HB synthesis is uncoupled with cell growth.* Microbial Cell Factories, 2013. **12**: p. 123.

47. Nelson, T., et al., *The Extraneural Distribution of γ-Hydroxybutyrate.* Journal of Neurochemistry, 1981. **37**(5): p. 1345-1348.

48. Klein, C., et al., *Pharmacological doses of gamma-hydroxybutyrate (GHB) potentiate histone acetylation in the rat brain by histone deacetylase inhibition.* Neuropharmacology, 2009. **57**(2): p. 137-47.

49. Zhang, G.F., et al., *Metabolism of gamma-hydroxybutyrate in perfused rat livers.* Biochem J, 2012. **444**(2): p. 333-41.

50. Bay, T., et al., *GHB receptor targets in the CNS: focus on high-affinity binding sites.* Biochem Pharmacol, 2014. **87**(2): p. 220-8.

51. Nelson, T., et al., *The extraneural distribution of g-hydroxybutyrate.* Journal of Neurochemistry, 1981. **37**(5): p. 1345-1348.

52. Mamelak, M., *Alzheimer' s disease, oxidative stress and gammahydroxybutyrate.* Neurobiol Aging, 2007. **28**(9): p. 1340-60.

53. Spaeth, M., et al., *Sodium oxybate therapy provides multidimensional improvement in fibromyalgia: results of an international phase 3 trial.* Ann Rheum Dis, 2012. **71**(6): p. 935-42.

54. Spaeth, M., et al., *Long-term tolerability and maintenance of therapeutic response to sodium oxybate in an open-label extension study in patients with fibromyalgia.* Arthritis Research & Therapy, 2013. **15**: p. R185.

55. Donohoe, D.R., et al., *The Warburg effect dictates the mechanism of butyrate-mediated histone acetylation and cell proliferation.* Mol Cell, 2012. **48**(4): p. 612-26.

56. Donohoe, D.R., et al., *The microbiome and butyrate regulate energy metabolism and autophagy in the mammalian colon.* Cell Metab, 2011. **13**(5): p. 517-26.

57. Park, J.S., et al., *Anti-inflammatory effects of short chain fatty acids in IFN-gamma-stimulated RAW 264.7 murine macrophage cells: involvement of NF-kappaB and ERK signaling pathways.* Int Immunopharmacol, 2007. **7**(1): p. 70-7.

58. Campbell, Y., M.L. Fantacone, and A.F. Gombart, *Regulation of antimicrobial peptide gene expression by nutrients and by-products of microbial metabolism.* Eur J Nutr, 2012. **51**(8): p. 899-907.

59. Jiang, W., et al., *Differential regulation of human cathelicidin LL-37 by free fatty acids and their analogs.* Peptides, 2013. **50**: p. 129-38.

60. Steinmann, J., et al., *Phenylbutyrate induces antimicrobial peptide expression.* Antimicrob Agents Chemother, 2009. **53**(12): p. 5127-33.

61. Daghighi, S., et al., *Infection resistance of degradable versus non-degradable biomaterials: an assessment of the potential mechanisms.* Biomaterials, 2013. **34**(33): p. 8013-7.

62. Busscher, H.J., et al., *Biomaterial-Associated Infection: Locating the Finish Line in the Race for the Surface.* Science Translational Medicine, 2012. **4**(153): p. 153rv10-153rv10.

63. Engelsman, A.F., et al., *The phenomenon of infection with abdominal wall reconstruction.* Biomaterials, 2007. **28**(14): p. 2314-27.

64. Perez-Kohler, B., et al., *Inhibition of Staphylococcus aureus Adhesion to the Surface of a Reticular Heavyweight Polypropylene Mesh Soaked in a Combination of Chlorhexidine and Allicin: An In vitro Study.* PLoS One, 2015. **10**(5): p. e0126711.

65. Cohen, L.E., et al., *Comparison of Antibiotic-Coated versus Uncoated Porcine Dermal Matrix.* Plast Reconstr Surg, 2016. **138**(5): p. 844e-855e.

66. Zaat, S., C. Broekhuizen, and M. Riool, *Host tissue as a niche for biomaterial-associated infection.* Future Microbiology, 2010. **5**(8): p. 1149-1151.

67. Brown, B.N. and S.F. Badylak, *Expanded applications, shifting paradigms and an improved understanding of host-biomaterial interactions.* Acta Biomater, 2013. **9**(2): p. 4948-55.

68. Ji, J., et al., *Microbial metabolite butyrate facilitates M2 macrophage polarization and function.* Sci Rep, 2016. **6**: p. 24838.

69. Bruns, H., et al., *Vitamin D–dependent induction of cathelicidin in human macrophages results in cytotoxicity against high-grade B cell lymphoma.* Science Translational Medicine, 2015. **7**(282).

70. De Smet, K. and R. Contreras, *Human antimicrobial peptides: defensins, cathelicidins and histatins.* Biotechnol Lett, 2005. **27**(18): p. 1337-47.

71. Heilborn, J.D., et al., *The cathelicidin anti-microbial peptide LL-37 is involved in re-epithelialization of human skin wounds and is lacking in chronic ulcer epithelium.* J Invest Dermatol, 2003. **120**(3): p. 379-89.

72. Schwab, M., et al., *Role of nuclear hormone receptors in butyrate-mediated up-regulation of the antimicrobial peptide cathelicidin in epithelial colorectal cells.* Mol Immunol, 2007. **44**(8): p. 2107-14.

73. Meng, F.W., et al., *Solubilized extracellular matrix from brain and urinary bladder elicits distinct functional and phenotypic responses in macrophages.* Biomaterials, 2015. **46**: p. 131-40.

74. Dziki, J.L., et al., *Solubilized extracellular matrix bioscaffolds derived from diverse source tissues differentially influence macrophage phenotype.* J Biomed Mater Res A, 2017. **105**(1): p. 138-147.

75. Huleihel, L., et al., *Macrophage phenotype in response to ECM bioscaffolds.* Semin Immunol, 2017. **29**: p. 2-13.

76. Huleihel, L., et al., *Matrix-Bound Nanovesicles Recapitulate Extracellular Matrix Effects on Macrophage Phenotype.* Tissue Eng Part A, 2017. **23**(21-22): p. 1283-1294.

77. Martin, D.P., et al., *Characterization of poly-4-hydroxybutyrate mesh for hernia repair applications.* J Surg Res, 2013. **184**(2): p. 766-73.

78. Gao, Y., et al., *Methodology of fibroblast and mesenchymal stem cell coating of surgical meshes: a pilot analysis.* J Biomed Mater Res B Appl Biomater, 2014. **102**(4): p. 797-805.

79. Cavallo, J.A., et al., *Remodeling characteristics and biomechanical properties of a crosslinked versus a non-crosslinked porcine dermis scaffolds in a porcine model of ventral hernia repair.* Hernia, 2015. **19**(2): p. 207-18.

80. Sicari, B.M., et al., *The promotion of a constructive macrophage phenotype by solubilized extracellular matrix.* Biomaterials, 2014. **35**(30): p. 8605-12.

81. Freytes, D.O., et al., *Preparation and rheological characterization of a gel form of the porcine urinary bladder matrix.* Biomaterials, 2008. **29**(11): p. 1630-7.

82. Englen, M.D., et al., *Granulocyte/macrophage colony-stimulating factor is expressed and secreted in cultures of murine L929 cells.* J Immunol Methods, 1995. **184**(2): p. 281-3.

83. Shearer, J.D., et al., *Differential regulation of macrophage arginine metabolism: a proposed role in wound healing.* Am J Physiol, 1997. **272**(2 Pt 1): p. E181-90.

84. Brown, B.N., et al., *Macrophage polarization: an opportunity for improved outcomes in biomaterials and regenerative medicine.* Biomaterials, 2012. **33**(15): p. 3792-802.

85. Yu, K., et al., *Engineering biomaterials surfaces to modulate the host response.* Colloids Surf B Biointerfaces, 2014. **124**: p. 69-79.

86. Al-Maawi, S., et al., *In vivo cellular reactions to different biomaterials-Physiological and pathological aspects and their consequences.* Semin Immunol, 2017. **29**: p. 49-61.

87. Morris, A.H., D.K. Stamer, and T.R. Kyriakides, *The host response to naturally-derived extracellular matrix biomaterials.* Semin Immunol, 2017. **29**: p. 72-91.

88. Ganapathy, V., et al., *Transporters and receptors for short-chain fatty acids as the molecular link between colonic bacteria and the host.* Curr Opin Pharmacol, 2013. **13**(6): p. 869-74.

89. Bhutia, Y.D., et al., *SLC transporters as a novel class of tumour suppressors: identity, function and molecular mechanisms.* Biochem J, 2016. **473**(9): p. 1113-24.

90. Thangaraju, M., et al., *GPR109A is a G-protein-coupled receptor for the bacterial fermentation product butyrate and functions as a tumor suppressor in colon.* Cancer Res, 2009. **69**(7): p. 2826-32.

91. Gambhir, D., et al., *GPR109A as an anti-inflammatory receptor in retinal pigment epithelial cells and its relevance to diabetic retinopathy.* Invest Ophthalmol Vis Sci, 2012. **53**(4): p. 2208-17.

92. Graff, E.C., et al., *Anti-inflammatory effects of the hydroxycarboxylic acid receptor 2.* Metabolism, 2016. **65**(2): p. 102-13.

93. Tan, J., et al., *The role of short-chain fatty acids in health and disease.* Adv Immunol, 2014. **121**: p. 91-119.

94. Sun, M., et al., *Microbiota metabolite short chain fatty acids, GPCR, and inflammatory bowel diseases.* J Gastroenterol, 2017. **52**(1): p. 1-8.

95. Offermanns, S., *Hydroxy-Carboxylic Acid Receptor Actions in Metabolism.* Trends Endocrinol Metab, 2017. **28**(3): p. 227-236.

96. Feingold, K.R., et al., *Inflammation stimulates niacin receptor (GPR109A/HCA2) expression in adipose tissue and macrophages.* J Lipid Res, 2014. **55**(12): p. 2501-8.

97. Digby, J.E., et al., *Anti-inflammatory effects of nicotinic acid in human monocytes are mediated by GPR109A dependent mechanisms.* Arterioscler Thromb Vasc Biol, 2012. **32**(3): p. 669-76.

98. Fukushima, K., *Poly(trimethylene carbonate)-based polymers engineered for biodegradable functional biomaterials.* Biomater Sci, 2015. **4**(1): p. 9-24.

99. Bat, E., et al., *Macrophage-mediated erosion of gamma irradiated poly(trimethylene carbonate) films.* Biomaterials, 2009. **30**(22): p. 3652-61.

100. Romero-Garcia, S., et al., *Lactate Contribution to the Tumor Microenvironment: Mechanisms, Effects on Immune Cells and Therapeutic Relevance.* Front Immunol, 2016. **7**: p. 52.

101. Errea, A., et al., *Lactate Inhibits the Pro-Inflammatory Response and Metabolic Reprogramming in Murine Macrophages in a GPR81-Independent Manner.* PLoS One, 2016. **11**(11): p. e0163694.

102. Chen, P., et al., *Gpr132 sensing of lactate mediates tumor-macrophage interplay to promote breast cancer metastasis.* Proc Natl Acad Sci U S A, 2017. **114**(3): p. 580-585.

103. Baardman, J., et al., *Metabolic-epigenetic crosstalk in macrophage activation.* Epigenomics, 2015. **7**(7): p. 1155-64.

104. Reing, J.E., et al., *The effects of processing methods upon mechanical and biologic properties of porcine dermal extracellular matrix scaffolds.* Biomaterials, 2010. **31**(33): p. 8626-33.

105. Pourcet, B. and I. Pineda-Torra, *Transcriptional regulation of macrophage arginase 1 expression and its role in atherosclerosis.* Trends Cardiovasc Med, 2013. **23**(5): p. 143-52.

106. Xiong, H., et al., *Butyrate upregulates endogenous host defense peptides to enhance disease resistance in piglets via histone deacetylase inhibition.* Sci Rep, 2016. **6**: p. 27070.

107. Kida, Y., T. Shimizu, and K. Kuwano, *Sodium butyrate up-regulates cathelicidin gene expression via activator protein-1 and histone acetylation at the promoter region in a human lung epithelial cell line, EBC-1.* Mol Immunol, 2006. **43**(12): p. 1972-81.

108. Schauber, J., et al., *Histone-deacetylase inhibitors induce the cathelicidin LL-37 in gastrointestinal cells.* Mol Immunol, 2004. **41**(9): p. 847-54.

109. Sarker, P., et al., *Phenylbutyrate counteracts Shigella mediated downregulation of cathelicidin in rabbit lung and intestinal epithelia: a potential therapeutic strategy.* PLoS One, 2011. **6**(6): p. e20637.

110. Gall, W.E., et al., *alpha-hydroxybutyrate is an early biomarker of insulin resistance and glucose intolerance in a nondiabetic population.* PLoS One, 2010. **5**(5): p. e10883.

111. Owen, O.E., et al., *Brain Metabolism during Fasting.* The Journal of Clinical Investigation, 1967. **46**(10): p. 1589-1595.

112. Kimura, I., et al., *Short-chain fatty acids and ketones directly regulate sympathetic nervous system via G protein-coupled receptor 41 (GPR41).* PNAS, 2011. **108**(19): p. 8030–8035.

113. Brennan, E.P., et al., *Antibacterial Activity within Degradation Products of Biological Scaffolds Composed of Extracellular Matrix.* Tissue Engineering, 2006. **12**(10): p. 2949-2955.

114. Cleries, R., et al., *BootstRatio: A web-based statistical analysis of fold-change in qPCR and RT-qPCR data using resampling methods.* Comput Biol Med, 2012. **42**(4): p. 438-45.

115. Mottamal, M., et al., *Histone deacetylase inhibitors in clinical studies as templates for new anticancer agents.* Molecules, 2015. **20**(3): p. 3898-941.

116. Shimazu, T., et al., *Suppression of oxidative stress by beta-hydroxybutyrate, an endogenous histone deacetylase inhibitor.* Science, 2013. **339**(6116): p. 211-4.

117. Ahmed, K., S. Tunaru, and S. Offermanns, *GPR109A, GPR109B and GPR81, a family of hydroxy-carboxylic acid receptors.* Trends Pharmacol Sci, 2009. **30**(11): p. 557-62.

118. Zeng, X., et al., *Induction of porcine host defense peptide gene expression by short-chain fatty acids and their analogs.* PLoS One, 2013. **8**(8): p. e72922.

119. Yonezawa, T., Y. Kobayashi, and Y. Obara, *Short-chain fatty acids induce acute phosphorylation of the p38 mitogen-activated protein kinase/heat shock protein 27 pathway via GPR43 in the MCF-7 human breast cancer cell line.* Cell Signal, 2007. **19**(1): p. 185-93.

120. Miraglia, E., et al., *Entinostat up-regulates the CAMP gene encoding LL-37 via activation of STAT3 and HIF-1alpha transcription factors.* Sci Rep, 2016. **6**: p. 33274.

121. Khan, S. and G.B. Jena, *Protective role of sodium butyrate, a HDAC inhibitor on beta-cell proliferation, function and glucose homeostasis through modulation of p38/ERK MAPK and apoptotic pathways: study in juvenile diabetic rat.* Chem Biol Interact, 2014. **213**: p. 1-12.

122. Jamaluddin, M., et al., *TNF-alpha-induced NF-kappaB/RelA Ser(276) phosphorylation and enhanceosome formation is mediated by an ROS-dependent PKAc pathway.* Cell Signal, 2007. **19**(7): p. 1419-33.

123. Kefaloyianni, E., C. Gaitanaki, and I. Beis, *ERK1/2 and p38-MAPK signalling pathways, through MSK1, are involved in NF-kappaB transactivation during oxidative stress in skeletal myoblasts.* Cell Signal, 2006. **18**(12): p. 2238-51.

124. Guha, M. and N. Mackman, *LPS induction of gene expression in human monocytes.* Cell Signal, 2001. **13**(2): p. 85-94.

125. Chakraborty, K., et al., *cAMP stringently regulates human cathelicidin antimicrobial peptide expression in the mucosal epithelial cells by activating cAMP-response element-binding protein, AP-1, and inducible cAMP early repressor.* J Biol Chem, 2009. **284**(33): p. 21810-27.

126. Elloumi, H.Z. and S.M. Holland, *Complex regulation of human cathelicidin gene expression: novel splice variants and 5'UTR negative regulatory element.* Mol Immunol, 2008. **45**(1): p. 204-17.

127. Ta, A., et al., *Double-stranded RNA induces cathelicidin expression in the intestinal epithelial cells through phosphatidylinositol 3-kinase-protein kinase Czeta-Sp1 pathway and ameliorates shigellosis in mice.* Cell Signal, 2017. **35**: p. 140-153.

128. Cederlund, A., et al., *Label-free quantitative mass spectrometry reveals novel pathways involved in LL-37 expression.* J Innate Immun, 2014. **6**(3): p. 365-76.

129. Takada, Y., et al., *Nonsteroidal anti-inflammatory agents differ in their ability to suppress NF-kappaB activation, inhibition of expression of cyclooxygenase-2 and cyclin D1, and abrogation of tumor cell proliferation.* Oncogene, 2004. **23**(57): p. 9247-58.

130. Ture, Z., et al., *The role of nonsteroidal anti-inflammatory drugs intramuscular injection in the development and severity of deep soft tissue infection in mice.* Fundam Clin Pharmacol, 2017.

131. Bryant, A.E., et al., *The roles of injury and nonsteroidal anti-inflammatory drugs in the development and outcomes of severe group A streptococcal soft tissue infections.* Curr Opin Infect Dis, 2015. **28**(3): p. 231-9.

132. Weng, T.C., et al., *Ibuprofen worsens Streptococcus pyogenes soft tissue infections in mice.* J Microbiol Immunol Infect, 2011. **44**(6): p. 418-23.

133. Beale, E.W., et al., *The role of biologic mesh in abdominal wall reconstruction: a systematic review of the current literature.* Am J Surg, 2012. **204**(4): p. 510-7.

134. Bilsel, Y. and I. Abci, *The search for ideal hernia repair; mesh materials and types.* Int J Surg, 2012. **10**(6): p. 317-21.

135. Payne, R., J. Aldwinckle, and S. Ward, *Meta-analysis of randomised trials comparing the use of prophylactic mesh to standard midline closure in the reduction of incisional herniae.* Hernia, 2017. **21**(6): p. 843-853.

136. Bellon, J.M., et al., *Partially absorbable meshes for hernia repair offer advantages over nonabsorbable meshes.* Am J Surg, 2007. **194**(1): p. 68-74.

137. Ulrich, D., et al., *A preclinical evaluation of alternative synthetic biomaterials for fascial defect repair using a rat abdominal hernia model.* PLoS One, 2012. **7**(11): p. e50044.

138. Brown, B.N., et al., *Effects of age-related shifts in cellular function and local microenvironment upon the innate immune response to implants.* Semin Immunol, 2017. **29**: p. 24-32.

139. Todros, S., et al., *Synthetic surgical meshes used in abdominal wall surgery: Part II-Biomechanical aspects.* J Biomed Mater Res B Appl Biomater, 2015.

140. Todros, S., P.G. Pavan, and A.N. Natali, *Synthetic surgical meshes used in abdominal wall surgery: Part I-materials and structural conformation.* J Biomed Mater Res B Appl Biomater, 2015.

141. Huber, A., et al., *Polypropylene-containing synthetic mesh devices in soft tissue repair: a meta-analysis.* J Biomed Mater Res B Appl Biomater, 2012. **100**(1): p. 145-54.

142. Hu, Z., et al., *Immunomodulatory ECM-like Microspheres for Accelerated Bone Regeneration in Diabetes Mellitus.* ACS Appl Mater Interfaces, 2018. **10**(3): p. 2377-2390.

143. Sicari, B., N. Turner, and S.F. Badylak, *An in vivo model system for evaluation of the host response to biomaterials.* Methods Mol Biol, 2013. **1037**: p. 3-25.

144. Valentin, J.E., et al., *Extracellular Matrix Bioscaffolds for Orthopaedic Applications.* The Journal of Bone and Joint Surgery, 2006. **88-A**(12): p. 2673-2686.

145. Londono, R. and S.F. Badylak, *Biologic Scaffolds for Regenerative Medicine: Mechanisms of In vivo Remodeling.* Ann Biomed Eng, 2014.

146. Brown, B.N., B.M. Sicari, and S.F. Badylak, *Rethinking regenerative medicine: a macrophage-centered approach.* Front Immunol, 2014. **5**: p. 510.

147. Wynn, T.A., *Type 2 cytokines: mechanisms and therapeutic strategies.* Nat Rev Immunol, 2015. **15**(5): p. 271-82.

148. Nucera, S., D. Biziato, and M. De Palma, *The interplay between macrophages and angiogenesis in development, tissue injury and regeneration.* Int J Dev Biol, 2011. **55**(4-5): p. 495-503.

149. Haldar, M. and K.M. Murphy, *Origin, development, and homeostasis of tissue-resident macrophages.* Immunological Reviews, 2014. **262**: p. 25-35.

150. Wynn, T.A., A. Chawla, and J.W. Pollard, *Macrophage biology in development, homeostasis and disease.* Nature, 2013. **496**(7446): p. 445-55.

151. Gordon, S. and L. Martinez-Pomares, *Physiological roles of macrophages.* Pflugers Arch, 2017. **469**(3-4): p. 365-374.

152. Tidball, J.G. and M. Wehling-Henricks, *Macrophages promote muscle membrane repair and muscle fibre growth and regeneration during modified muscle loading in mice in vivo.* J Physiol, 2007. **578**(Pt 1): p. 327-36.

153. Tidball, J.G. and S.A. Villalta, *Regulatory interactions between muscle and the immune system during muscle regeneration.* Am J Physiol Regul Integr Comp Physiol, 2010. **298**(5): p. R1173-87.

154. Godwin, J.W., A.R. Pintoa, and N.A. Rosenthal, *Macrophages are required for adult salamander limb regeneration.* Proceedings of the National Academy of Sciences, 2013. **110**(23): p. 9415–9420.

155. Wynn, T.A. and K.M. Vannella, *Macrophages in Tissue Repair, Regeneration, and Fibrosis.* Immunity, 2016. **44**(3): p. 450-462.

156. Vannella, K.M. and T.A. Wynn, *Mechanisms of Organ Injury and Repair by Macrophages.* Annu Rev Physiol, 2017. **79**: p. 593-617.

157. Amid, P.K., *Classification of Biomaterials and Their Related Complications in Abdominal Wall Hernia Surgery.* Hernia, 1997. **1**(1): p. 15-21.

158. Hjort, H., et al., *Three-year results from a preclinical implantation study of a long-term resorbable surgical mesh with time-dependent mechanical characteristics.* Hernia, 2012. **16**(2): p. 191-7.

159. Pascual, G., et al., *Repair of abdominal wall defects with biodegradable laminar prostheses: polymeric or biological?* PLoS One, 2012. **7**(12): p. e52628.

160. Sun, W.Q., et al., *Process-induced extracellular matrix alterations affect the mechanisms of soft tissue repair and regeneration.* J Tissue Eng, 2013. **4**: p. 2041731413505305.

161. Russo, I., et al., *Butyrate attenuates lipopolysaccharide-induced inflammation in intestinal cells and Crohn's mucosa through modulation of antioxidant defense machinery.* PLoS One, 2012. **7**(3): p. e32841.

162. Anderson, J., *Foreword,* in *Host Response to Biomaterials: The Impact of Host Response on Biomaterial Selection*. 2015, Academic Press. p. xiii.

163. Burger, J.W.A., et al., *Long-term Follow-up of a Randomized Controlled Trial of Suture Versus Mesh Repair of Incisional Hernia.* Transactions of the ... Meeting of the American Surgical Association, 2004. **CXXII**(&NA;): p. 176-183.

164. Gravante, G., D. Venditti, and V. Filingeri, *The Role of Single-Shot Antibiotic Prophylaxis in Inguinal Hernia Repair A Meta-Analysis Approach of 4336 Patients.* Annals of Surgery, 2008. **248**(3): p. 496-497.

165. Berger, R.L., et al., *Development and validation of a risk-stratification score for surgical site occurrence and surgical site infection after open ventral hernia repair.* J Am Coll Surg, 2013. **217**(6): p. 974-82.

166. Brown, R.H., et al., *Comparison of infectious complications with synthetic mesh in ventral hernia repair.* Am J Surg, 2013. **205**(2): p. 182-7.

167. Ousley, J., et al., *Previous Methicillin-Resistant Staphylococcus aureus Infection Independent of Body Site Increases Odds of Surgical Site Infection after Ventral Hernia Repair*. J Am Coll Surg, 2015. **221**(2): p. 470-7.

168. Gandhi, D., et al., *Chronic abdominal pain secondary to mesh erosion into cecum following incisional hernia repair: a case report and literature review*. Ann Gastroenterol, 2011. **24**(4): p. 321-324.

169. Kingsnorth, A. and K. LeBlanc, *Hernias: inguinal and incisional.* Lancet, 2003. **362**(9395): p. 1561-71.

170. Hong, Y., et al., *Mechanical properties and in vivo behavior of a biodegradable synthetic polymer microfiber-extracellular matrix hydrogel biohybrid scaffold.* Biomaterials, 2011. **32**(13): p. 3387-94.

171. Cavallaro, A., *Use of biological meshes for abdominal wall reconstruction in highly contaminated fields.* World Journal of Gastroenterology, 2010. **16**(15): p. 1928.

172. Garcia, A. and A. Baldoni, *Complex ventral hernia repair with a human acellular dermal matrix and component separation: A case series.* Ann Med Surg (Lond), 2015. **4**(3): p. 271-8.

173. Cheng, A.W., M.A. Abbas, and T. Tejirian, *Outcome of Abdominal Wall Hernia Repair with Biologic Mesh: Permacolversus Strattice.* The American Surgeon, 2014. **80**: p. 999-1002.

174. Perez-Kohler, B., et al., *Preclinical Bioassay of a Polypropylene Mesh for Hernia Repair Pretreated with Antibacterial Solutions of Chlorhexidine and Allicin: An In Vivo Study.* PLoS One, 2015. **10**(11): p. e0142768.

175. Carbonell, A.M., et al., *Outcomes of synthetic mesh in contaminated ventral hernia repairs.* J Am Coll Surg, 2013. **217**(6): p. 991-8.

176. Angelos, P.C., T.E. Brennan, and D.M. Toriumi, *Biomechanical properties of superficial musculoaponeurotic system tissue with vs without reinforcement with poly-4-hydroxybutyric acid absorbable mesh.* JAMA Facial Plast Surg, 2014. **16**(3): p. 199-205.

177. Primus, F.E. and H.W. Harris, *A critical review of biologic mesh use in ventral hernia repairs under contaminated conditions.* Hernia, 2013. **17**(1): p. 21-30.

178. Pouton, C.W. and S. Akhtar, *Biosynthetic polyhydroxyalkanoates and their potential in drug delivery.* Advanced Drug Delivery Reviews, 1996. **18**: p. 133-162.

179. Li, Z. and X.J. Loh, *Water soluble polyhydroxyalkanoates: future materials for therapeutic applications.* Chem Soc Rev, 2015. **44**: p. 2865-2879.

180. Fu, N., et al., *Electrospun P34HB fibres: a scaffold for tissue engineering.* Cell Proliferation, 2014. **47**: p. 465-475.

181. Holihan, J.L., et al., *Adverse Events after Ventral Hernia Repair: The Vicious Cycle of Complications.* J Am Coll Surg, 2015. **221**(2): p. 478-85.

182. Badylak, S.F., et al., *Host Protection against Deliberate Bacterial Contamination of an Extracellular Matrix Bioscaffold versus Dacron™ Mesh in a Dog Model of Orthopedic Soft Tissue Repair.* J Biomed Mater Res Part B: Appl Biomater, 2003. **67B**: p. 648–654.

183. Blatnik, J.A., et al., *In vivo analysis of the morphologic characteristics of synthetic mesh to resist MRSA adherence.* J Gastrointest Surg, 2012. **16**(11): p. 2139-44.

184. Remlinger, N.T., et al., *Urinary bladder matrix promotes site appropriate tissue formation following right ventricle outflow tract repair.* Organogenesis, 2013. **9**(3): p. 149-60.

185. Tatara, A.M., et al., *Infected animal models for tissue engineering.* Methods, 2015. **84**: p. 17-24.

186. Schleicher, U., et al., *TNF-Mediated Restriction of Arginase 1 Expression in Myeloid Cells Triggers Type 2 NO Synthase Activity at the Site of Infection.* Cell Rep, 2016. **15**(5): p. 1062-1075.

187. Rath, M., et al., *Metabolism via Arginase or Nitric Oxide Synthase: Two Competing Arginine Pathways in Macrophages.* Front Immunol, 2014. **5**: p. 532.

188. Ruffell, D., et al., *A CREB-C/EBPbeta cascade induces M2 macrophage-specific gene expression and promotes muscle injury repair.* Proc Natl Acad Sci U S A, 2009. **106**(41): p. 17475-80.

189. Azad, A.K., M.V. Rajaram, and L.S. Schlesinger, *Exploitation of the Macrophage Mannose Receptor (CD206) in Infectious Disease Diagnostics and Therapeutics.* J Cytol Mol Biol, 2014. **1**(1).

190. Ni, Y.H., et al., *Microlocalization of CD68+ tumor-associated macrophages in tumor stroma correlated with poor clinical outcomes in oral squamous cell carcinoma patients.* Tumour Biol, 2015. **36**(7): p. 5291-8.

191. Iqbal, A.J., et al., *Human CD68 promoter GFP transgenic mice allow analysis of monocyte to macrophage differentiation in vivo.* Blood, 2014. **124**(15): p. e33-44.

192. Subauste, C.S., R. de Waal Malefyt, and F. Fuh, *Role of CD80 (B7.1) and CD86 (B7.2) in the Immune Response to an Intracellular Pathogen.* The Journal of Immunology, 1998. **160**: p. 1831-1840.

193. Gensel, J.C., et al., *Predictive screening of M1 and M2 macrophages reveals the immunomodulatory effectiveness of post spinal cord injury azithromycin treatment.* Sci Rep, 2017. **7**: p. 40144.

194. Nolan, A., et al., *Differential role for CD80 and CD86 in the regulation of the innate immune response in murine polymicrobial sepsis.* PLoS One, 2009. **4**(8): p. e6600.

195. Lin, H.H., et al., *The macrophage F4/80 receptor is required for the induction of antigen-specific efferent regulatory T cells in peripheral tolerance.* J Exp Med, 2005. **201**(10): p. 1615-25.

196. Raes, G., et al., *Differential expression of FIZZ1 and Ym1 in alternatively versus classically activated macrophages.* J Leukoc Biol, 2002. **71**(4): p. 597-602.

197. Madej, M.P., et al., *Different Regulation of Interleukin-1 Production and Activity in Monocytes and Macrophages: Innate Memory as an Endogenous Mechanism of IL-1 Inhibition.* Front Pharmacol, 2017. **8**: p. 335.

198. Gu, M., et al., *Protein phosphatase PP1 negatively regulates the Toll-like receptor- and RIG-I-like receptor-triggered production of type I interferon by inhibiting IRF3 phosphorylation at serines 396 and 385 in macrophage.* Cell Signal, 2014. **26**(12): p. 2930-9.

199. Moore, T.C. and T.M. Petro, *IRF3 and ERK MAP-kinases control nitric oxide production from macrophages in response to poly-I:C.* FEBS Lett, 2013. **587**(18): p. 3014-20.

200. Kurotaki, D., et al., *Essential role of the IRF8-KLF4 transcription factor cascade in murine monocyte differentiation.* Blood, 2013. **121**(10): p. 1839-1849.

201. Kapoor, N., et al., *Transcription factors STAT6 and KLF4 implement macrophage polarization via the dual catalytic powers of MCPIP.* J Immunol, 2015. **194**(12): p. 6011-23.

202. Wang, K., et al., *SUMOylation of KLF4 promotes IL-4 induced macrophage M2 polarization.* Cell Cycle, 2017. **16**(4): p. 374-381.

203. Date, D., et al., *Kruppel-like transcription factor 6 regulates inflammatory macrophage polarization.* J Biol Chem, 2014. **289**(15): p. 10318-29.

204. Vincent, E.E., et al., *Mitochondrial Phosphoenolpyruvate Carboxykinase Regulates Metabolic Adaptation and Enables Glucose-Independent Tumor Growth.* Mol Cell, 2015. **60**(2): p. 195-207.

205. Luu, K., et al., *STAT1 plays a role in TLR signal transduction and inflammatory responses.* Immunol Cell Biol, 2014. **92**(9): p. 761-9.

206. Leopold Wager, C.M., et al., *STAT1 signaling within macrophages is required for antifungal activity against Cryptococcus neoformans.* Infect Immun, 2015. **83**(12): p. 4513-27.

207. Sheikh, F., et al., *An essential role for IFN-beta in the induction of IFN-stimulated gene expression by LPS in macrophages.* J Leukoc Biol, 2014. **96**(4): p. 591-600.

208. Abdul-Sater, A.A., et al., *Different STAT Transcription Complexes Drive Early and Delayed Responses to Type I IFNs.* J Immunol, 2015. **195**(1): p. 210-216.

209. Dimberg, A., et al., *Inhibition of monocytic differentiation by phosphorylation-deficient Stat1 is associated with impaired expression of Stat2, ICSBP/IRF8 and C/EBPepsilon.* Scand J Immunol, 2006. **64**(3): p. 271-9.

210. Bode, J.G., C. Ehlting, and D. Haussinger, *The macrophage response towards LPS and its control through the p38(MAPK)-STAT3 axis.* Cell Signal, 2012. **24**(6): p. 1185-94.

211. Wang, W.L., et al., *Prostaglandin I(2) analogues suppress TNF-alpha expression in human monocytes via mitogen-activated protein kinase pathway.* Inflamm Res, 2011. **60**(7): p. 655-63.

212. Chang, N.C., et al., *A macrophage protein, Ym1, transiently expressed during inflammation is a novel mammalian lectin.* J Biol Chem, 2001. **276**(20): p. 17497-506.

213. Welch, J.S., et al., *TH2 cytokines and allergic challenge induce Ym1 expression in macrophages by a STAT6-dependent mechanism.* J Biol Chem, 2002. **277**(45): p. 42821-9.

214. Lee, P.H., et al., *Expression of an additional cathelicidin antimicrobial peptide protects against bacterial skin infection.* Proc Natl Acad Sci U S A, 2005. **102**(10): p. 3750-5.

215. Chong, K.T., R.R. Thangavel, and X. Tang, *Enhanced expression of murine beta-defensins (MBD-1, -2,- 3, and -4) in upper and lower airway mucosa of influenza virus infected mice.* Virology, 2008. **380**(1): p. 136-43.

216. van der Does, A.M., et al., *Vitamin D(3) and phenylbutyrate promote development of a human dendritic cell subset displaying enhanced antimicrobial properties.* J Leukoc Biol, 2014. **95**(6): p. 883-91.